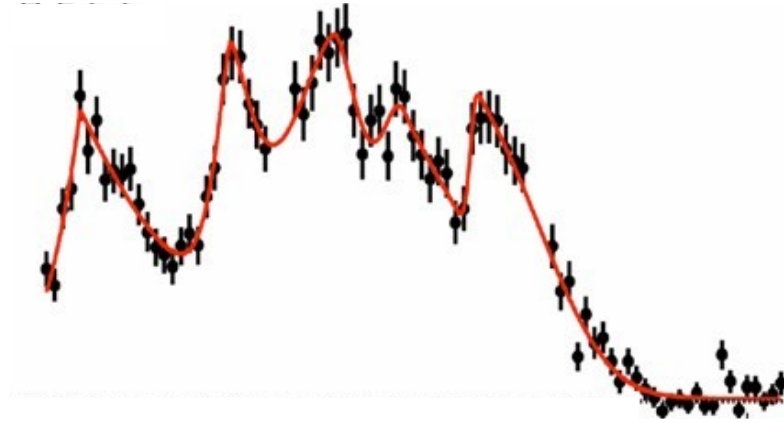
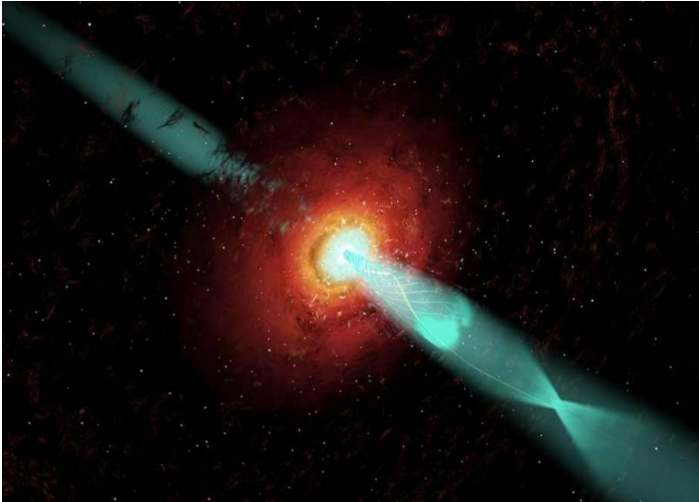


# Variable emission from Active Galactic Nuclei



A. Zech

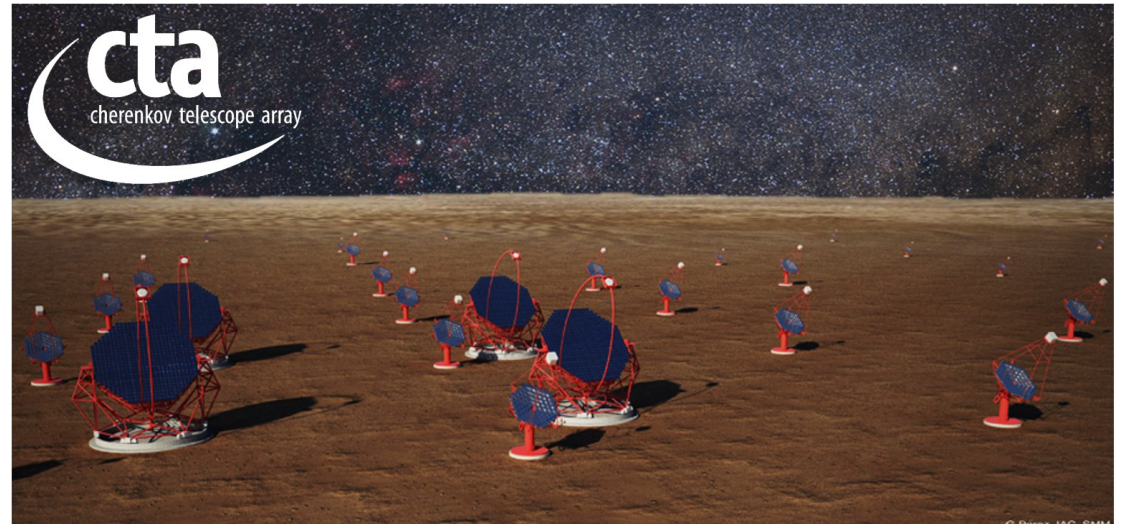
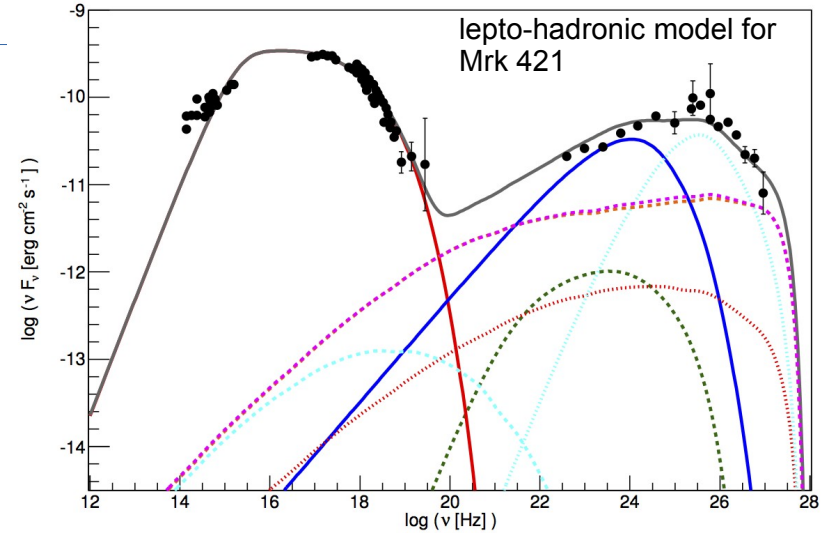
LUTH – Observatoire de Paris  
andreas.zech@obspm.fr

“The Transient Universe 2023”  
Cargèse, Corsica

## Andreas Zech

associate professor  
director of the teaching department  
LUTH , Observatoire de Paris (Meudon)

- very-high-energy gamma-ray astronomy
- > observations with the H.E.S.S. array in Namibia
- > preparation of the CTA (Cherenkov Telescope Array)
- development of emission models for the multi-wavelength emission from blazars



---

## **AGNs as transient sources**

What are the emission mechanisms of AGNs ?

What variability signatures are observed at different time scales ?

What do we know about their physical origin ?

# Content

---

## 1) a short introduction to AGNs

- structure of an AGN
- emission components
- AGN types

## 2) variability from the central engine

- variable flux from radio-quiet AGNs
- reverberation mapping

## 3) emission from blazars and radio-galaxies

- physics of relativistic jets
- emission mechanisms in the jet

## 4) variability from the jet

- flux and polarisation variability in blazars
- quasi-periodic oscillations

## 5) modelling blazar flares

- variability in the one-zone model
- multi-zone models


## 6) the puzzle of very rapid flares

- constraints from minute-scale flares
- models for very rapid flares

## 7) flares and multi-messengers

- what we have learnt from TXS 0506+056

## 8) conclusions & outlook

The image shows the Hercules A galaxy, a radio galaxy with a central active galactic nucleus (AGN). The central region is bright and contains a complex structure of jets and lobes. Two large, diffuse lobes of radio emission extend outwards from the center, one towards the upper left and one towards the lower right. The background is filled with numerous stars of various colors, including white, yellow, and blue. The text "1) a short introduction to AGNs" is overlaid in the center of the image.

# 1) a short introduction to AGNs

# discovery of active galaxies

Active galaxies were first discovered in 1908 due to the very large width of their emission lines. Seyfert galaxies were seen to have line widths of up to  $\Delta v \sim 8500$  km/s , when interpreted as **Doppler broadening**.

(reminder :  $\frac{\Delta\lambda}{\lambda} \approx \frac{\Delta v}{c}$  )

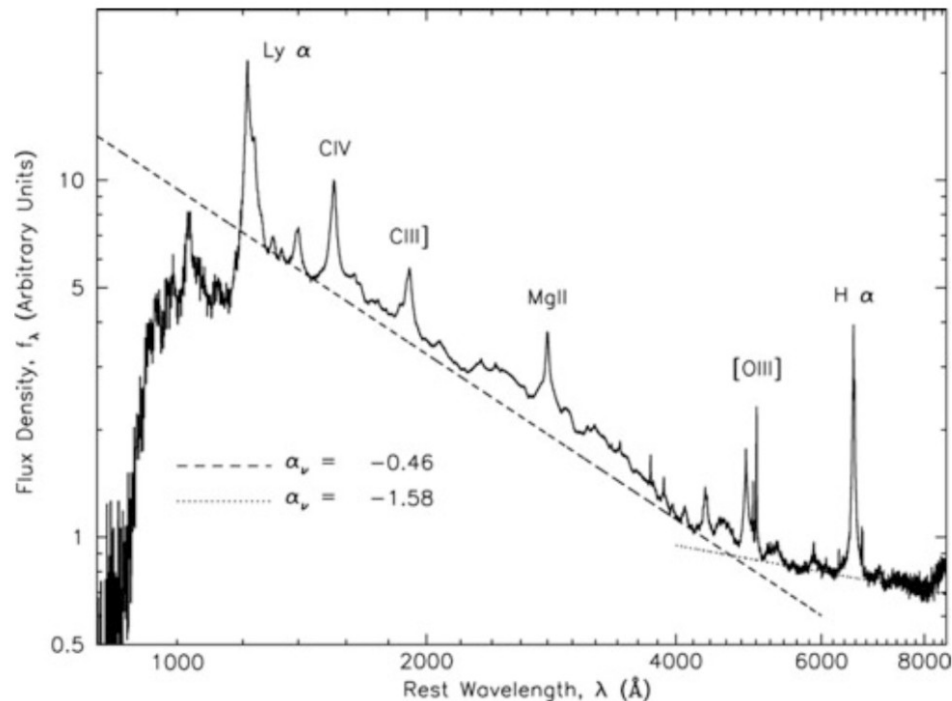
They show intense emission from unresolved core regions with radius  $r < 100$  pc.

For emission from a gravitationally bound gas

$$\Rightarrow v^2 \simeq \frac{GM}{r}$$

The broad emission lines from a very compact region imply thus a very large mass density in the core of such objects !

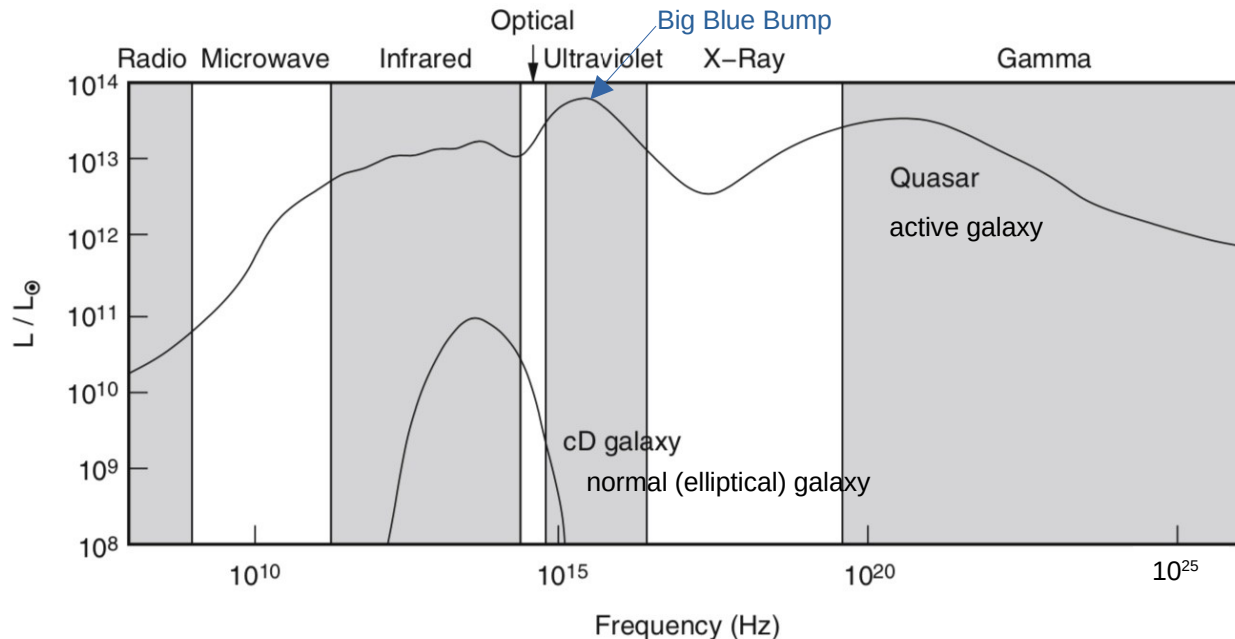
$$M(r) > 10^{10} \left( \frac{r}{100 \text{ pc}} \right) M_{\odot}$$



Combined optical spectrum of 2200 QSOs - a type of active galaxy - from the SDSS.

P. Schneider 2015

# discovery of active galaxies

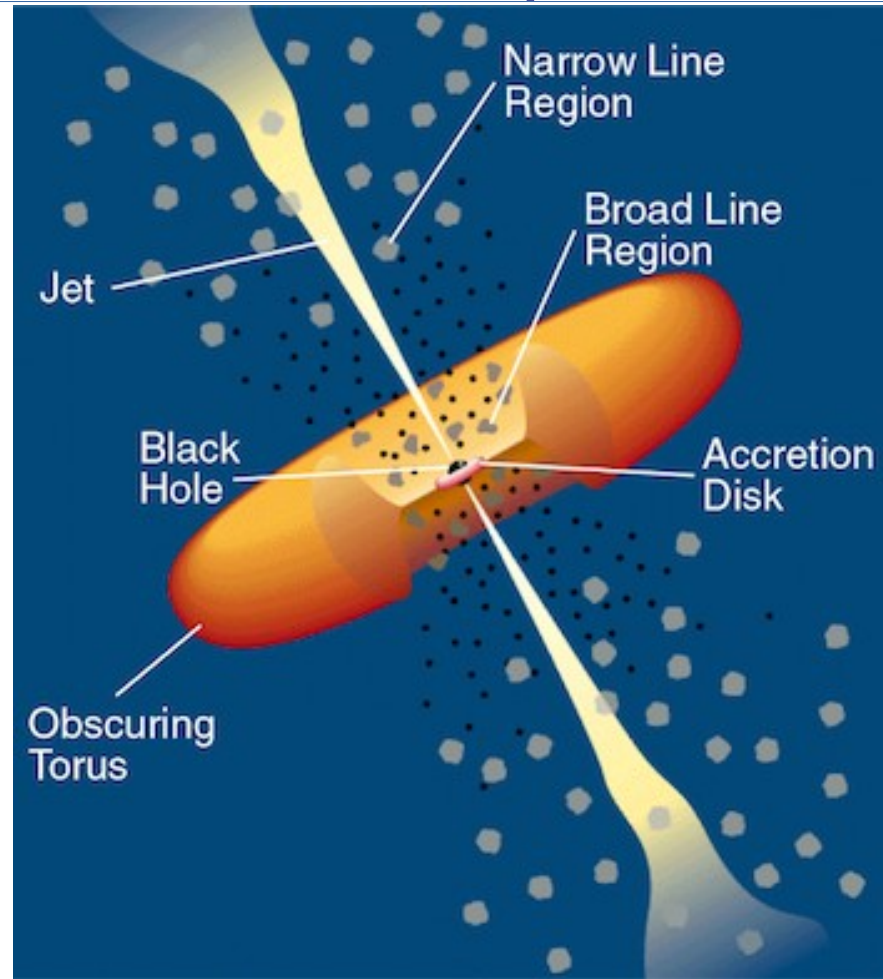


Active galaxies were found to have a vastly **larger spectrum** than normal galaxies. Some types emit from the radio band up to very-high energies.

Their spectral continuum can be approximated with **power laws** in different spectral bands, which indicates a **non-thermal** origin for their emission. Their emission was also found to be polarised.

Active galaxies show in general rapid flux variability - more rapid with shorter wavelengths.

# AGN components



*Trevor C. Weekes, Very High Energy Gamma-Ray Astronomy*



# AGN components: central engine - SMBH

The compact, high-luminosity center of active galaxies has been identified with a *central engine* in the form of a **super-massive black hole (SMBH) accreting nearby matter**.

The existence of a black hole is necessary for energetic reasons:

- luminosity  $L \sim 10^{47} \text{ erg / s}$   
lifetime (from extension of radio lobes)  $\Delta t > 10^7 \text{ yr}$   
-> energy requirement  $E_{\text{req}} \sim 3 \times 10^{61} \text{ erg}$
- size of the central engine:  $R < 3 \times 10^{15} \text{ cm}$   
(from observations of flux variability on the time-scale of a day)

If one assumes this energy is gained by fusion:

- max. efficiency  $\epsilon \sim 0.8\%$  :  $\epsilon m c^2 \sim E_{\text{req}}$  ->  $m \sim 2 \times 10^9 M_{\odot}$ .
- Such a massive object has a Schwarzschild radius  $r_s \sim 6 \times 10^{14} \text{ cm}$

A SMBH seems the only possible candidate and in this case, gravitational energy production is far more efficient than nuclear fusion:  $\epsilon \sim 6\%$  for Schwarzschild BH,  $\epsilon$  up to 29% for Kerr BH.



*first direct image of the central  
black hole of M87 with EHT  
(EHT Collaboration)*

# AGN components: central engine - accretion disk

## accretion:

Gas falling onto a compact object sees its potential (gravitational) energy converted into kinetic energy.

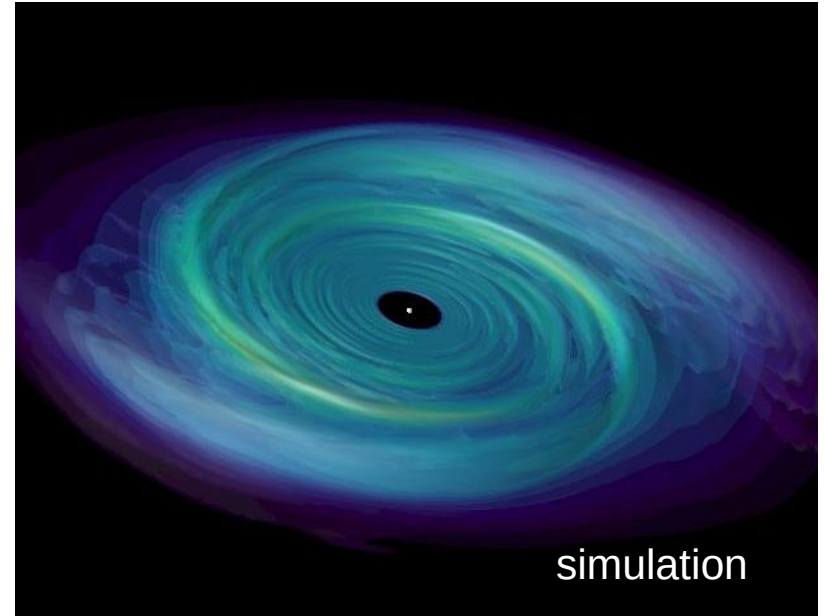
In general, the gas has finite angular momentum and, through internal friction, settles into an accretion disk oriented perpendicularly to the angular momentum vector.

The disk rotates differentially following Kepler's laws. This causes friction that heats the disk and leads to a deceleration. The gas moves slowly inwards and more potential energy is converted first into kinetic energy and then internal energy (heat) that is radiated away.

## geometrically thin, optically thick disk:

One can show that, in a first approximation, a geometrically thin, optically thick disk radiates as a superposition of Planck spectra with a radial temperature profile following :

$$T(r) = \left( \frac{3c^6}{64 \pi \sigma_{SB} G^2} \right)^{1/4} \dot{m}^{1/4} M_{BH}^{-1/2} \left( \frac{r}{r_s} \right)^{-3/4}$$



<https://apod.nasa.gov/apod/ap050312.html>

with  $\dot{m}$  the mass accretion rate and

$$r_s = \frac{2GM_{BH}}{c^2} \text{ the Schwarzschild radius.}$$

In AGNs, accretion disks radiate mostly in the UV range (leading to a “big blue bump” in the spectrum).

# AGN components: central engine - accretion disk

Approximate derivation :

- energy released by a mass  $m$  falling from  $r + \Delta r$  to  $r$  in the potential of  $M_{BH}$  :

$$\Delta E = \frac{G M_{BH} m}{r} - \frac{G M_{BH} m}{r + \Delta r} = \frac{G M_{BH} m}{r} \left( 1 - \frac{1}{1 + \Delta r/r} \right) \approx \frac{G M_{BH} m}{r} \frac{\Delta r}{r}$$

- according to the Virial theorem, half of this potential energy is converted into kinetic energy, i.e. rotational energy of the disk:  $\langle E_{rot} \rangle = \frac{1}{2} \langle \Delta E \rangle$

- the other half can be converted into internal energy (heat). Locally, for an optically thick (two-sided !) disk, this leads to a luminosity that can be described by a black body:

$$\Delta L = \frac{G M_{BH} \dot{m}}{2r^2} \Delta r = 2 \cdot 2 \pi r \Delta r \sigma_{SB} T^4(r)$$

- This yields an approximate description of  $T(r)$  :

$$T(r) = \left( \frac{G M_{BH} \dot{m}}{8 \pi \sigma_{SB} r^3} \right)^{1/4} \quad \text{valid for } r \gg r_s$$

( The different factor on the previous page comes from a more accurate description of the energy dissipation by friction and advection of heat. Plus,  $r$  has been scaled with  $r_s$ . )

The inner radius of the accretion disk is determined by the size of the *innermost stable circular orbit* (ISCO) of the SMBH.

# Eddington accretion rate

For matter to be able to fall into the gravitational potential, the radiation force from the emitted light must be smaller than then gravitational force. One considers a fully ionised gas falling onto an isotropic radiation field. The principal interaction is through **Thomson scattering of electrons**:

$$F_{rad} = \sigma_T \frac{L}{4 \pi r^2 c}$$

The gravitational force on the plasma is dominated by the protons :

$$F_{grav} = \frac{G M_{BH} m_p}{r^2}$$

Accretion proceeds as long as  $F_{rad} < F_{grav}$  i.e.  $L < \frac{4 \pi G c m_p}{\sigma_T} M_{BH} \equiv L_{edd} \approx 1.26 \times 10^{38} \left( \frac{M_{BH}}{M_{\odot}} \right) \text{erg/s}$

This defines the **Eddington luminosity** of a black hole with given mass.

Inversely, this relation provides a lower limit for the mass of SMBH for a given luminosity.

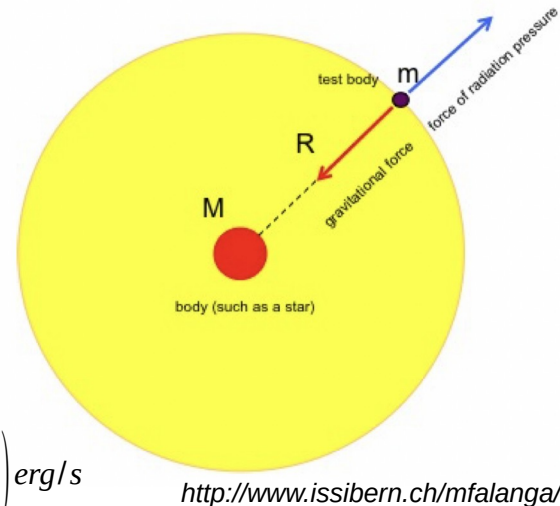
Luminous AGN have typically  $M_{BH} > 10^8 M_{\odot}$  , while less luminous ones have  $M_{BH} > 10^6 M_{\odot}$  .

If the efficiency  $\epsilon$  of conversion from potential energy to radiation is known, the mass accretion rate is given by

$$\dot{m} = \frac{L}{\epsilon c^2} \approx 0.18 \frac{1}{\epsilon} \left( \frac{L}{10^{46} \text{erg/s}} \right) M_{\odot} / \text{yr}$$

and its maximum is

$$\dot{m}_{Edd} = \frac{L_{Edd}}{\epsilon c^2} \approx \frac{1}{\epsilon} 2 \times 10^{-9} M_{BH} / \text{yr}$$



# AGN components: central engine - accretion disk

**low accretion rate**  $\dot{m}/\dot{m}_{Edd} \ll 10^{-6}$

- *accretion torus* : radiatively inefficient, optically thin, non-thermal emission → possible presence of a wind, no jets

**intermediate accretion rate**

- *standard disk, geometrically thin & optically thick* (Shakura et Sunyaev en 1973)

viscosity depends on sound speed ( $c_s$ ), thickness of disk ( $H \ll r$ ) and viscosity parameter  $\alpha$  :  $v_{vis} = \alpha c_s H$

- *magnetically arrested disk* (MAD) (Bisnovatyi-Kogan & Ruzmaikin 1974, Narayan et al. 2003)

strong poloidal magnetic field disrupts the axisymmetric accretion flow, causing discrete 'blobs' of material and sporadic eruption events  
→ powers relativistic jets in MHD simulations (Tchekhovskoy et al. 2012) through Blandford-Znajek mechanism

- *standard and normal evolution* (SANE) (Narayan et al. 2012)

weaker poloidal magnetic field, angular momentum is transported outward by turbulence in the disc (mainly magnetorotational instability)  
→ seem to lead to less powerful jets

- *accretion dominated advection flow* (ADAF)

radiatively inefficient, low luminosity, ADAFs are cooled by advection, geometrically extended, similar in shape to a sphere (or a "corona") rather than a disk. ADAFs emit a power-law, non-thermal radiation.

**high accretion rate**  $\dot{m}/\dot{m}_{Edd} \gg 0.1$

optically thick "*doughnuts*", radiatively inefficient, strong wind dominates emission (Abramowicz, Jaroszynski, Paczyński, Sikora, 1980s)

# AGN components: central engine - accretion disk

Marck's enhanced image: black hole lit by accretion disc.

approaching side  
(blueshift)



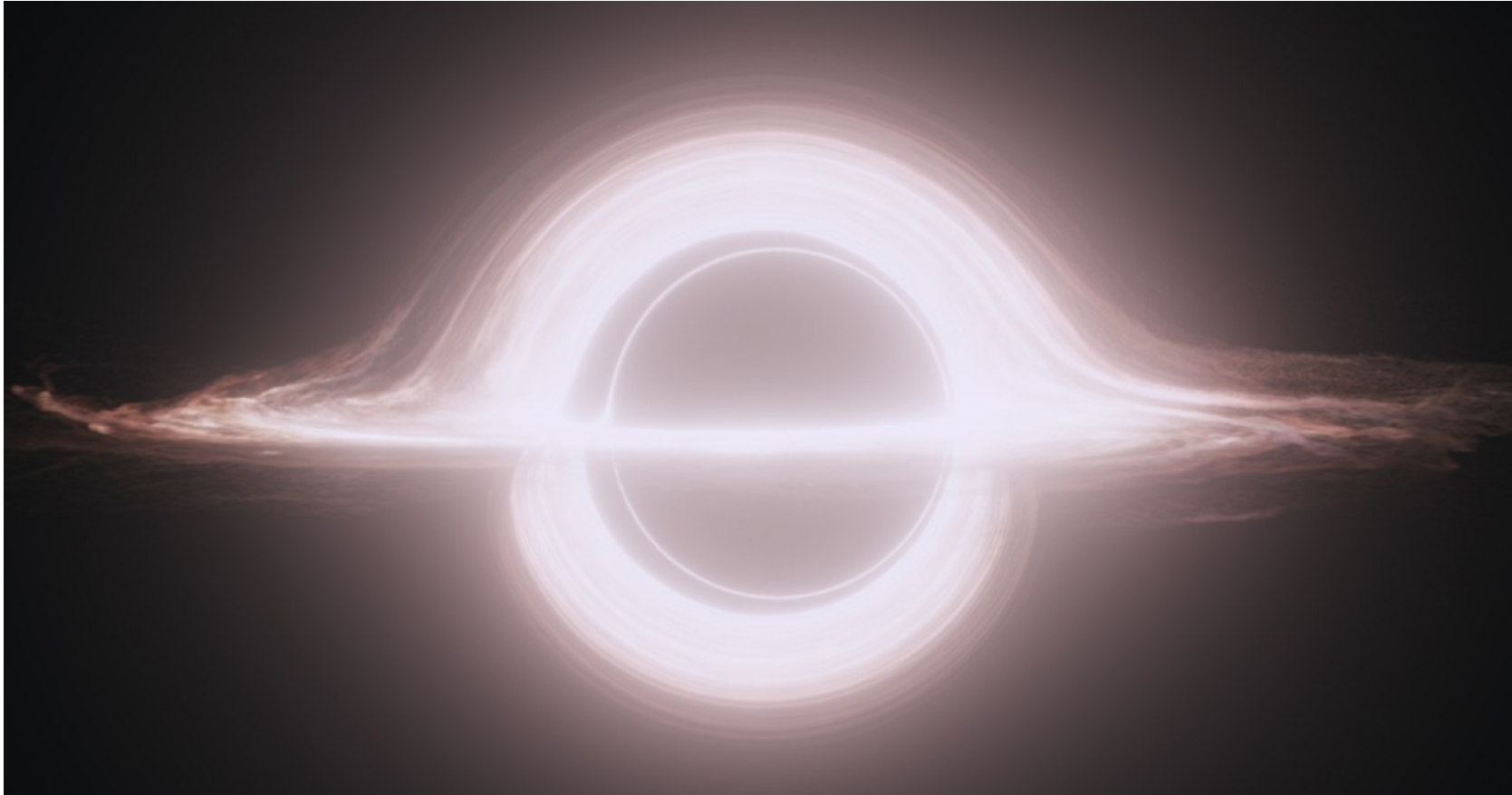
receding side  
(redshift)

simulated view of an accretion disc  
incorporating all relativistic effects  
*wikipedia, image J.A. Marck, OP, 1995*

# AGN components: central engine - accretion disk

---

the  
Hollywood  
version



Gargantua: A variant of the black-hole accretion disk seen in the film Interstellar. Credit: DNEG/Warner Bros. Entertainment Inc./CQG 32 065001

# AGN components: corona

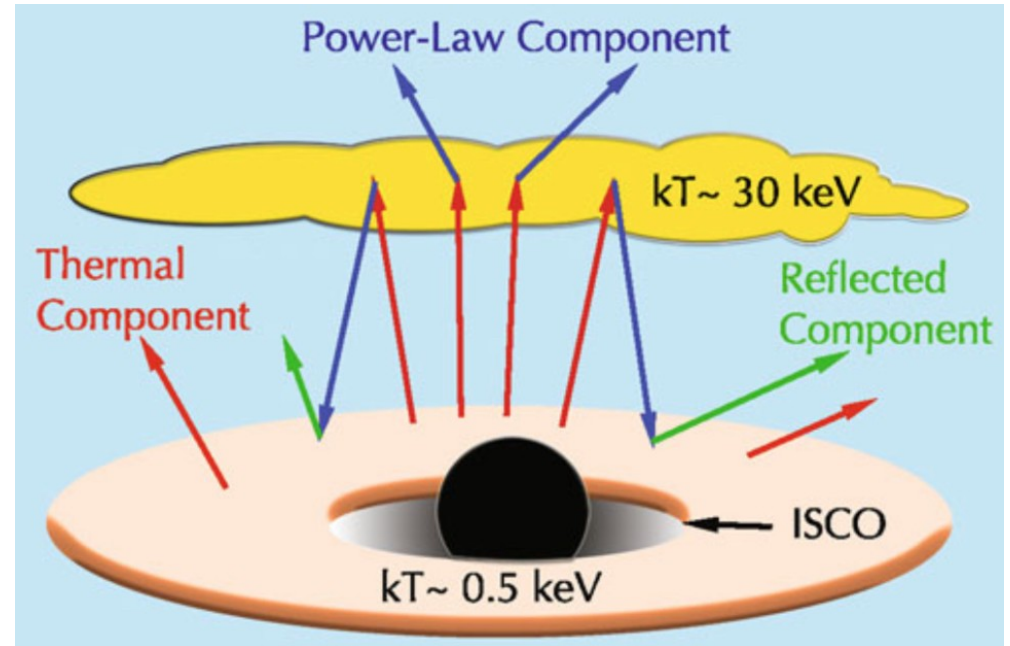
An additional emission of **X-rays** comes from the close vicinity of the disk.

In analogy to stellar atmospheres, a hot layer of gas is expected to form above the optically thick disk - the **corona**. This gas is optically thin and does not cool efficiently. It is expected to have a very high energy (10s to 100s of keV), maybe reaching the *virial temperature*:

$$k_B T \approx G M_{BH} m / r$$

Photons from the disk can be up-scattered in this gas via the *Inverse Compton effect*. The corona emits these up-scattered photons in the form of a power law with a cut-off at  $\sim 100$  keV.

In addition, part of the photons from the corona are emitted back towards the disk and form a “**reflected component**”. These photons are down-scattered in energy on the electrons in the disk.

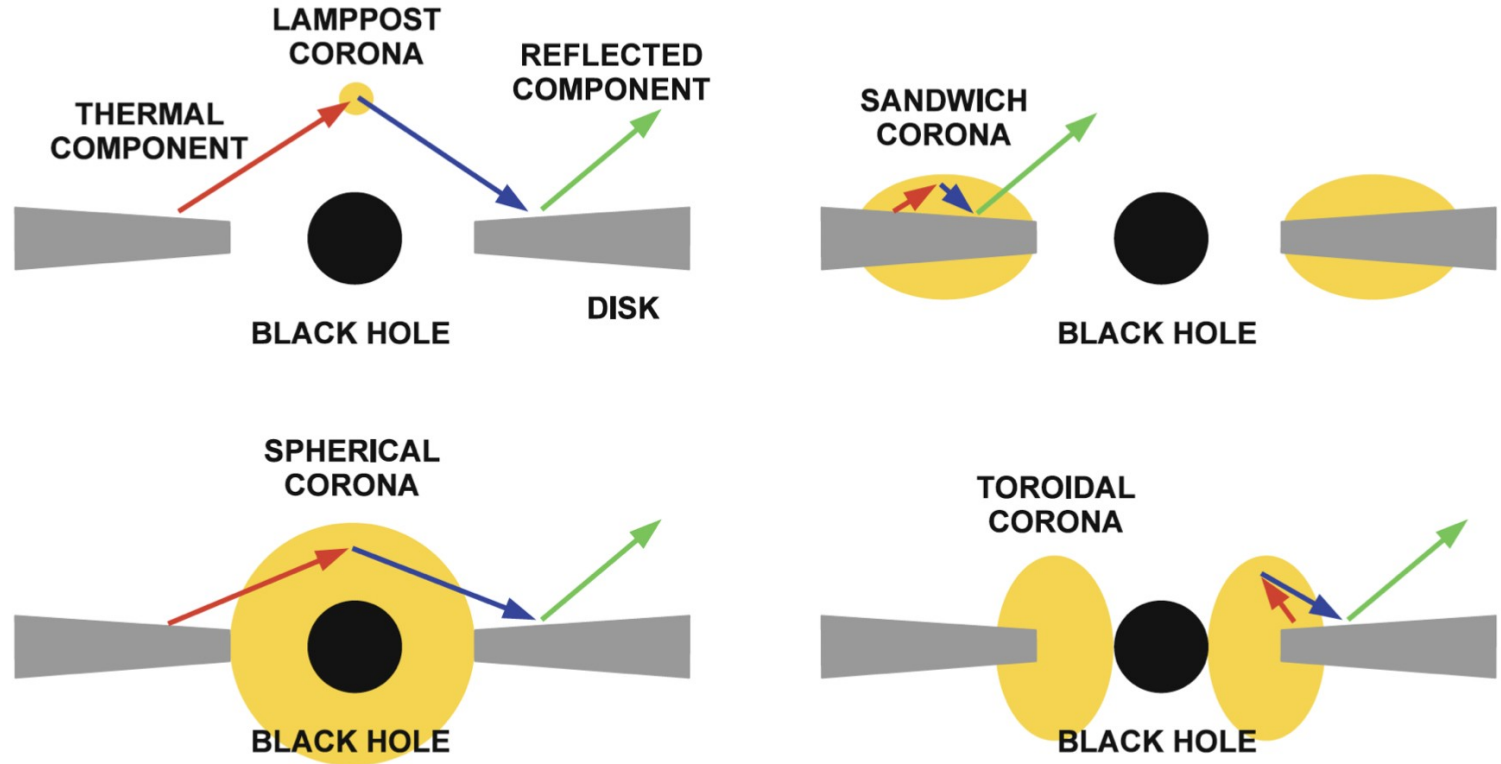


P. Schneider 2015



# AGN components: corona

The actual geometry of the corona is not known. A variety of scenarios have been proposed and several coronas might co-exist in a source.



Bambi  
2017

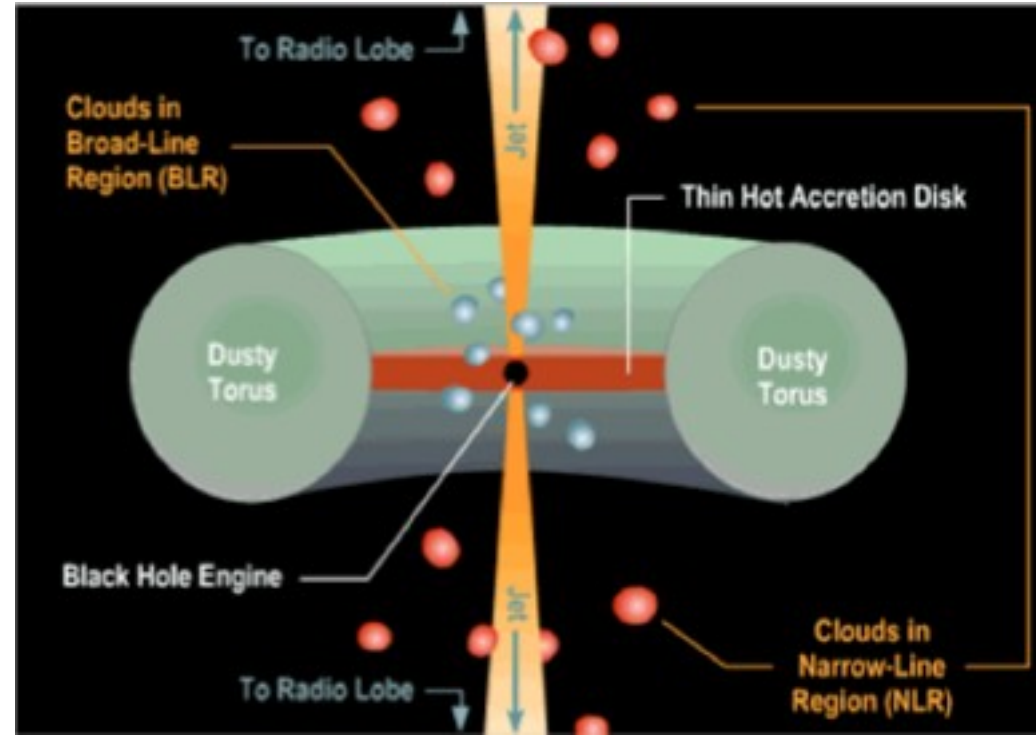
# AGN components: broad line region

The broad emission lines detected from many active galaxies must come from a gas of very high velocity ( $\sim 10\,000$  km/s). This gas seems to be located close to the central engine, since for Keplerian motion in the gravitational potential:

$$v_{\text{rot}} = \sqrt{\frac{GM_{\text{BH}}}{r}}, \text{ thus } r \sim 500 r_{\text{S}} \text{ (sub-pc range).}$$

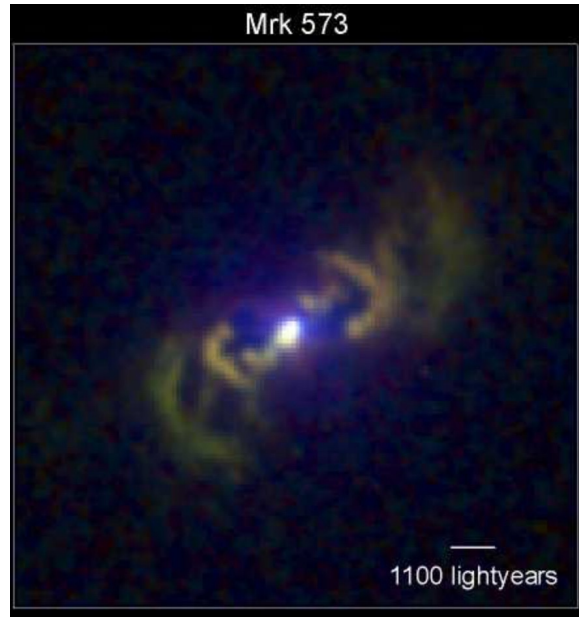
The **broad line region (BLR)** seems to consist of a very large number of fast-moving dense clouds of a typical temperature  $T \sim 20\,000$  K. They are partially ionised through radiation from the central engine.

Characteristics of this medium are deduced from observations of the emission lines (width, intensity, absence of forbidden lines,...).

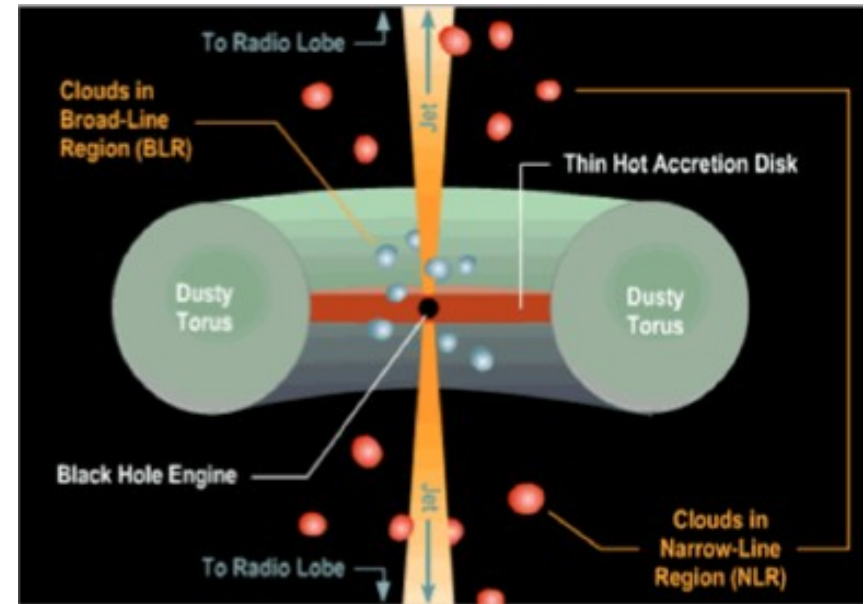


<http://ay20-eric.blogspot.com/2011/10/clarifications-on-agn.html>

# AGN components: narrow line region



HST, NASA, <http://www.astro.ru.nl/~falcke/trans1.jpg>



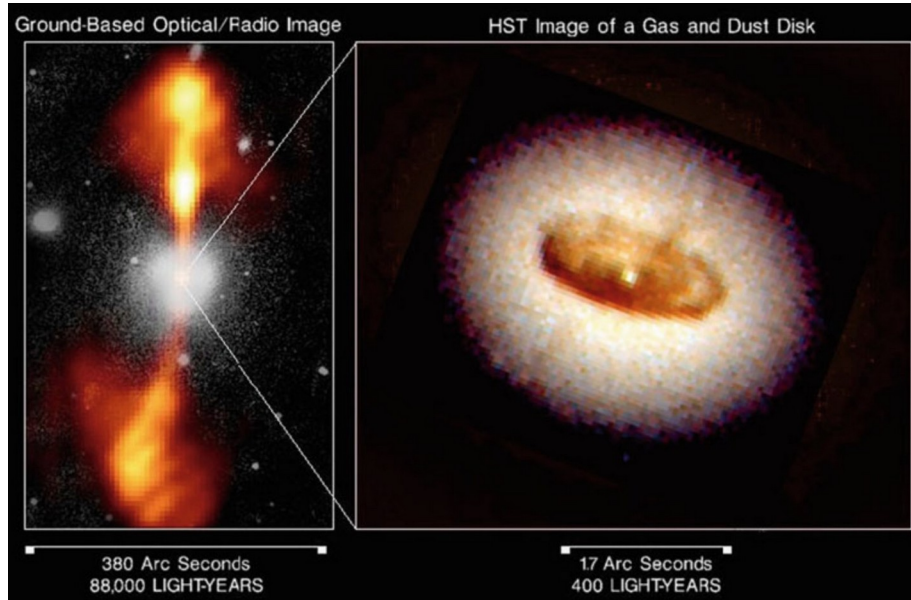
<http://ay20-eric.blogspot.com/2011/10/clarifications-on-agn.html>

Most AGNs emit also narrow lines, with typical widths  $\sim 400$  km/s. These include the “forbidden” [OIII] line, indicating that the **narrow line region (NLR)** is much less dense than the BLR.

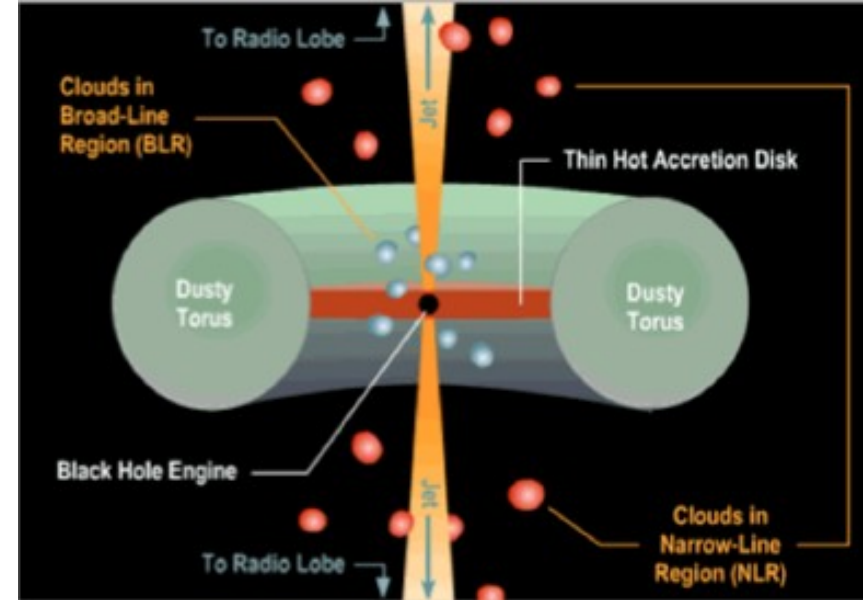
The NLR is thought to extend to  $\sim 100$  pc and to consist of clouds as well. The gas temperature is  $T \sim 15\,000$  K. It can be spatially resolved in certain Seyfert galaxies and shows the shape of two cones above and below the disk.

It seems that the ionisation of the gas in the NLR is not isotropic, but occurs in “ionisation cones”.

# AGN components: dusty torus



P. Schneider 2015



<http://ay20-eric.blogspot.com/2011/10/clarifications-on-agn.html>

In the current picture, a torus of gas and dust surrounds the accretion disk, with a size about an order of magnitude larger than the BLR. It consists of dense clouds. The dust in these clouds absorbs radiation from the central engine in the direction of the plane of the accretion disk. This leads to heating of the torus, which radiates in the **infrared**.

The **dusty torus** is difficult to observe directly and its characteristics are not well known. Its temperature would be  $T \lesssim 1000$  K, limited by the dust sublimation temperature.

It plays an important role in the AGN unification scheme since it obscures emission for certain viewing angles.

# AGN components: relativistic jet

A small fraction of AGNs (~10%) are qualified as “**radio-loud**” and present a significant **non-thermal emission** from relativistic jets.

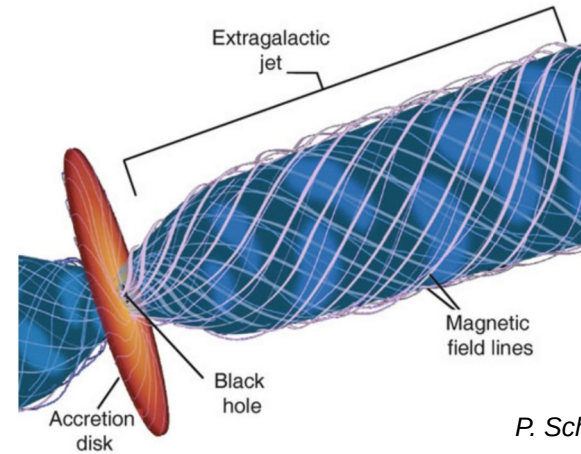
These jets are thought to be launched close to the central engine: from magnetic field lines dragged either by a rotating SMBH or from the accretion disk

They consist of relativistic plasma (pair plasma or ion-electron plasma) carrying magnetic fields. A **magnetic field with a helical large-scale structure** is thought to assure their stability.

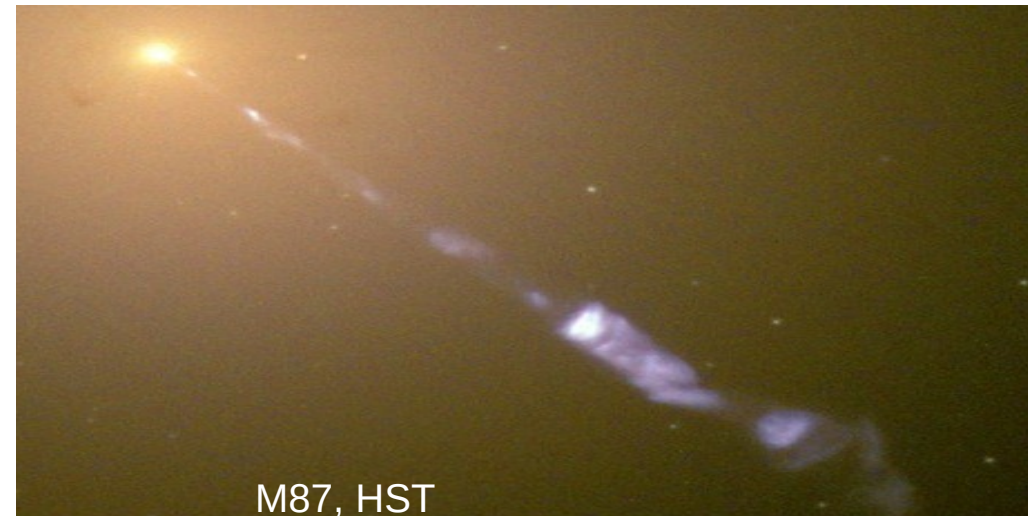
AGN jets are found at scales of **pc to kpc**. They can even extend to **Mpc scales** where they end in large radio lobes.

Jets emit electromagnetic radiation over a very large frequency range. From radio to UV/X-rays it is due to **synchrotron radiation**.

At larger frequencies (X-rays up to very high energies), it is probably due to **Inverse Compton emission** (or hadronic emission processes).

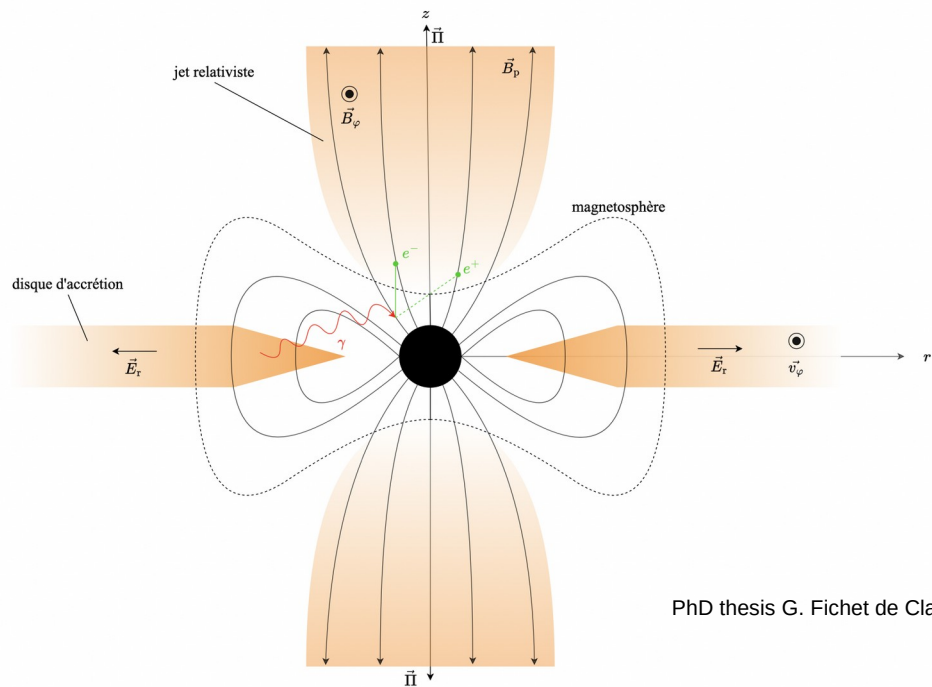


*P. Schneider 2015*

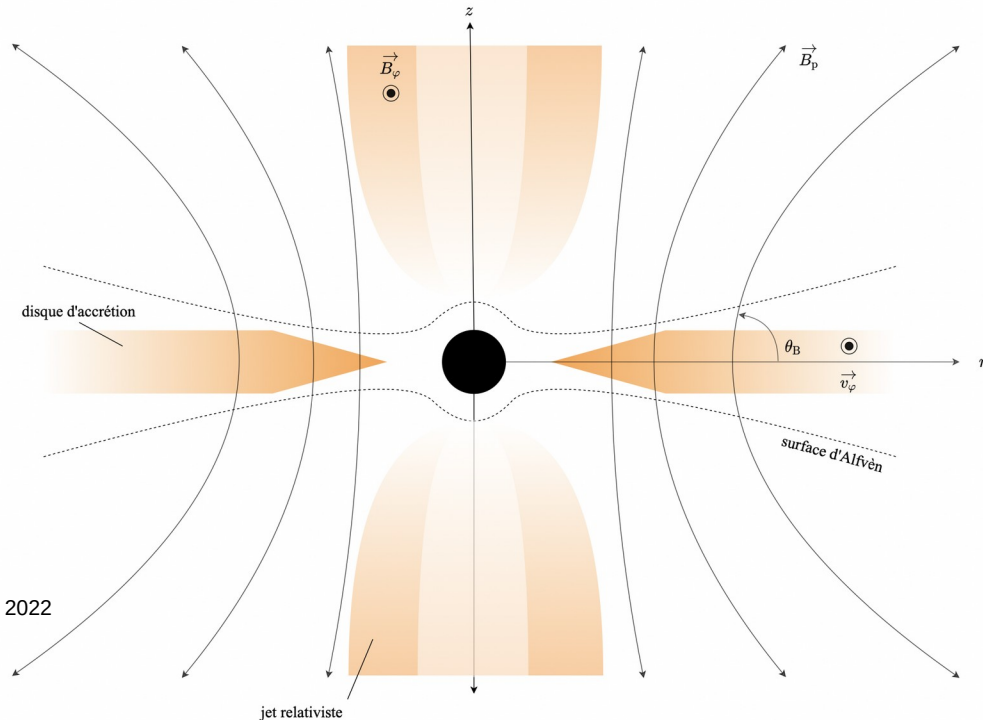


M87, HST

# jet launching



PhD thesis G. Fichet de Clairfontaine, 2022



## Blandford & Znajek 1977

- extraction of rotational energy from the BH spin through magnetic field lines from the disk threading the ergosphere
- launching of a Poynting jet (purely electromagnetic)
- $e^+ e^-$  pairs are created in the BH magnetosphere and follow field lines into the jet

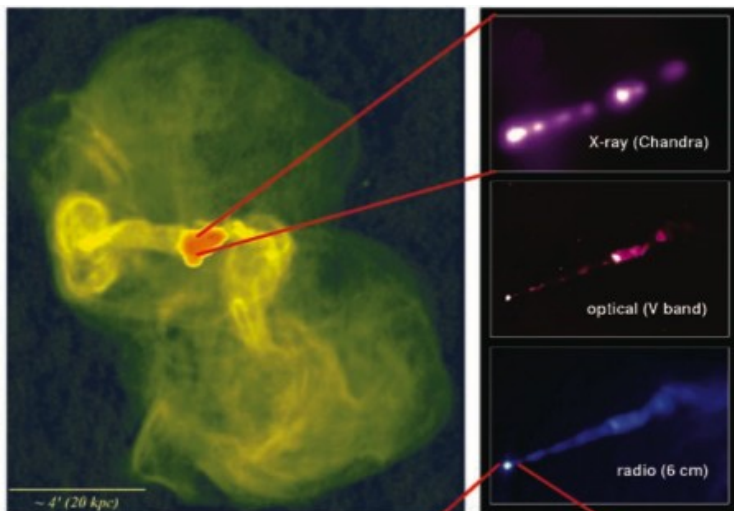
## Blandford & Payne 1982

- extraction of rotational energy from the disk through magnetic field lines anchored in the disk
- launching of a jet through magneto-centrifugal force
- jet is charged with leptons and baryons

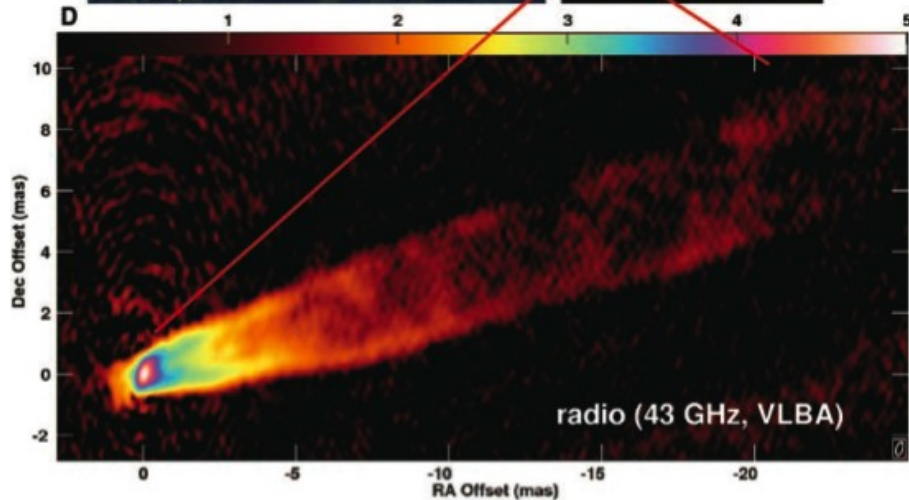
in both cases: jet collimation through helicoidal B-field

# M87 - a close look at a radio galaxy

VLA radio emission shows **kpc jets and radio lobes**



synchrotron emission from the **plasma jet, its core and bright knots** seen by Chandra, HST, VLA (size  $\sim 2$  kpc)

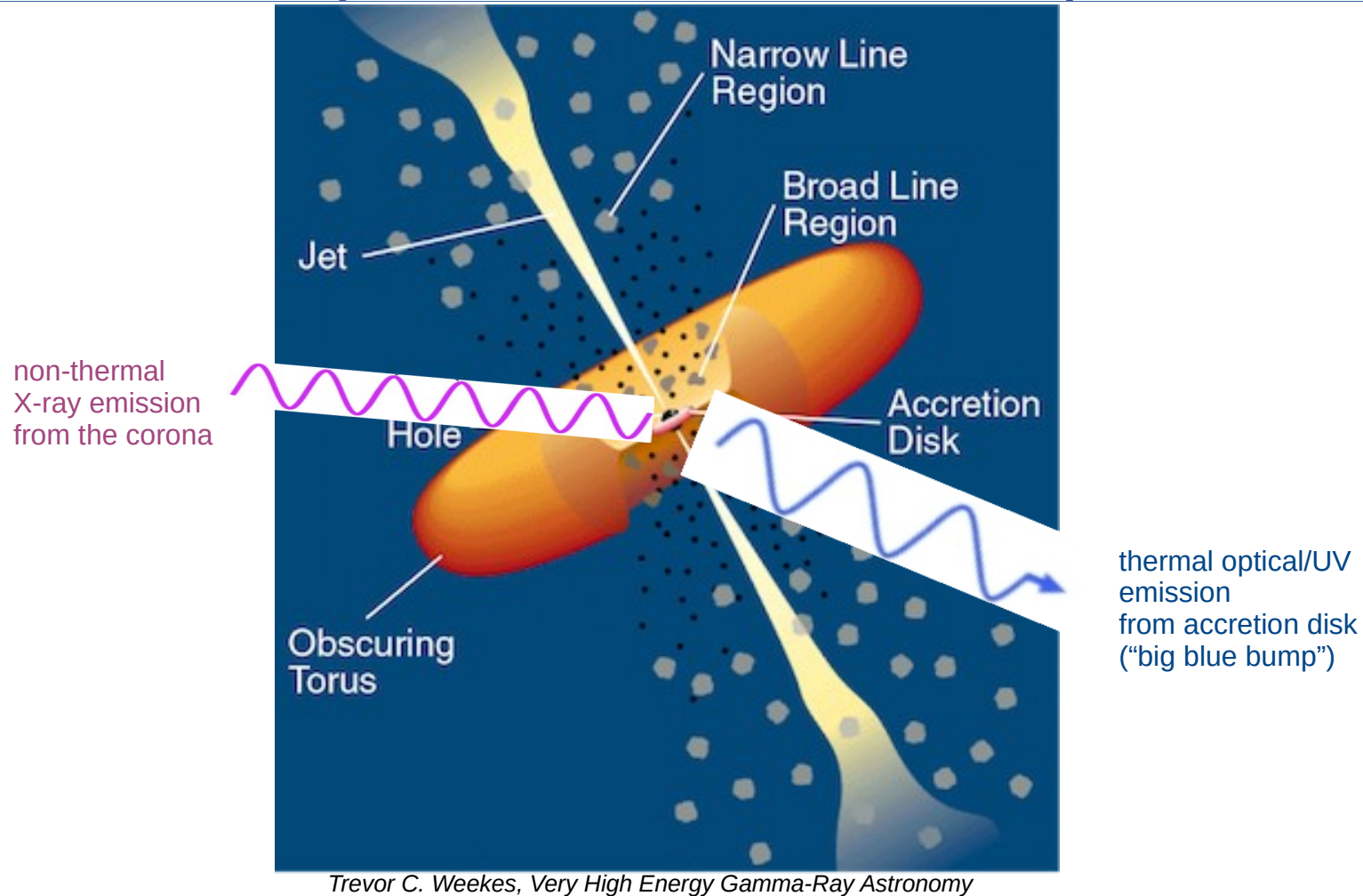


**inner jet and core** resolved by VLBA

The central black hole is thought to be found at a few  $10 R_s$  from the radio core at 43 GHz.

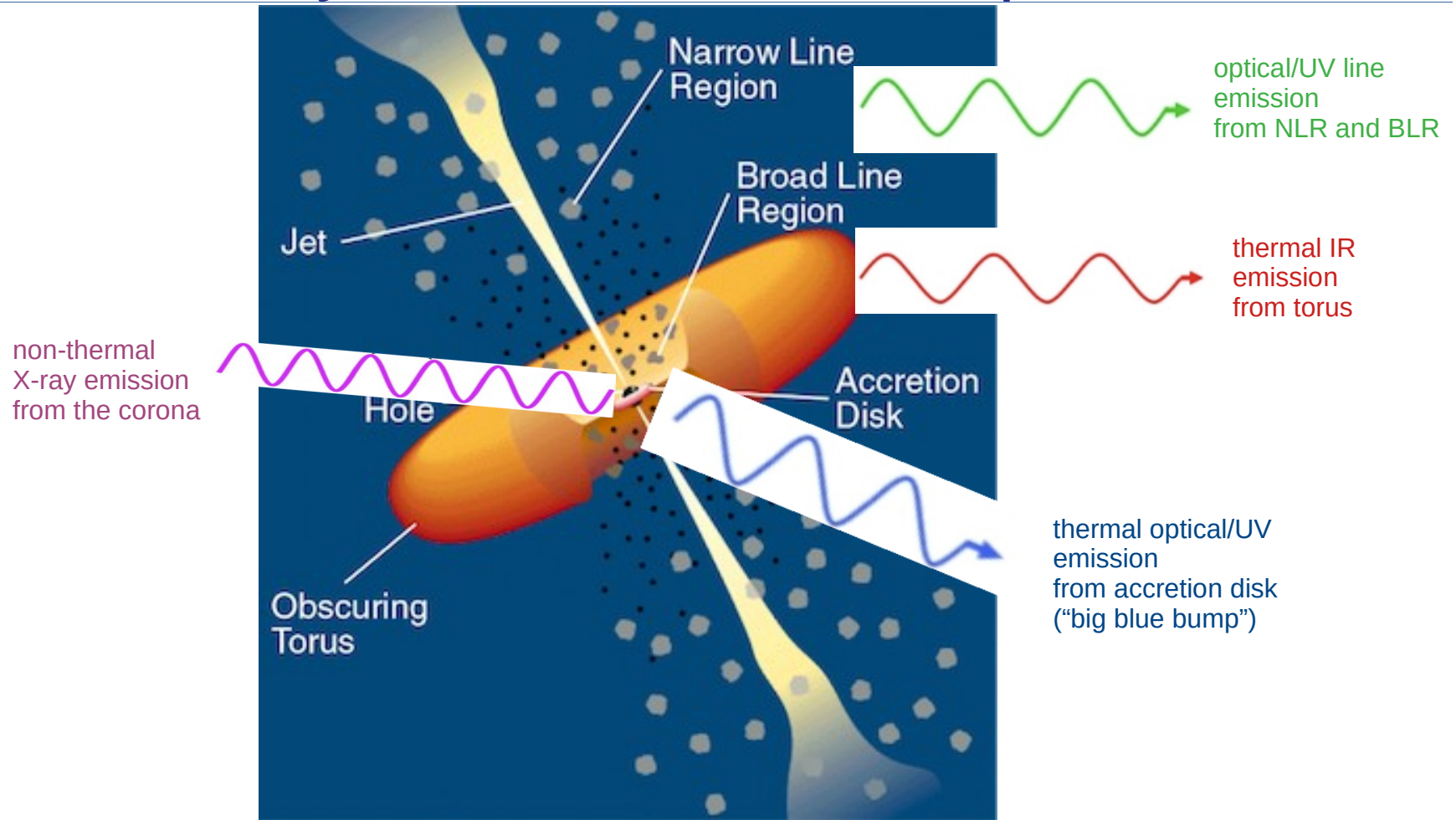
Veritas, HESS...,  
*Science*, 325, 444  
(2009)

# summary: AGN emission components



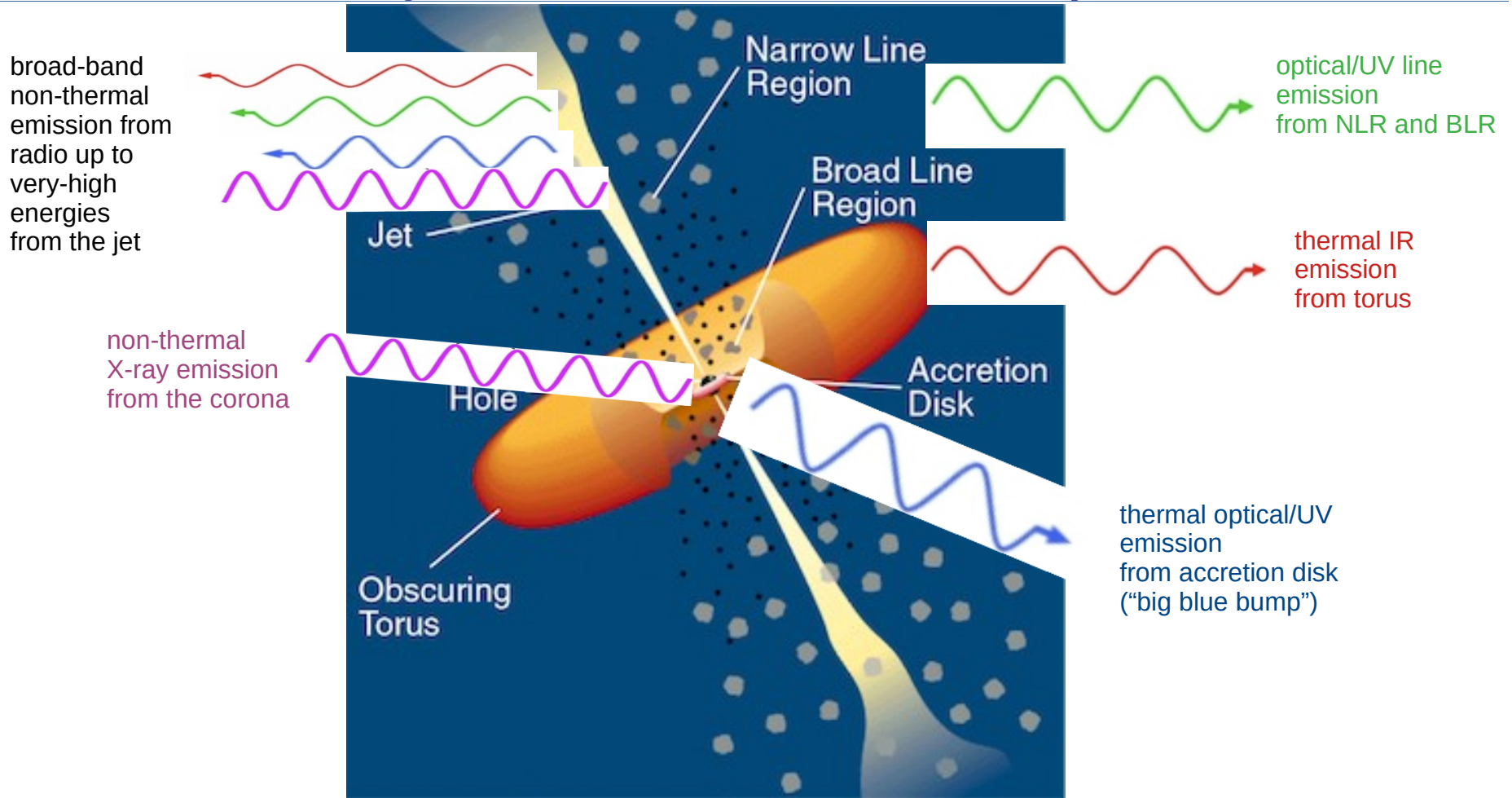


# summary: AGN emission components



Trevor C. Weekes, *Very High Energy Gamma-Ray Astronomy*

# summary: AGN emission components



Trevor C. Weekes, *Very High Energy Gamma-Ray Astronomy*

# AGN unified model

The unified model attempts to explain the large number of different AGN classes with a single physical object.

**Dichotomy** of “radio-loud” (jetted) and “radio-quiet” AGN.

Other differences in the observed emission (mostly) due to the **viewing angle**:

**- large angle (close to disk plane):**

View of the BLR is obstructed by the dusty torus. Spectra show only narrow emission lines. (*Narrow-Line Radio Galaxies, Seyfert 2*)

**- intermediate angle:**

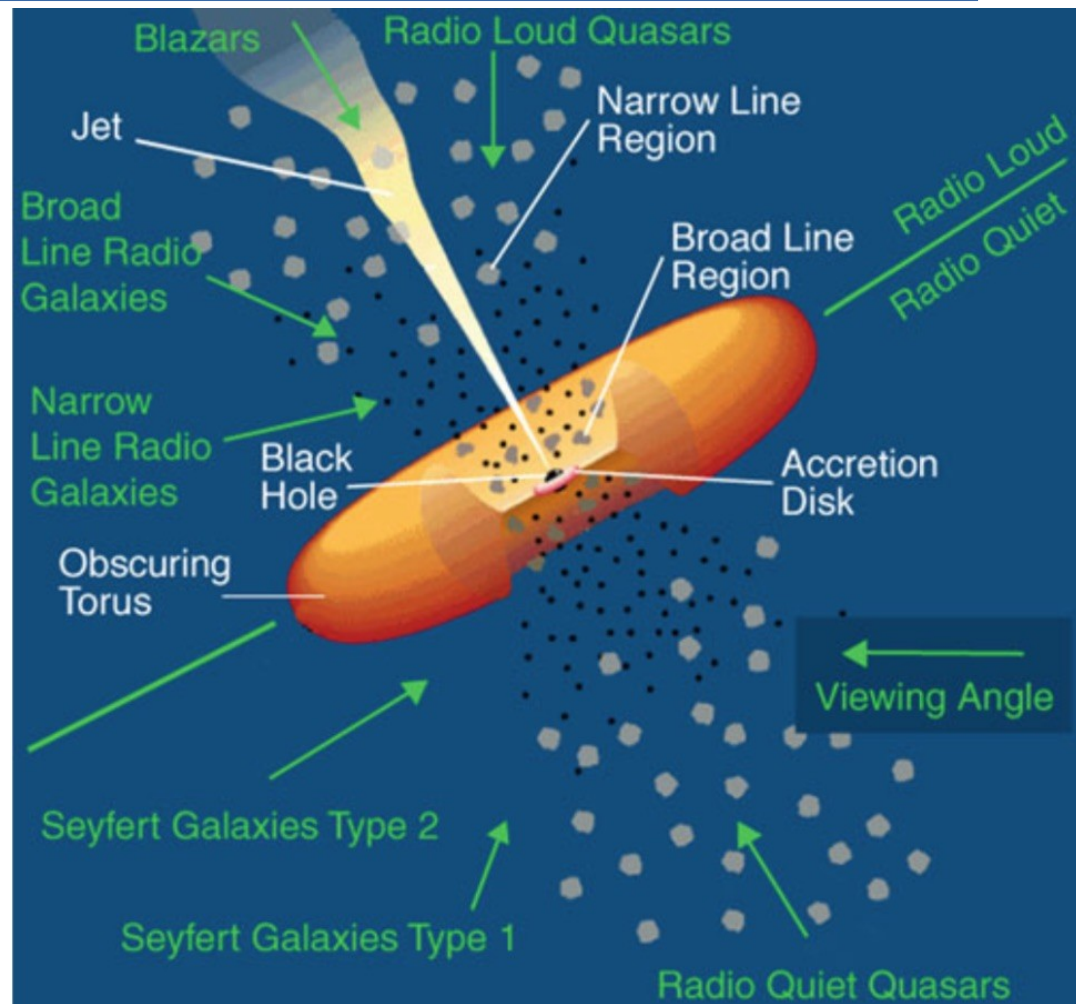
Broad emission lines can be observed. (*Broad-Line Radio Galaxies, Seyfert 1*)

**- small angle (closer to jet axis or disk normal):**

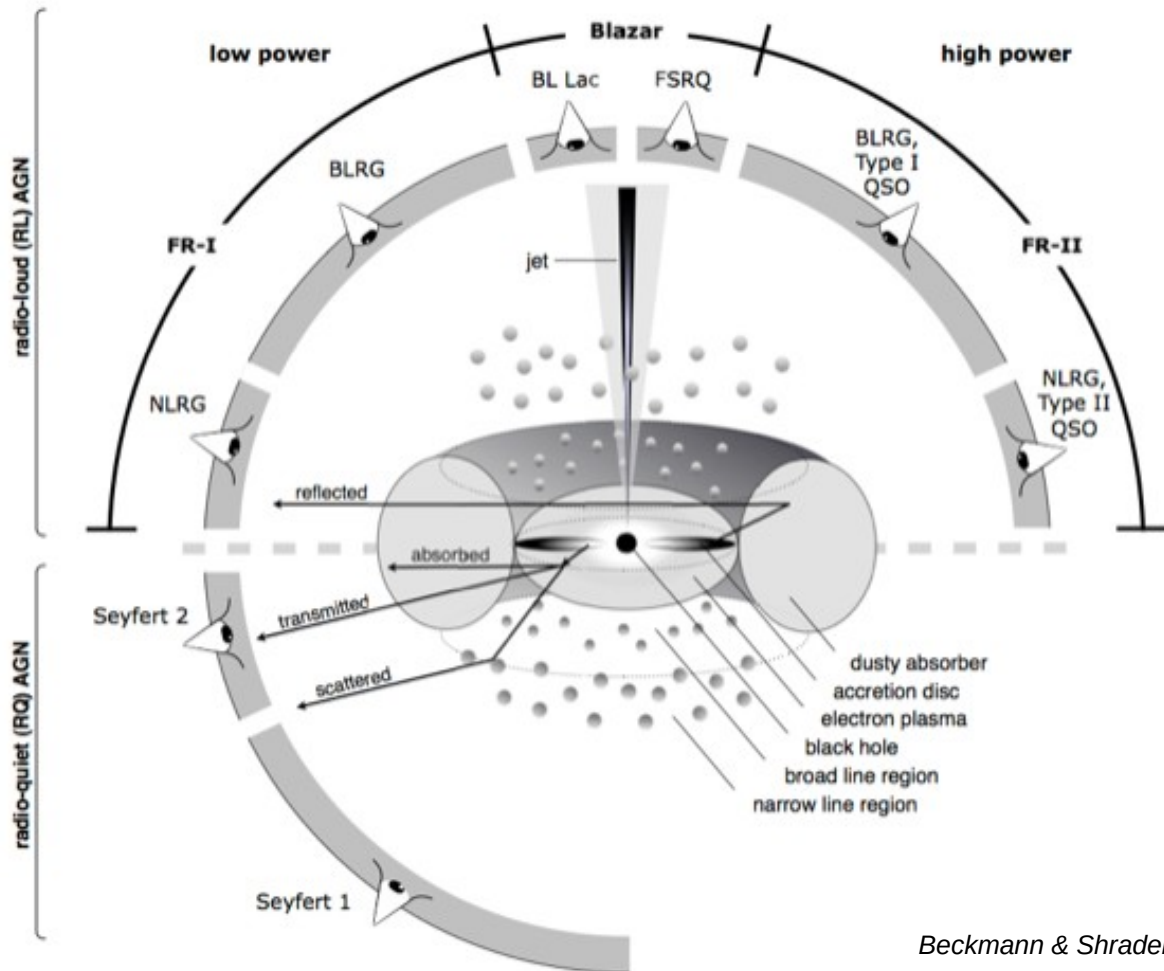
Bright emission from the central region (*radio-quiet & radio-loud quasars or QSOs*)

**- very small angle (~aligned with jet axis):**

For radio-loud objects, relativistic effects amplify the observed luminosity and reduce variability time scales. (*blazars*)



# AGN unified model



Beckmann & Shrader (2012)

# a few specimen

Galaxy NGC 7742

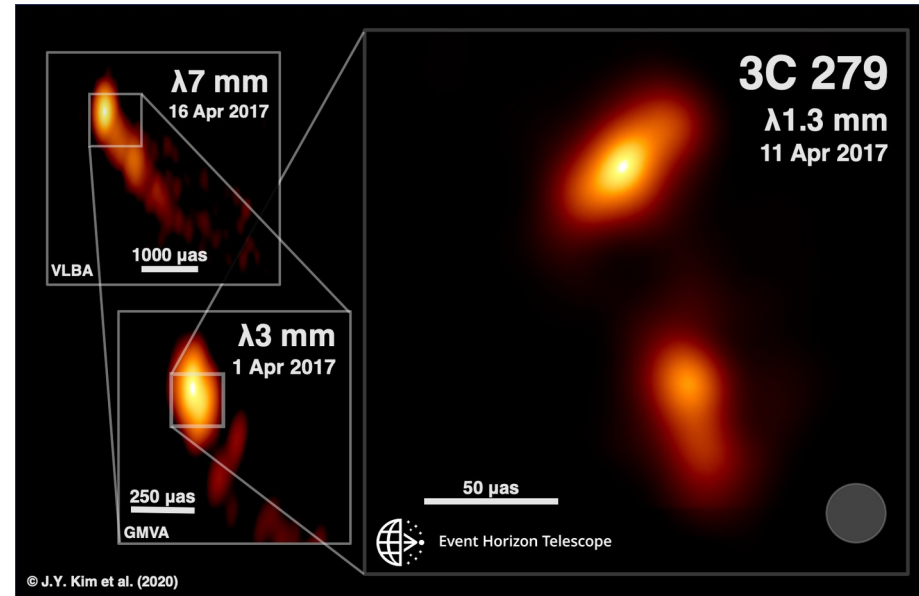


Hubble Heritage

PRC98-28 • Space Telescope Science Institute • Hubble Heritage Team

*the Seyfert galaxy NGC 7742 Image credit: Hubble Heritage Team (AURA/STScI/NASA)*

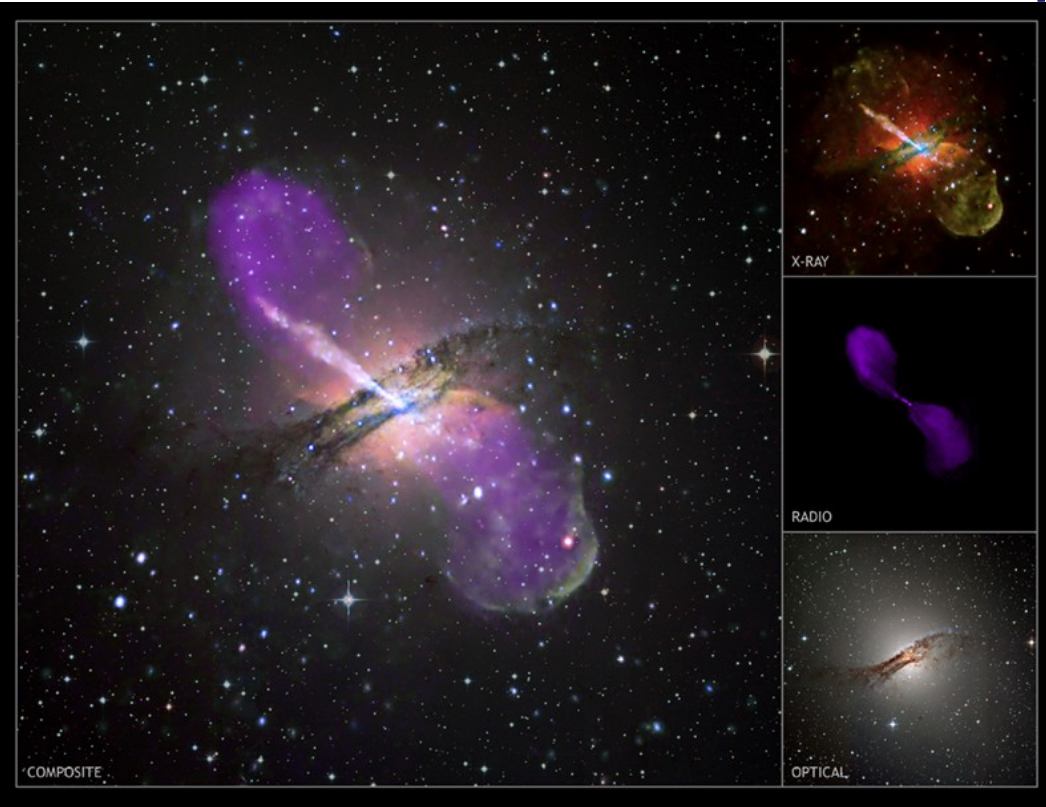
the blazar Mrk 421  
(Sloan Digital Sky Survey)



the blazar 3C 279

Credit: J.Y. Kim (MPIfR), Boston University Blazar Program (VLBA and GMVA), and the Event Horizon Telescope Collaboration

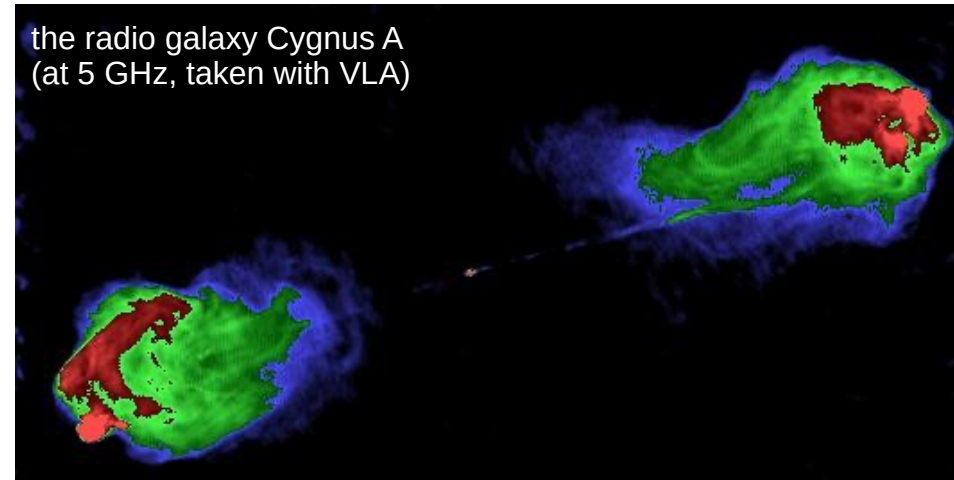
# a few specimen



the radio galaxy M87  
(NASA and The Hubble  
Heritage Team  
(STScI/AURA) )



the radio galaxy Cygnus A  
(at 5 GHz, taken with VLA)



the radio galaxy Centaurus A  
(Credit: X-ray: NASA/CXC/CfA/R.Kraft et al; Radio:  
NSF/VLA/Univ.Hertfordshire/M.Hardcastle; Optical:  
ESO/WFI/M.Rejkuba et al.)

# host galaxies of AGNs

---

To trigger accretion onto the SMBH, disturbances of the gravitational potential (through interactions with other galaxies) seem necessary for the gas to overcome the angular momentum barrier and approach the central region.

Both spiral and elliptical galaxies can host AGNs. Much is still unknown on the host galaxies of different AGN classes.

It seems that

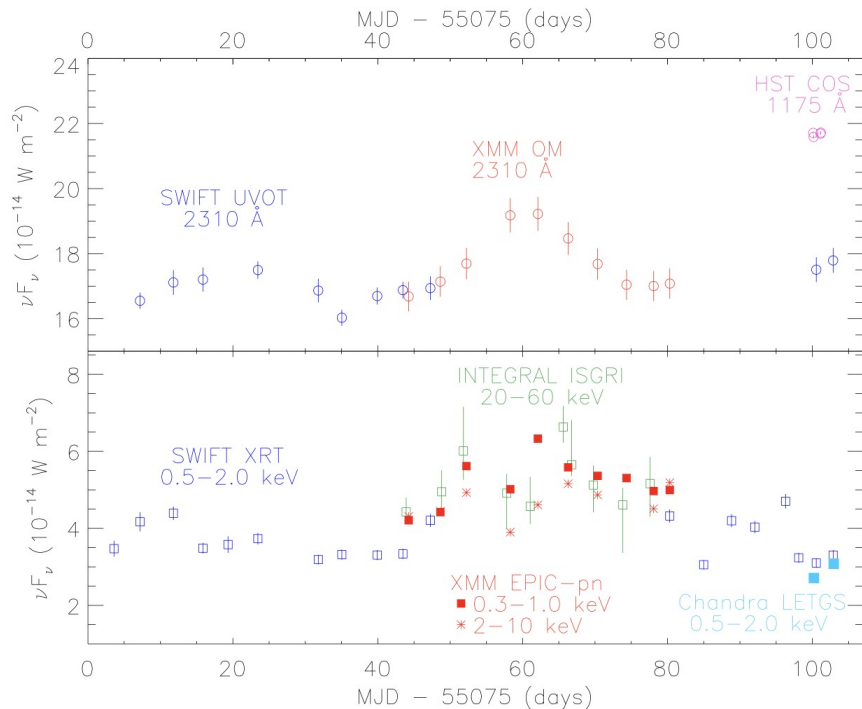
- Most Seyfert galaxies are spiral galaxies.
- Blazars are usually found in elliptical host galaxies.

**Feedback** between AGNs and their host galaxies is a very active field of research (which we will not go into here...).

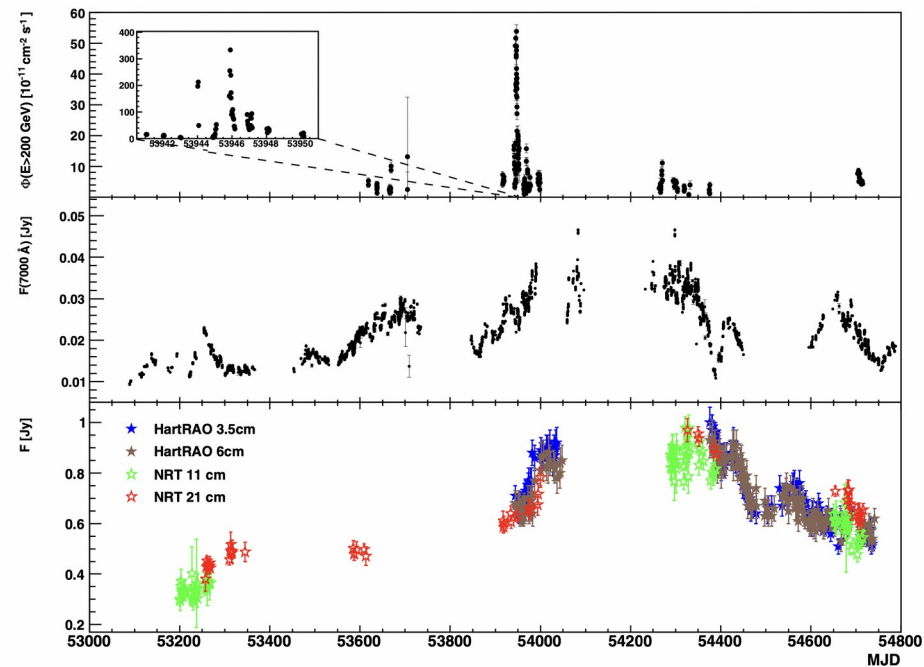
# AGN variability

Radio-loud and radio-quiet AGNs have shown **variability at all wavelengths**.

Variations are generally aperiodic (except for some cases of quasi-periodic oscillations) and have variable amplitude. The most rapid variability is observed at the shortest wavelengths.



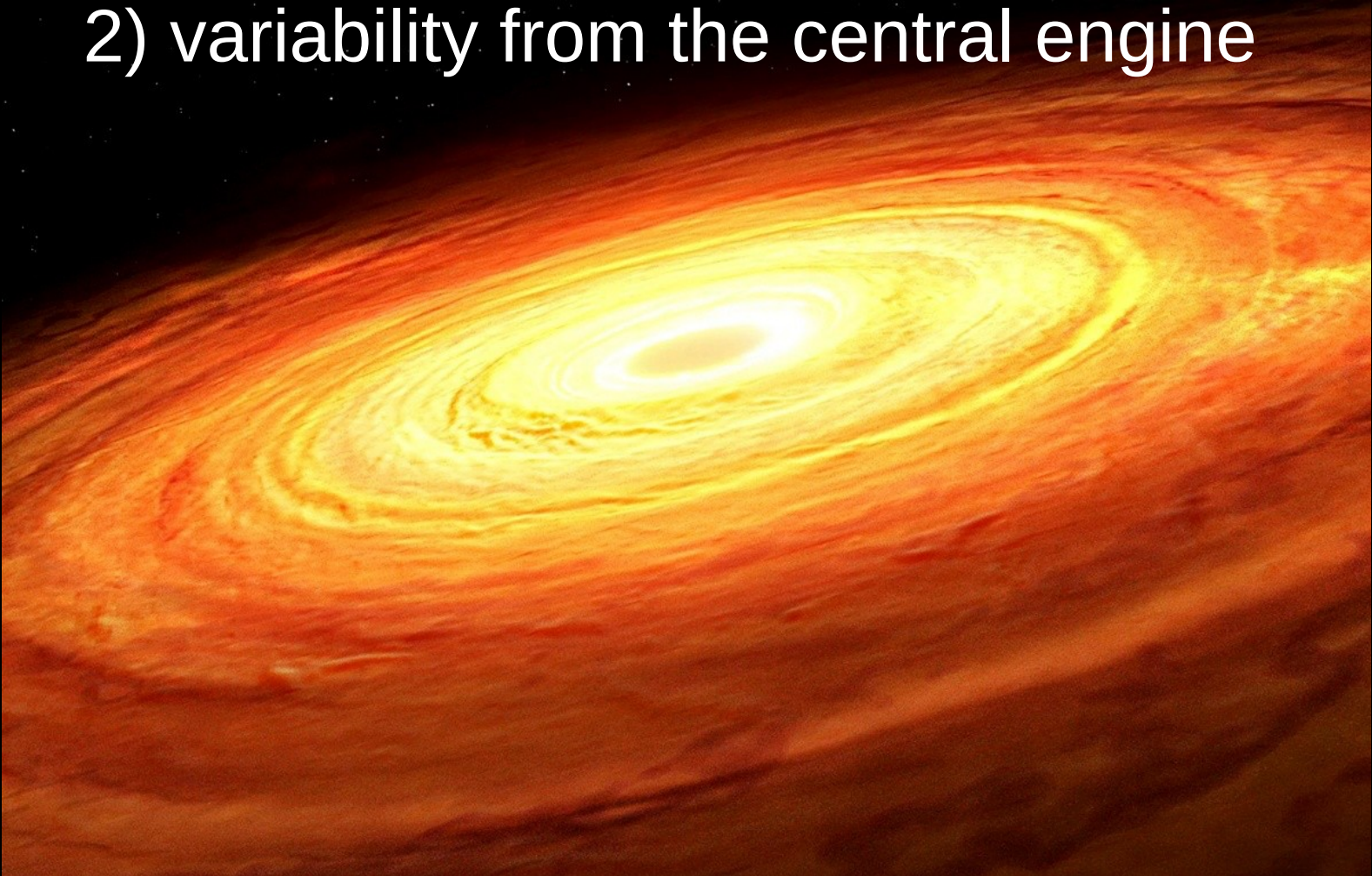
UV and X-ray light curves of the **Seyfert 1** galaxy Mrk 509 (Kaastra et al. 2011)



VHE, optical and radio light curves of the **blazar** PKS 2155-304 (HESS Collaboration 2012)



## 2) variability from the central engine



*An artist's impression of an accretion disk rotating around an unseen supermassive black hole. Credit: Mark A. Garlick/Simons Foundation*

# general characteristics of variability

## 1. linear relationship between flux and rms variability found in X-rays

→ variations on different time-scales are coupled

## 2. flux distributions are **lognormal**

→ flux variations are result of a multiplicative, rather than additive, process

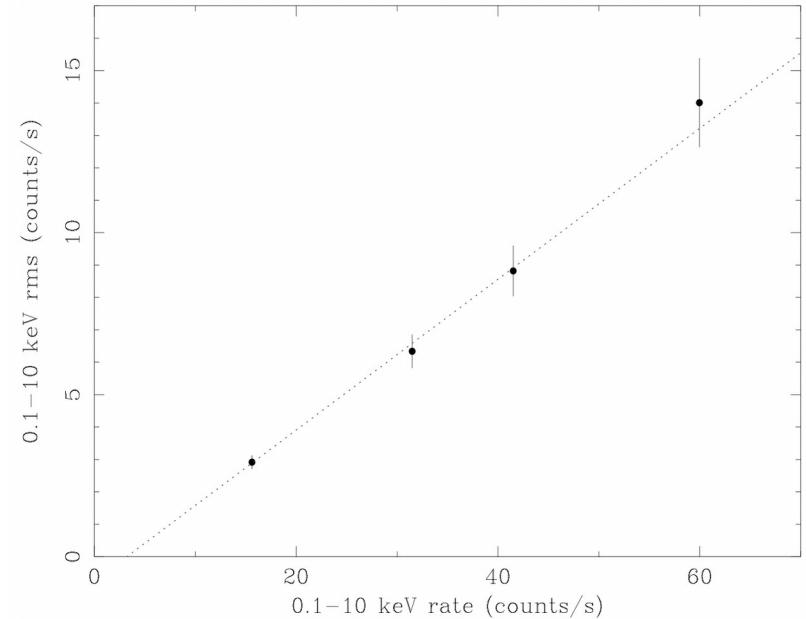
*Flux – rms relationship is actually a consequence of lognormal flux :*

*If the flux  $\Phi = f(x)$  function of a normally distributed quantity  $x$ , then a log-normal flux follows  $\Phi = f(x) = e^x$  .*

*Its variance is  $(\delta \Phi)^2 = \left(\frac{\partial f}{\partial x}(x_0)\right)^2 \delta x^2$  .*

*Thus the rms  $\delta \Phi \propto \Phi \Leftrightarrow f(x_0)^2 \propto (\delta \Phi)^2$  .*

*This is a known characteristic of  $e^x$  !*



**Right Panel rms-flux relationship for NGC4051 [17]**

*McHardy 2008*

# general characteristics of variability

- X-ray variability is a **red-noise or pink-noise process**, i.e.  $P(\nu) \propto \nu^{-\alpha}$  with  $\alpha \sim 1$
- power-spectrum density steepens above a particular frequency  $\nu_B = 1/T_B$ , where  $T_B \propto M_{BH}/\dot{m}$  (accretion rate is in Eddington units)
  - characteristic timescales scale with BH mass and inverse to accretion rate
  - origin in **variations of the accretion rate in the disc, propagating inwards and modulating X-ray emission**

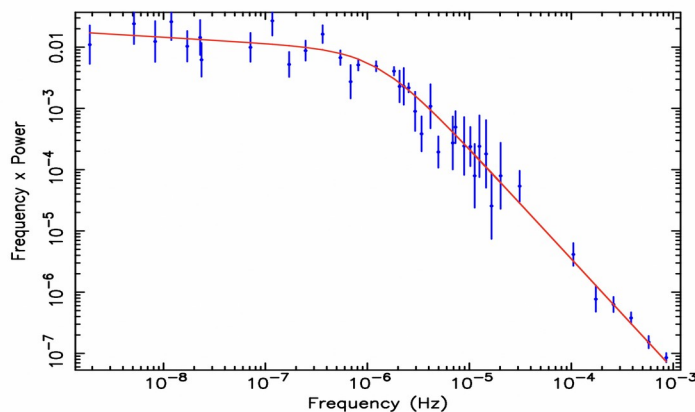
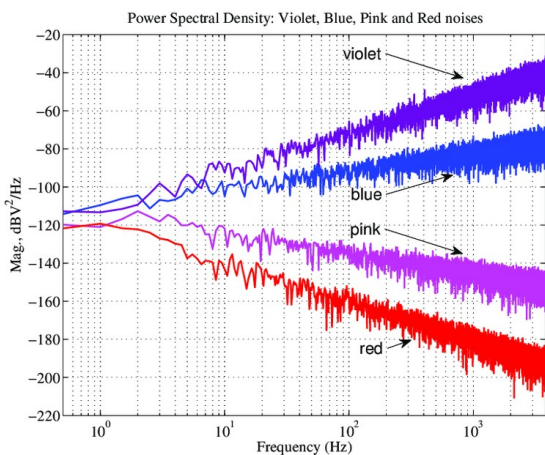
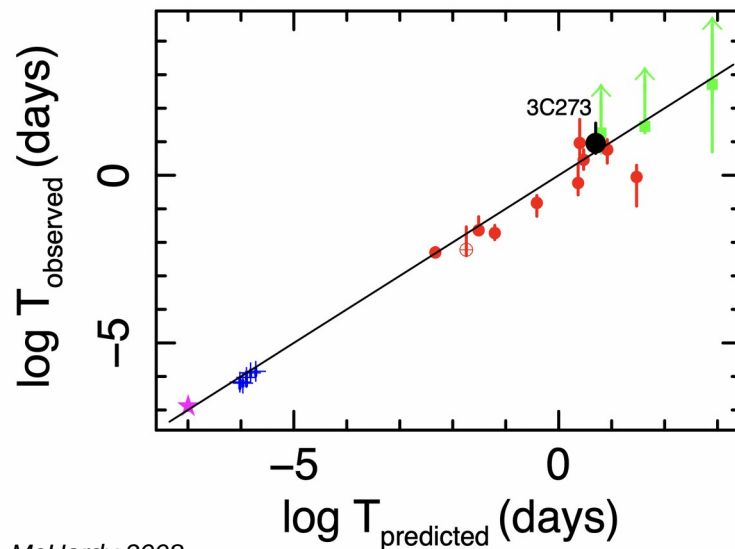


**Figure 6:** PSD of 3C273, derived from observations by *RXTE EXOSAT*, and many previous unfolded from the observational sampling pattern.



McHardy 2008

Santos et al. 2019

# time lags

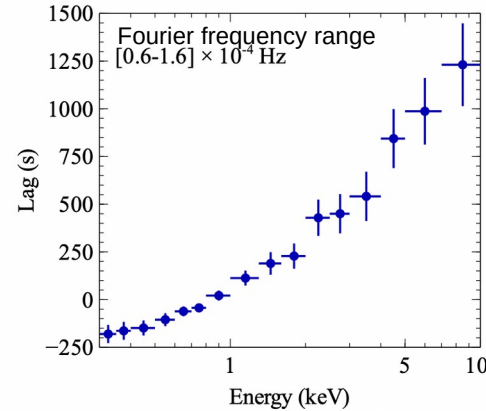
These inward propagating fluctuations in mass accretion rate can cause **time lags** in the X-ray continuum emission

(Lyubarskii 1997, Kotov et al. 2001, Arévalo & Uttley 2006, Ingram & Done 2011, Ingram & van der Klis 2013, Mushtukov et al. 2018).

In an extended corona, **hard lags** (high energies arrive later) are caused by:

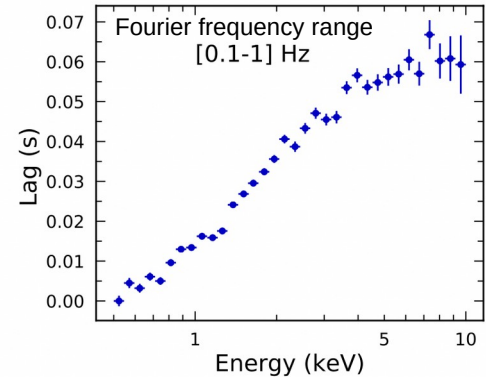
- accretion rate fluctuations first propagating through the cooler outer region of the corona (with a softer spectrum, i.e. dominated by lower energies)
- then, after a viscous propagation time, through the hotter inner region (with a harder spectrum).

AGN (Mass  $\sim 6 - 25$  million  $M_{\odot}$ ): Ark 564



similar time lags are found in AGNs and in X-ray Binaries

→ indicates similar mechanism



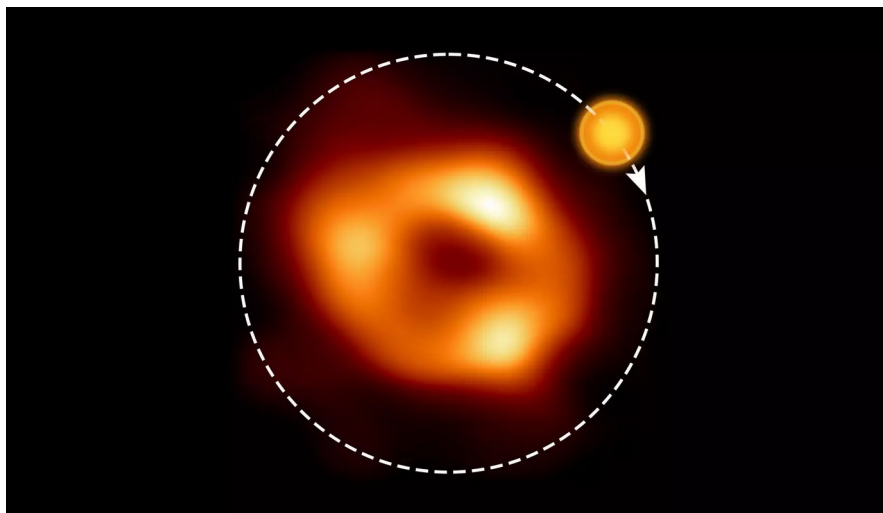
XRB (Mass  $\sim 7-8 M_{\odot}$ ): MAXI J1820+070

C. Bambi et al. 2021

# very rapid variability : Sgr A\* flares

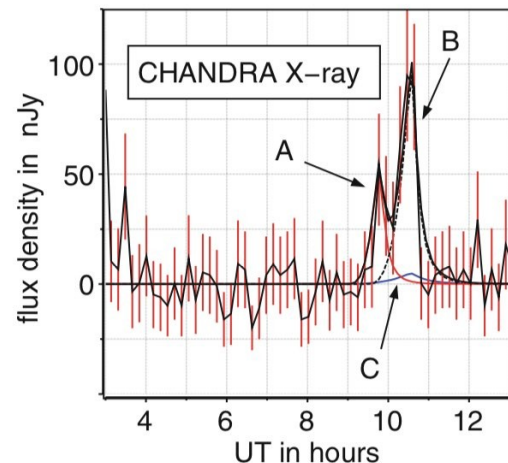
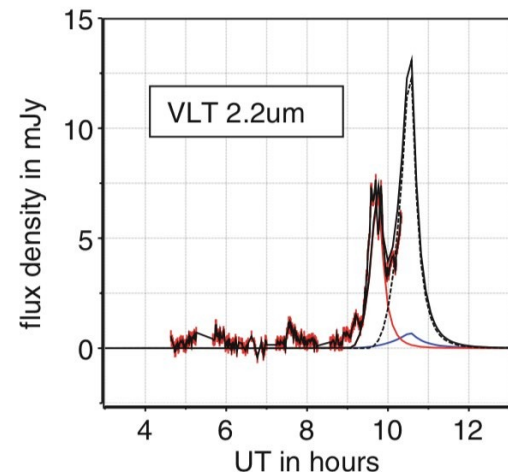
Very rapid flares, with durations of the hour scale and variability on **time-scales of several minutes**, were first observed from the direction of SgrA\* in X-rays, then in the IR and radio band as well. Such flares are frequent and occur ~once a day in X-rays.

The data from GRAVITY and ALMA both suggest the flares originate in a clump of gas (“hot spot”) orbiting the black hole at about 0.3 c in ~70 min. Magnetic reconnection is thought to be responsible for the flare emission.



© EHT-Kollaboration, ESO/M. Kornmesser (Acknowledgment: M. Wielgus)

<https://www.mpg.de/19276597/gas-bubble-sagittarius-a>



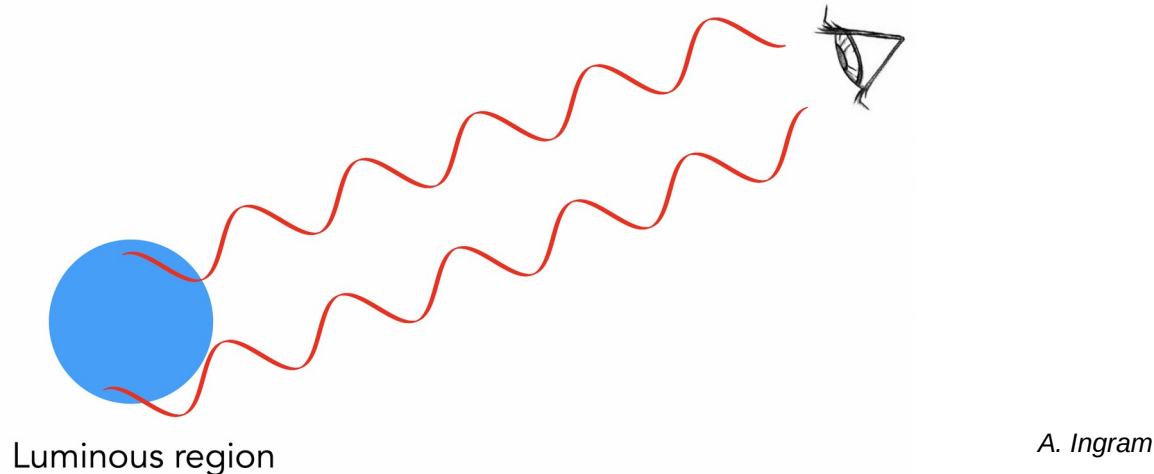
P. Schneider 2015

# rapid variability = compact emission region

Detection of rapid variability in quasars constrained the size of the emission region through the light travel time (or source coherence / causality) argument :

For a source to vary coherently in flux, the emission region must be causally connected, which implies a maximum size of  $R \leq c t_{\text{var}}$  for a typical variability time scale  $t_{\text{var}}$ . If this was not the case, stochastic variations from different source regions would average out.

→ Observation of day-scale variations in the optical band led to size constraints of a light day ( $\sim 3 \times 10^{15}$  cm) for the quasar emission region.



*A. Ingram*

# variability time scales connected to the central engine

**crossing time** of the X-ray emitting region :

$$t_{cross} = 0.011 M_7 \left( \frac{r}{10 R_{grav}} \right) \text{ days}$$

with a minimum given by the **BH size scale**:

$$t_{cross, min} = \frac{R_{grav}}{c}$$

**orbital period** :

$$t_{orbital} = 0.33 M_7 \left( \frac{r}{10 R_{grav}} \right)^{\frac{3}{2}} \text{ days}$$

duration of the development of **thermal instabilities** in the disk :

$$t_{thermal} = 5.3 \left( \frac{0.01}{\alpha} \right) M_7 \left( \frac{r}{10 R_{grav}} \right)^{\frac{3}{2}} \text{ days}$$

with  $\alpha$  the viscosity parameter

disk crossing time for **mechanical instabilities** :

$$t_{sound} = 33 \left( \frac{r}{100 H} \right) M_7 \left( \frac{r}{10 R_{grav}} \right)^{\frac{3}{2}} \text{ days}$$

with H the disk thickness

time scale for propagation of variations in the **accretion rate** through the disk :

$$t_{drift} = 53000 \left( \frac{r}{100 H} \right)^2 \left( \frac{0.01}{\alpha} \right) M_7 \left( \frac{r}{10 R_{grav}} \right)^{\frac{3}{2}} \text{ days}$$

Edelson R., & Nandra K.,  
ApJ, 514, 682, 1999.

# variability through absorption

Several observations of rapidly changing X-ray fluxes are attributed to **obscuration** of a central compact X-ray source through fast BLR clouds orbiting the SMBH.

A close analysis of the light curves and spectra concludes that the shape of the clouds is “cometary”, with a long tail of decreasing density.

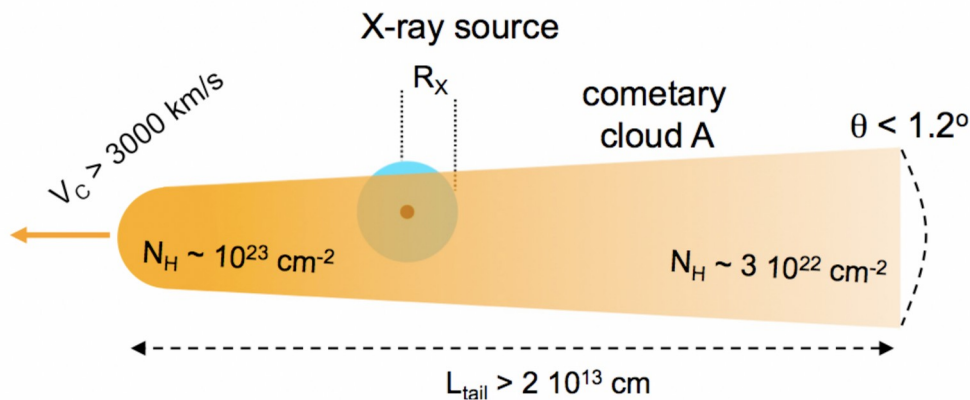
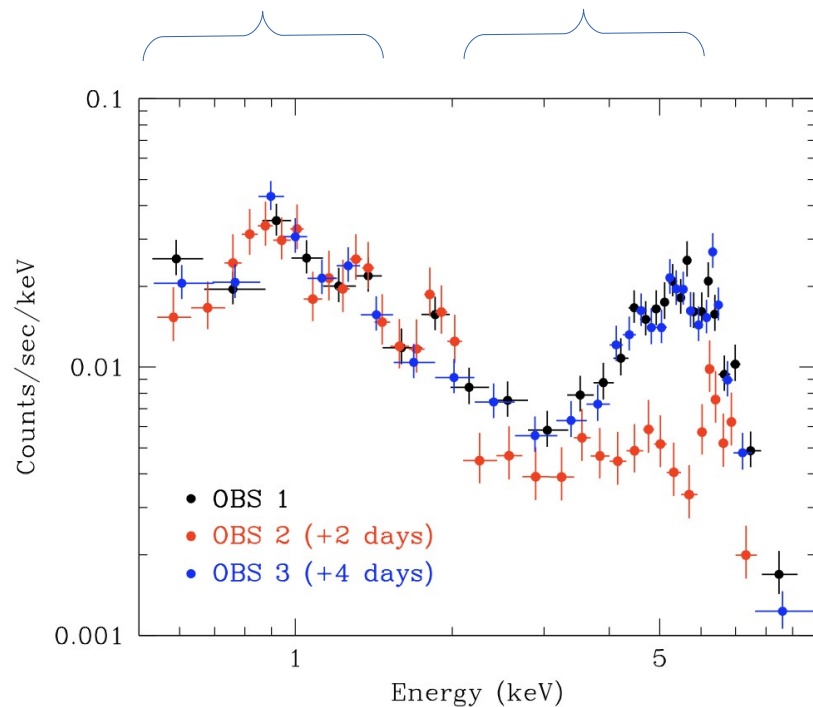


**Figure 2:** Structure of the absorbing cloud as obtained from a Suzaku observation of NGC 1365. The estimates are based on the hypothesis of Keplerian motion, and on a black hole mass of  $2 \times 10^6 M_\odot$  [45]. The cloud size is not in the correct scale: the tail is much longer when compared with the source size, which is of the order of a few  $10^{11}$  cm.

(Maiolino et al. 2010)

**soft thermal component :**  
hot plasma in star forming region + NLR + point sources (X-ray binaries...)

**non-thermal component :**  
mostly power-law emission from the corona

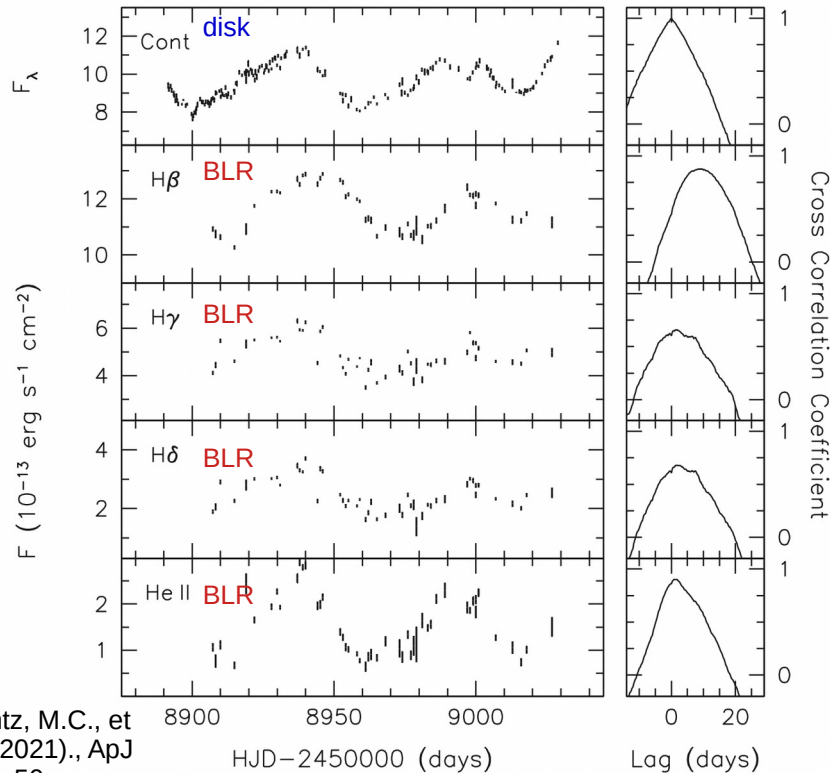


Spectra of the Seyfert galaxy NGC 1365, showing X-ray occultations due to BLR clouds (data from Chandra) (Bianchi et al. 2012)

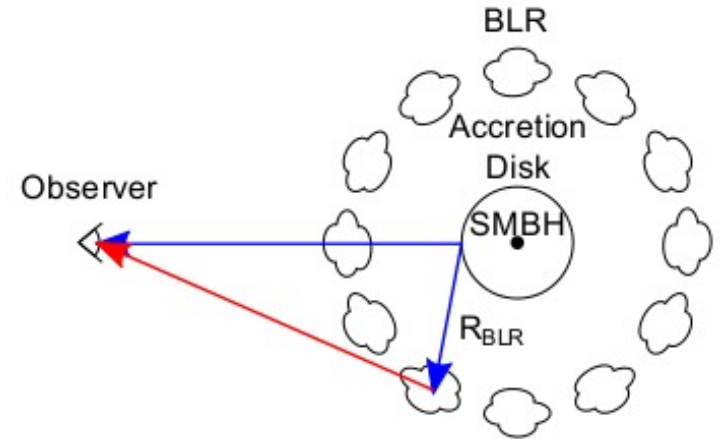


# reverberation mapping

In **reverberation mapping**, variations of the continuum emission from the central engine are compared to echoes in the line emission. The time delay between the two (due to the light travel time  $\Delta t \sim r/c$ ) provides information on the geometry of the BLR.



Bentz, M.C., et al. (2021), ApJ 906, 50.



<https://london.physics.ucdavis.edu/~reu/REU16/projects16.html>

Time lags are determined with **cross correlation functions** :

$$\text{CCF}(\tau) = \int_{-\infty}^{+\infty} L(t) C(t-\tau) dt$$

CCF provides the correlation coefficient (0 – 1) for a lag  $\tau$ . C and L are the light curves of the continuous (= disk) emission and the line (= BLR) emission.

# reverberation mapping

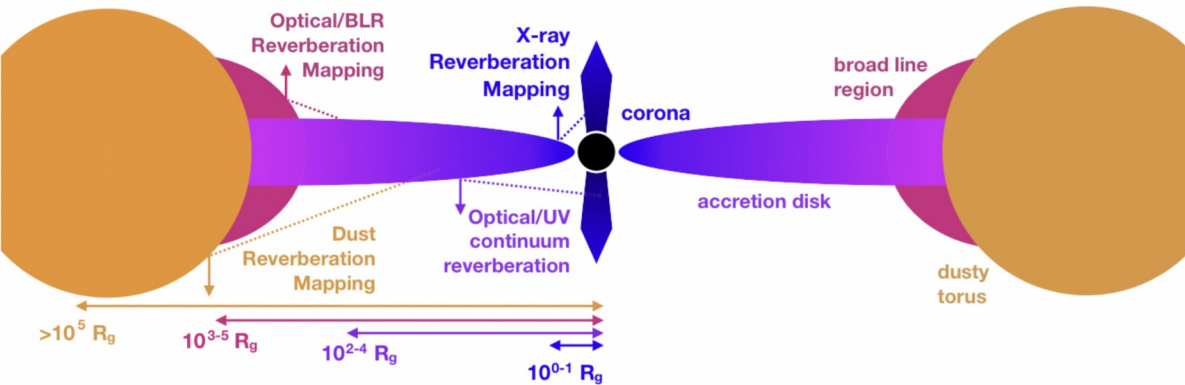
r.m. is also applied for the most precise measurements of the **BH mass**:  $M_{BH} = f r \sigma^2 / G$

The distance  $r$  for a given atomic line is determined with r.m.

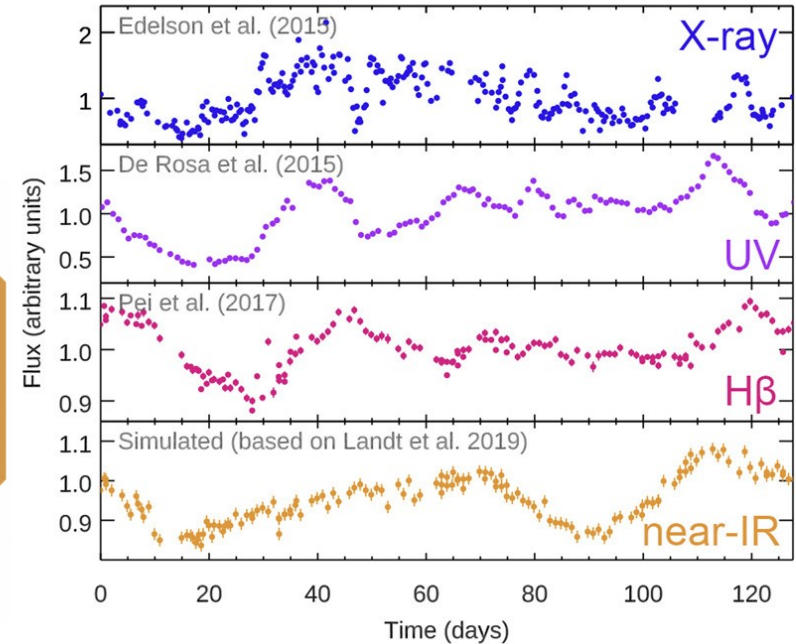
The gas velocity dispersion is deduced from its width ( $\sigma = c \Delta \lambda / \lambda$ ).

The geometric correction factor  $f$  accounts for departures from circular orbits seen edge-on.

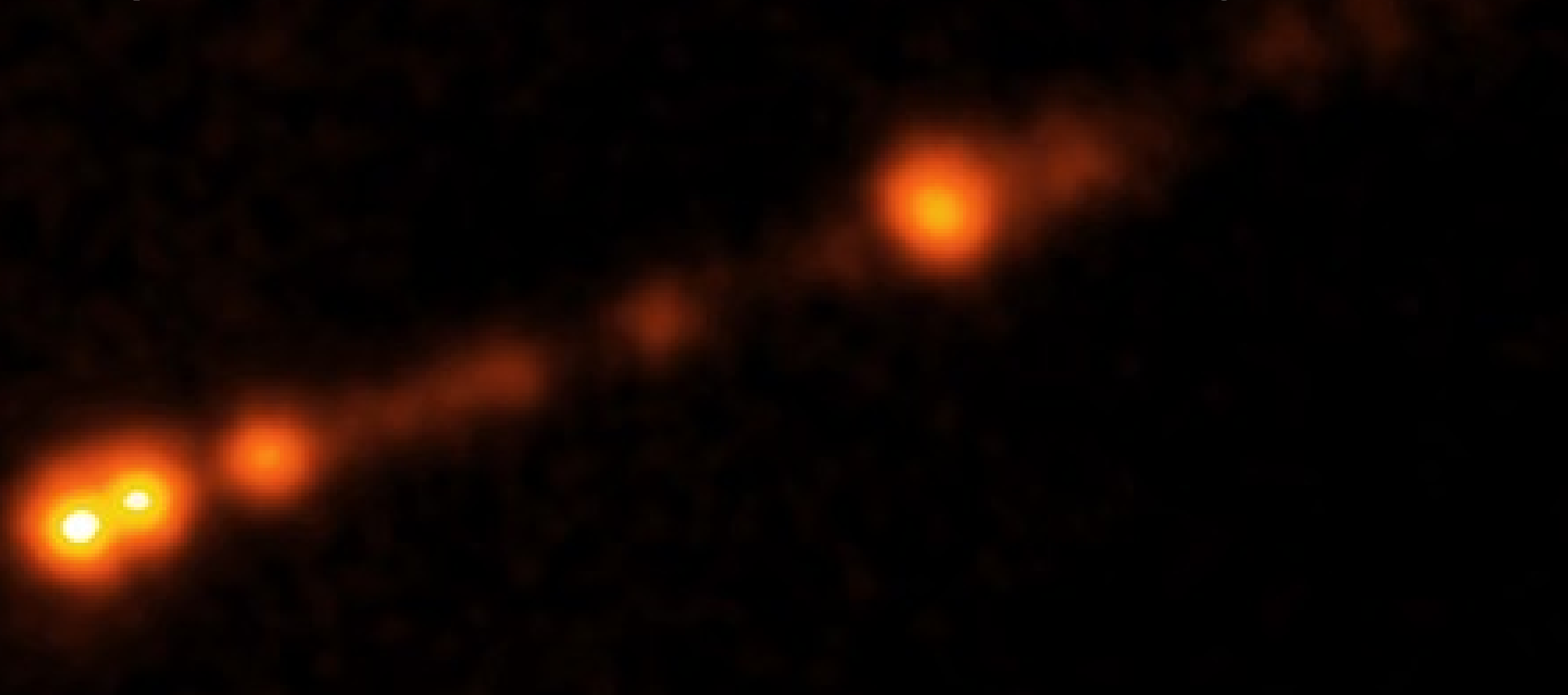
The principle of r.m. can also be applied to other regions of the AGN by observing delays in different wavelength bands.



E.M. Cackett et al. 2021



### 3) emission from blazars and radio-galaxies



# broad-band jet emission : steady-jet model

The steady-jet model by *Blandford & Königl (1979)* explains the observed flat emission spectrum ( in spectral flux density  $F_\nu$  [ $\text{erg s}^{-1} \text{cm}^{-2} \text{Hz}^{-1}$ ] ) through the **sum of synchrotron emission spectra** from a non-thermal electron plasma follow adiabatic expansion, leading to a conical jet.

Magnetic field strength and electron density decrease along the jet.

The lower region of the jet is **optically thick** to radiation of all frequencies. In the middle region, the jet becomes optically thin to radiation of progressively lower frequencies.

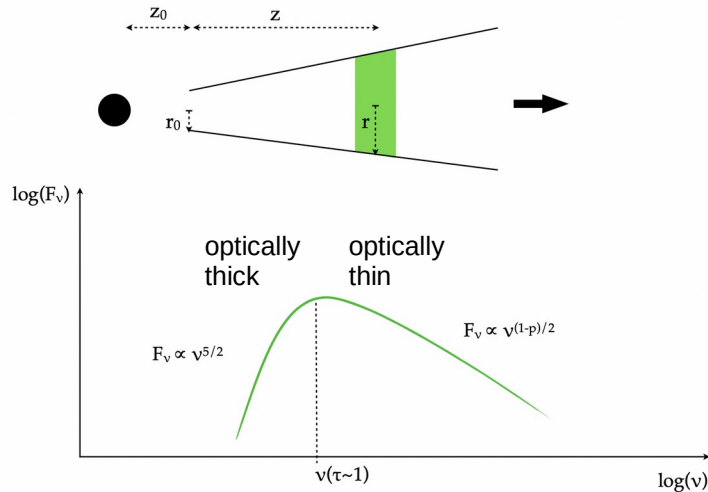


FIGURE 1.9 – Densité spectrale d'énergie d'une couche de jet de rayon  $r$  située à une distance  $z$  de la base.

M. Péault, PhD thesis 2019

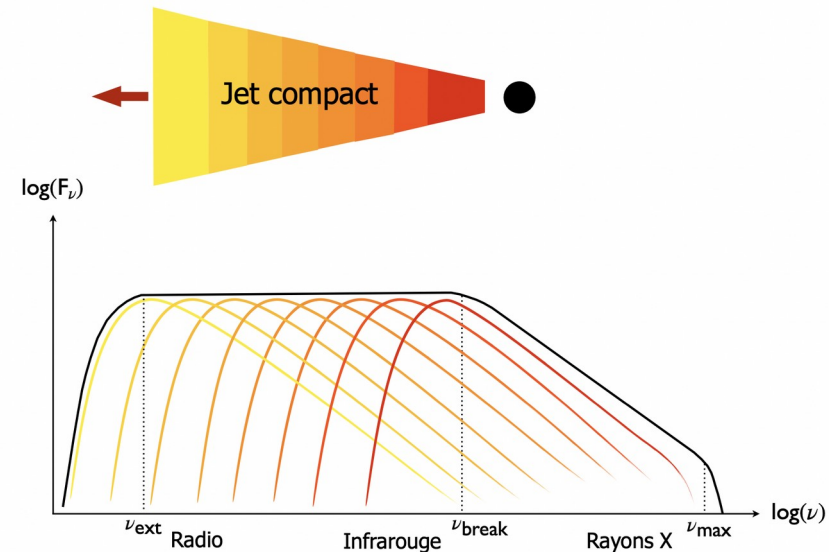
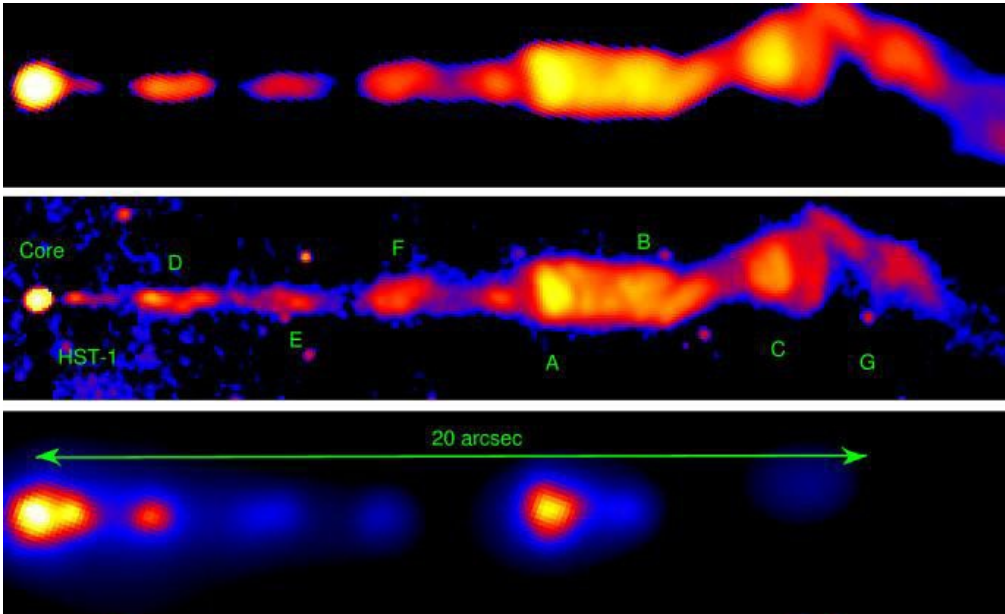
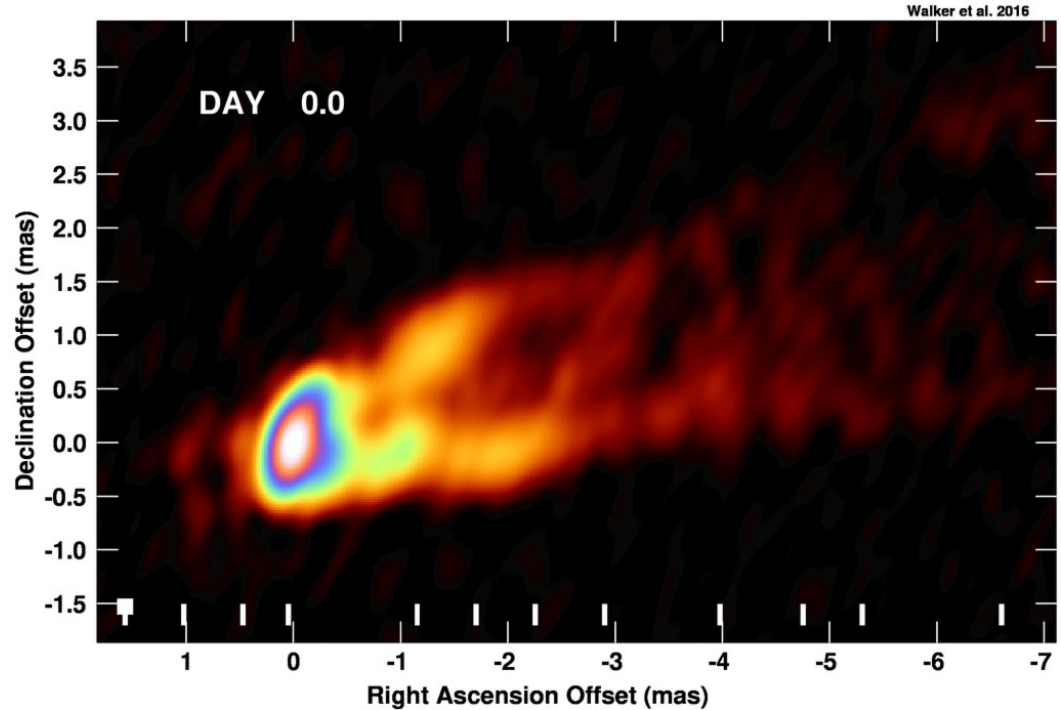


FIGURE 1.10 – Spectre d'émission du jet d'après le modèle de Blandford et Königl.

# broad-band jet emission : observations



Multi-wavelength view of the M87 jet. From top to bottom:  
radio (VLA), optical (HST), and X-ray (Chandra)  
(Marshall et al. 2002)



VLBI images of the M87 radio core  
(Walker et al. 2016)

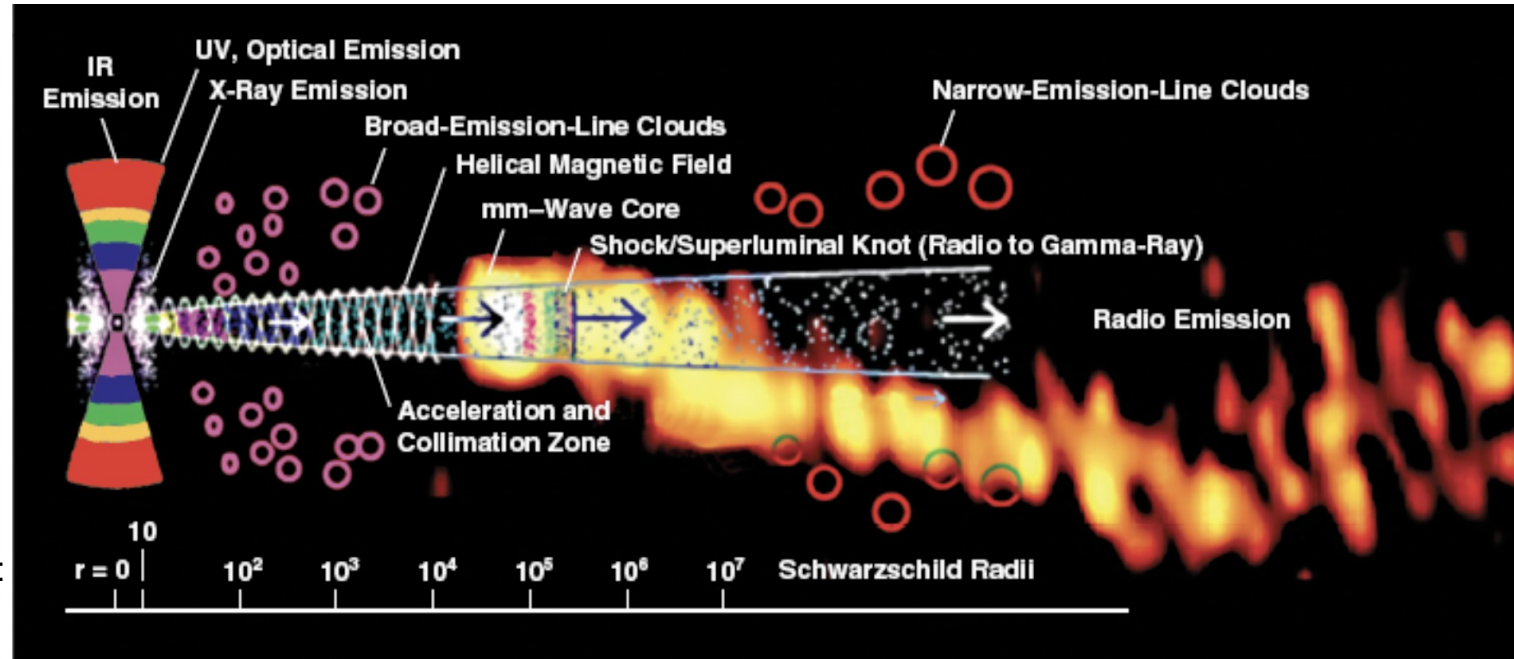
Jets from AGN are not homogeneous :

- standing and moving “knots” are seen from radio to X-ray bands
- some “knots” have superluminal velocities

# broad-band jet emission : the current picture

Overlay of a 3 mm radio image of the blazar 3C454.3 (Krichbaum, et al. 1999) on a diagram of a quasar from Marscher et al. (2008), not to scale.

A. E. Wehrle 2009



current standard picture of the inner jet (A. Marscher 2008), derived from VLBI and polarisation measurements :

- acceleration/collimation region with helical magnetic field and spiral streamlines  
→ emission region of high-energy emission ?
- conical standing shock (= recollimation shock?) is identified as the mm-wave core (VLBI core), from which superluminal knots are seen to detach. This conical shock is preceded by a region where the plasma is turbulent
- the position of the radio core does not coincide with the base of the jet, but is shifted due to frequency-dependent self-absorption (“core shift”)

# broad-band jet emission : observations

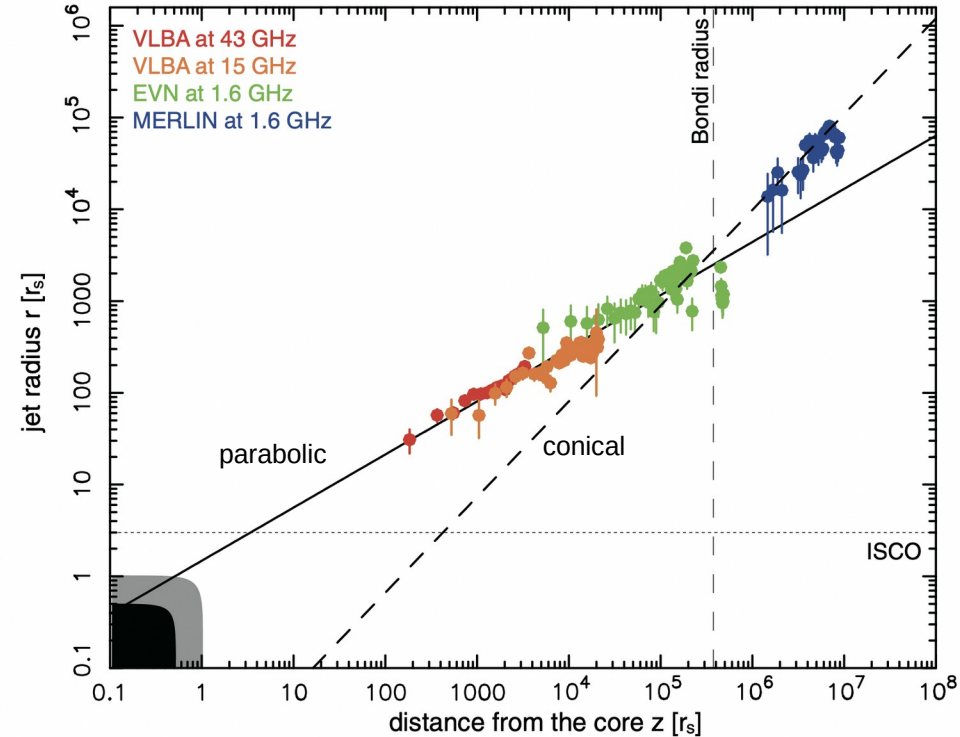
VLBI data from several sources show a **transition from a parabolic to a conical jet at  $\sim 10^5 - 10^6 r_s$** .

→ expected if ambient medium is governed by Bondi accretion (*Y.Y. Kovalev et al. 2020*).

→ in the transition region, the bulk plasma kinetic energy flux seems to become equal to the Poynting energy flux (acceleration saturates)

Often, **standing “knots”** are found in the transition region.

→ a recollimation shock or a shock caused by change in the ambient pressure ?



Jet profile of M87 from VLBI data  
*Asada & Nakamura 2012*

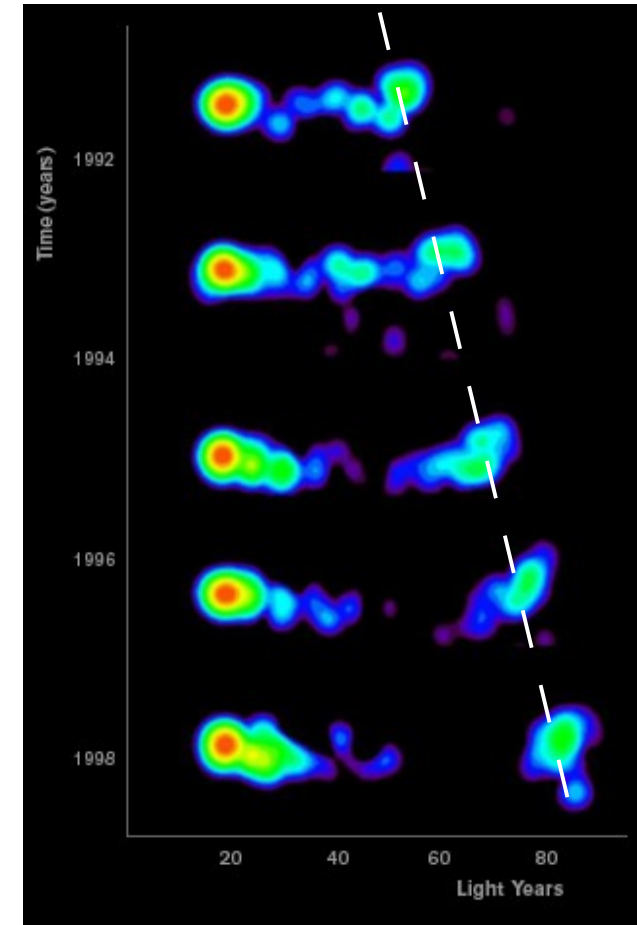
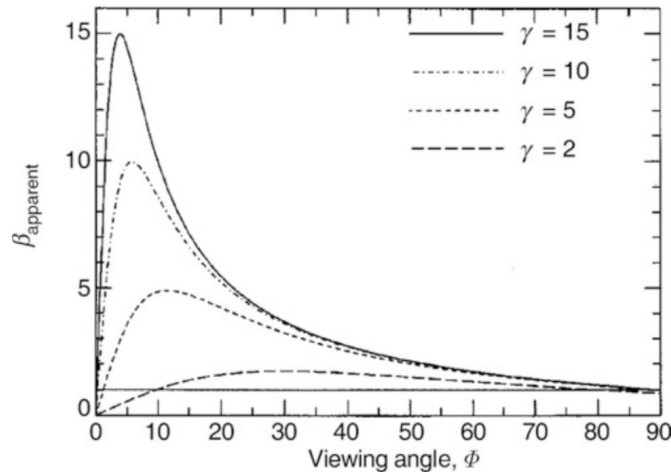
# superluminal motion

Apparent superluminal motion of components observed in some AGN with very long baseline interferometry (VLBI) helped identify the existence of relativistic jets.

The apparent movement of components with  $v_{app} > c$  (sometimes  $v_{app} = 6c$  or more !), is caused by the projection of emission from a relativistic jet pointing in our direction on the celestial plane.

$$v_{app} = \frac{v \sin \phi}{1 - \beta \cos \phi}$$

with  $v = \beta c$  the real velocity of the component along the jet and  $\phi$  the viewing angle of the jet



<http://user.astro.columbia.edu/~jules/UN2002/superluminal.html>



# superluminal motion explained

Demonstration:

- A “radio knot” is emitted from the core A of the jet at  $t = 0$ . Its distance from the core at time  $t = t_e$  is  $v t_e$  (position B).

We only observe the movement projected onto the sky, i.e. its transverse component  $\Delta r = v t_e \sin \phi$  (from C to B).

- Photons emitted from the new position B will take slightly less time to reach the observer. For the observer, the time interval between the signal from the core and from the new position is :

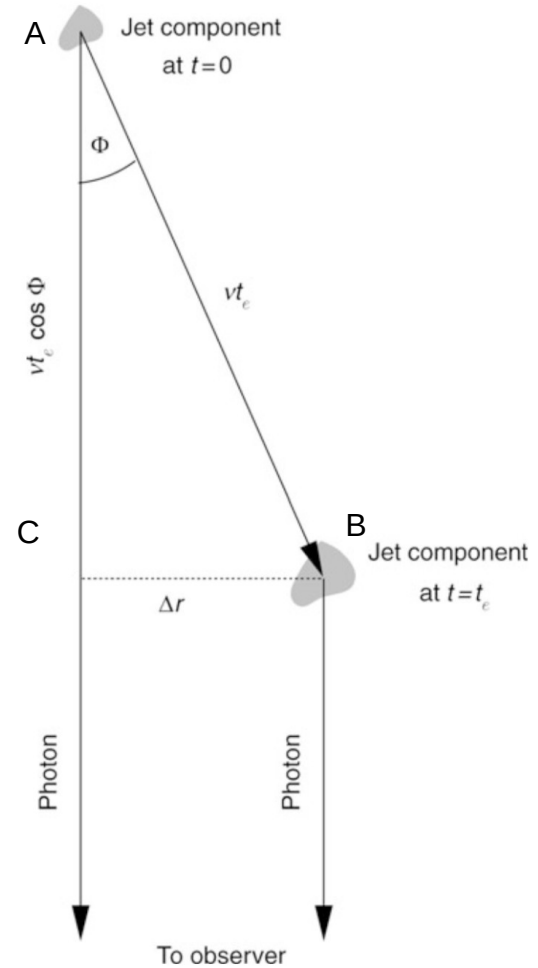
$$\Delta t = t_e - \frac{v t_e \cos \phi}{c} = t_e (1 - \beta \cos \phi)$$

- with  $v_{app} = \frac{\Delta r}{\Delta t}$  one obtains the above equation for  $v_{app}$ .

- For a given  $v$ , the maximum value of  $v_{app}$  is achieved if

$$\sin \phi = 1/\gamma \quad \text{with the Lorentz factor} \quad \gamma = \frac{1}{\sqrt{1-v^2/c^2}}$$

This leads to  $v_{app,max} = \gamma v$ .



# relativistic beaming

Emission from relativistic jets is subject to several relativistic effects :

- **Doppler effect:** Light emitted from a jet pointing at the observer under an angle  $\phi$  is blue-shifted

$$v_{obs} = \delta v_{em} \quad \text{by the Doppler factor} \quad \delta = \frac{1}{\gamma(1 - \beta \cos \phi)}$$

- **relativistic beaming** : Light emitted isotropically in the reference frame of the moving knot is emitted preferentially in the direction of movement of the plasma in the observer frame. This leads to an amplification (“Doppler boosting”) of the observed emission from the jet (and a de-amplification from the counter-jet).

The effect on the energy flux for an approaching jet is given by :  $I_{obs} = I_{em} \delta^4$

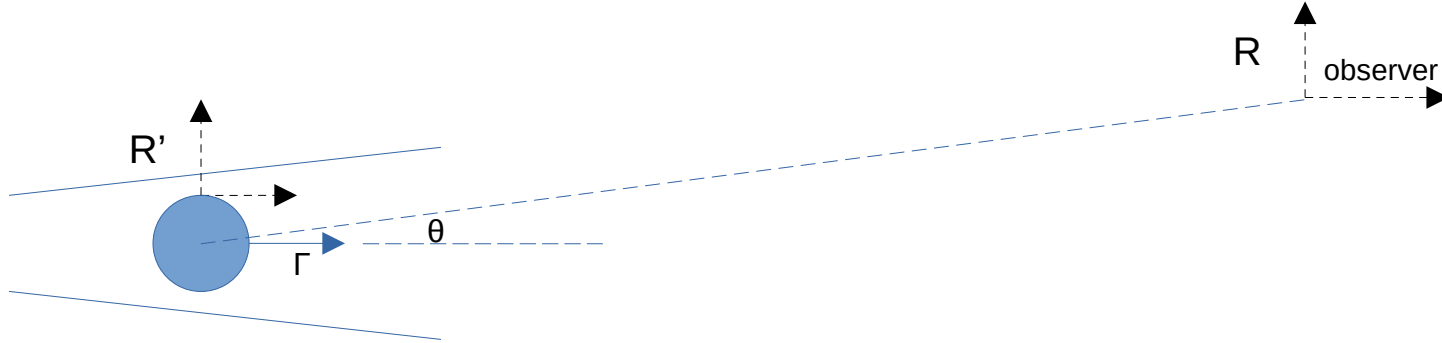
For typical Doppler factors of the order of 10, this leads to an amplification by a factor 10 000 !

The observed flux ratio of jet and counter-jet is :  $\frac{\Phi_+}{\Phi_-} = \left( \frac{1 + \beta \cos \phi}{1 - \beta \cos \phi} \right)^{2+\alpha}$

where  $\alpha$  is the spectral index of the emission for a power law  $S_\nu \propto \nu^{-\alpha}$

→ This explains why one often observes only a single jet.

# relativistic beaming explained



emitting region moving with Lorentz factor  $\Gamma = 1/\sqrt{1-\beta^2}$  along jet

- isotropic emission of light in comoving frame  $R'$

- emitted specific intensity  $I'_\nu(\nu')$

Doppler factor between  $R'$  and  $R$ :

$$\delta = \frac{1}{\Gamma(1-\beta \cos(\theta))}$$

observer frame  $R$  views jet axis under viewing angle  $\theta$

- observed specific intensity  $I_\nu(\nu)$

# relativistic beaming explained

---

Specific intensity is defined as  $I_\nu(\nu) = \frac{dE}{dt d\Omega dA d\nu}$  [ erg s<sup>-1</sup> cm<sup>-2</sup> sr<sup>-1</sup> Hz<sup>-1</sup> ] .

$I_\nu(\nu)/\nu^3 = I_{\nu'}(\nu')/\nu'^3$  is a Lorentz invariant ! (cf *Rybicki & Lightman* or consider the Planck distribution)

Thus :  $I_\nu(\nu) = I_{\nu'}(\nu') \left(\frac{\nu}{\nu'}\right)^3$  and  $\nu = \nu' \delta$

=>  $I_\nu(\nu) = I_{\nu'}(\nu') \delta^3$

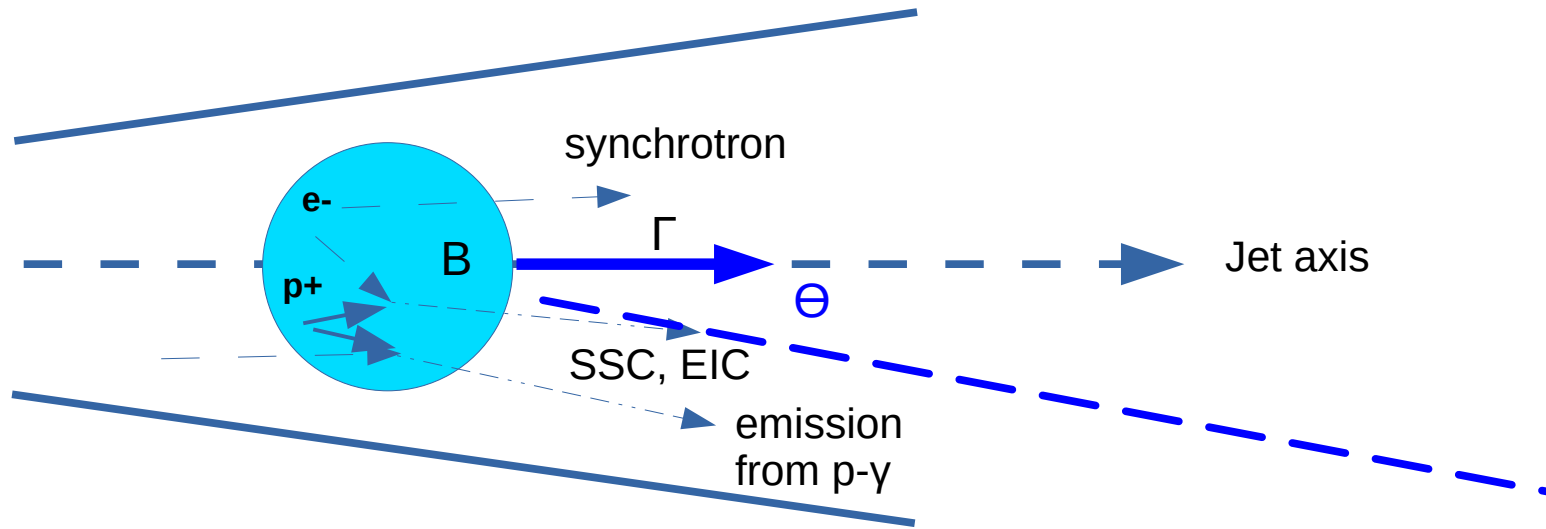
For the energy flux  $\frac{dE}{dt d\Omega dA}$  , this yields :  $\nu I_\nu(\nu) = \nu' I_{\nu'}(\nu') \delta^4$

If the specific intensity follows a power law :  $I_{\nu'}(\nu') = A (\nu')^{-\alpha} = A (\nu/\delta)^{-\alpha} = A \delta^\alpha (\nu)^{-\alpha}$

=>  $I_\nu(\nu) = \delta^{3+\alpha} I_{\nu'}(\nu')$

**attention:** The formulas above apply to emission from a discrete emission region inside the jet (“blob”). When describing the emission from the whole steady-state jet, the result changes, as discussed, for example, in the Appendix of *Sikora, M. et al. 1997*.

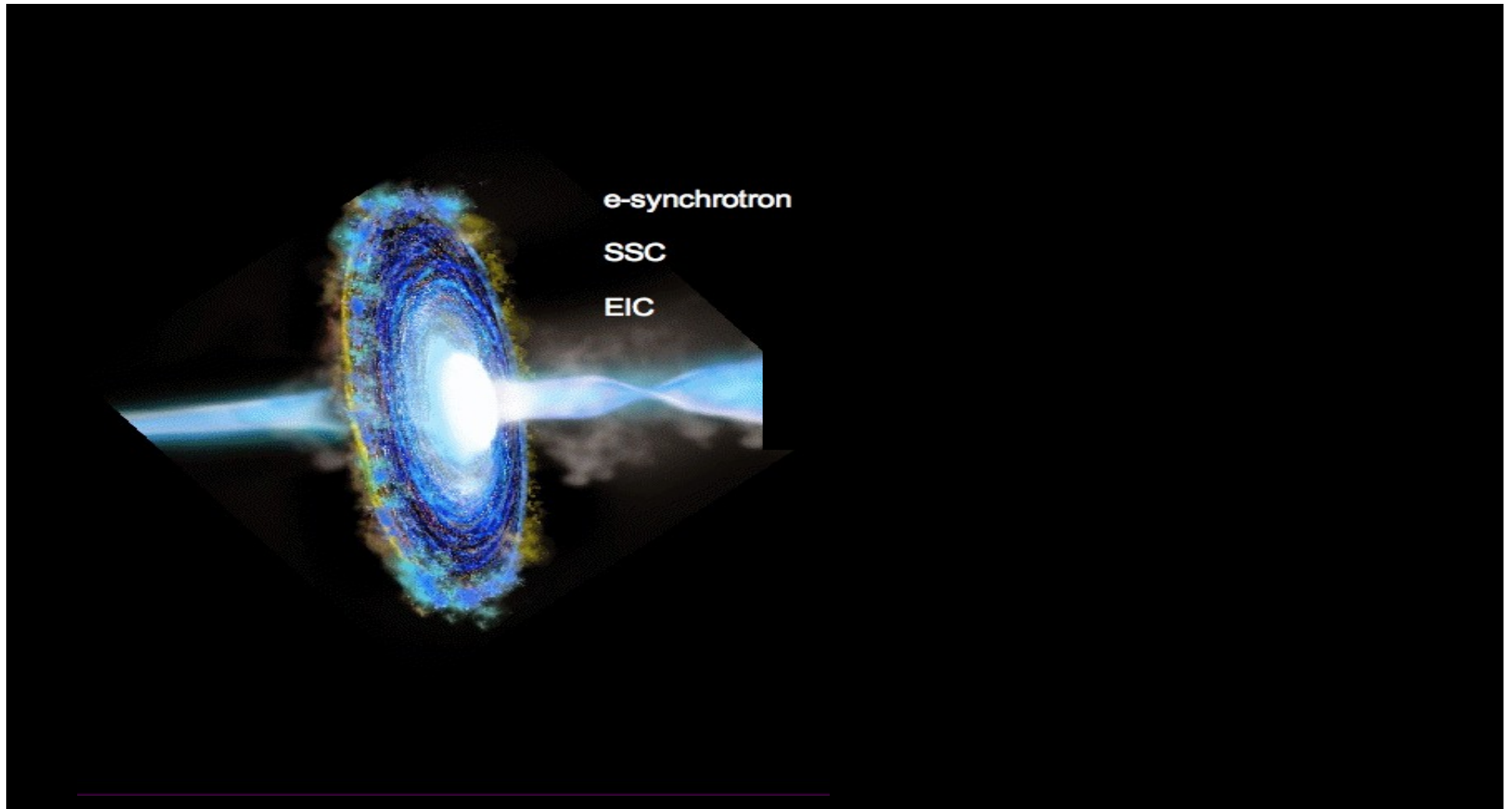
# blazar emission: one-zone models



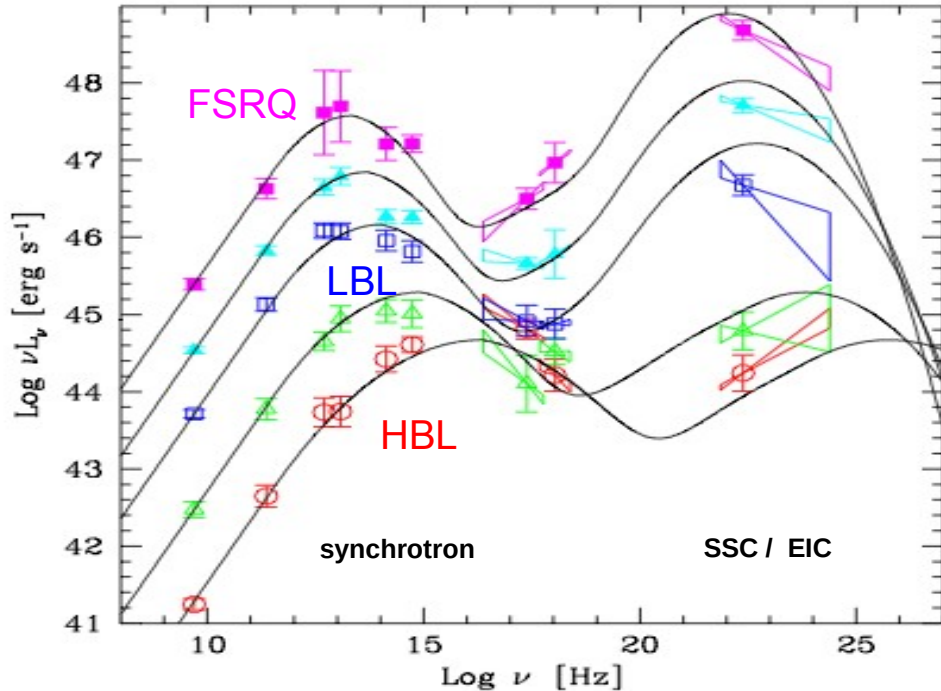
- plasma blob inside jet with turbulent magnetic field and high energy electrons / positrons (and protons)
- emission from radio to X-rays due to **synchrotron** radiation
- $\gamma$ -rays from **Synchrotron Self-Compton** or **External Inverse Compton** diffusion (on BLR or torus photons) or **interactions of protons** with magnetic or photon fields



# leptonic models

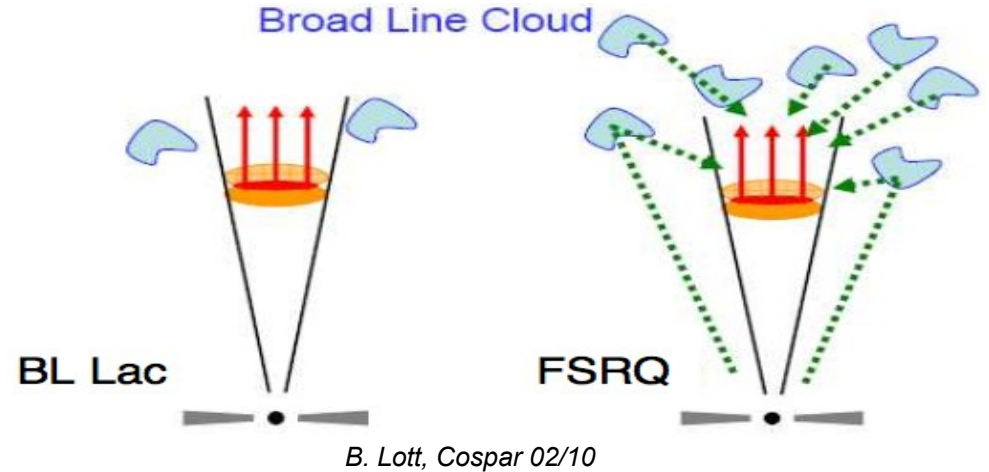


# blazar emission in the leptonic model



Donato et al. (2002), based on Fossati et al. (1998)

different blazar types : luminous FSRQs with high peaks in gamma band ↔ less luminous BL Lac objects with lower peaks in gamma band



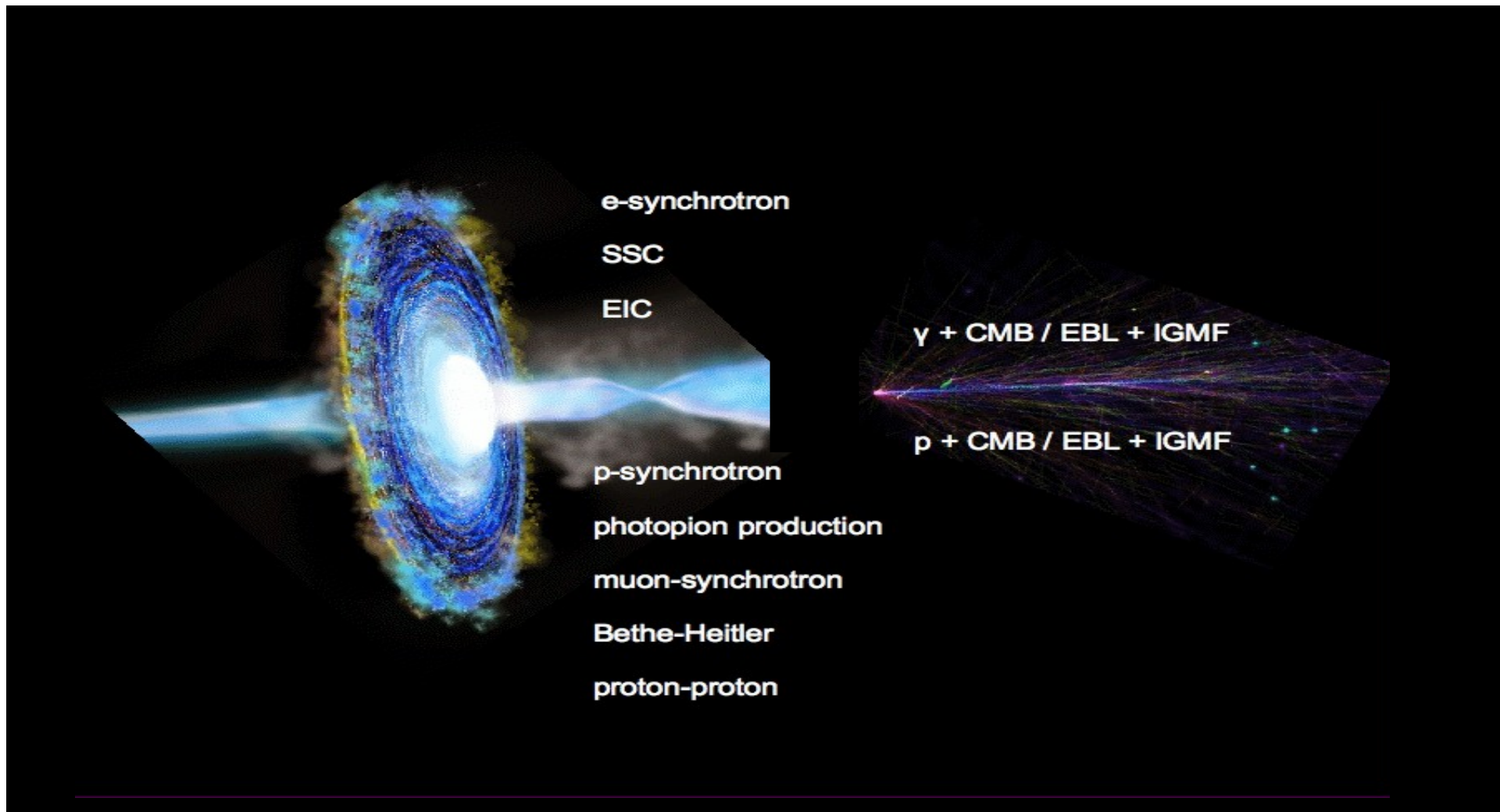
- Disk and Broad Line Region weak

-  $\gamma$ -rays due to Synchrotron Self Compton

- Disk and Broad Line Region strong

-  $\gamma$ -rays due to Synchrotron Self Compton & External Inverse Compton  
→ high Compton dominance

# lepto-hadronic models





# hadronic emission processes

---

## proton-synchrotron emission

$$p^+ + \vec{B} \rightarrow p^+ + \vec{B} + \gamma \quad (\text{for high energy peak, requires ultra-relativistic protons and } B \sim 10 - 100 \text{ G})$$

## proton-photon interactions

$$p^+ + \gamma \rightarrow p^+ + e^+ + e^- \quad (\text{Bethe-Heitler pair production})$$

$$p^+ + \gamma \rightarrow p^+ + \pi^0 \rightarrow p^+ + \gamma + \gamma \quad (\text{photo-pion production})$$

$$p^+ + \gamma \rightarrow n^0 + \pi^+ \rightarrow n^0 + \mu^+ + \nu_\mu \rightarrow n^0 + e^+ + \nu_\mu + \nu_e$$

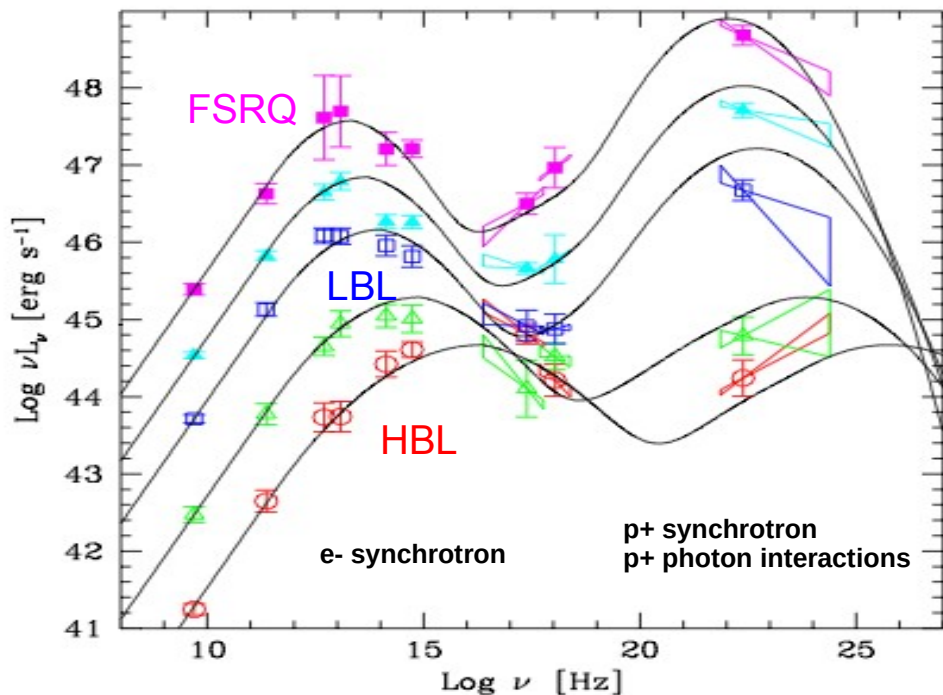
## synchrotron-pair cascades

leptons and gamma-rays produced in proton-photon interactions are at ultra-high energy and interact with photon field or B-field  
→ trigger cascades of synchrotron emission and pair production (or Inverse Compton emission and pair production)

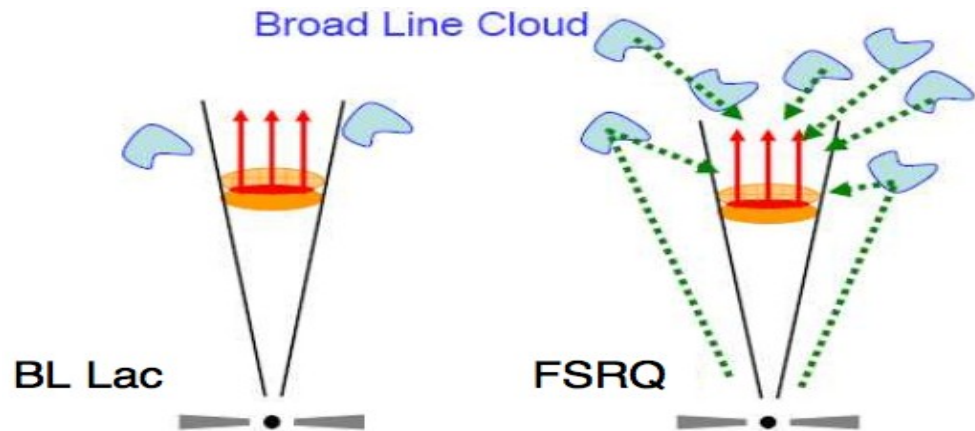
## proton-proton interactions

$$p^+ + p^+ \rightarrow p^+ + p^+ + \pi^0 + \pi^+ + \pi^- + \dots \quad (\text{only in very dense jets } \rightarrow \text{generally not applicable to blazar jets})$$

# blazar emission in the hadronic model



Donato et al. (2002), based on Fossati et al. (1998)



B. Lott, Cospar 02/10

- Disk and Broad Line Region weak

-  $\gamma$ -rays due to mostly proton synchrotron emission ?

- Disk and Broad Line Region strong

-  $\gamma$ -rays due to proton synchrotron and proton-photon emission ?

# leptonic vs. hadronic models

---

## leptonic models :

low B-fields ( $\sim 0.01-1$  G)

+ rapid variability

+ jet power  $\ll L_{\text{edd}}$

- description of “orphan” gamma-ray flares difficult

- no link with multi-messengers

## hadronic models:

high B-fields ( $\sim 1-100$  G)

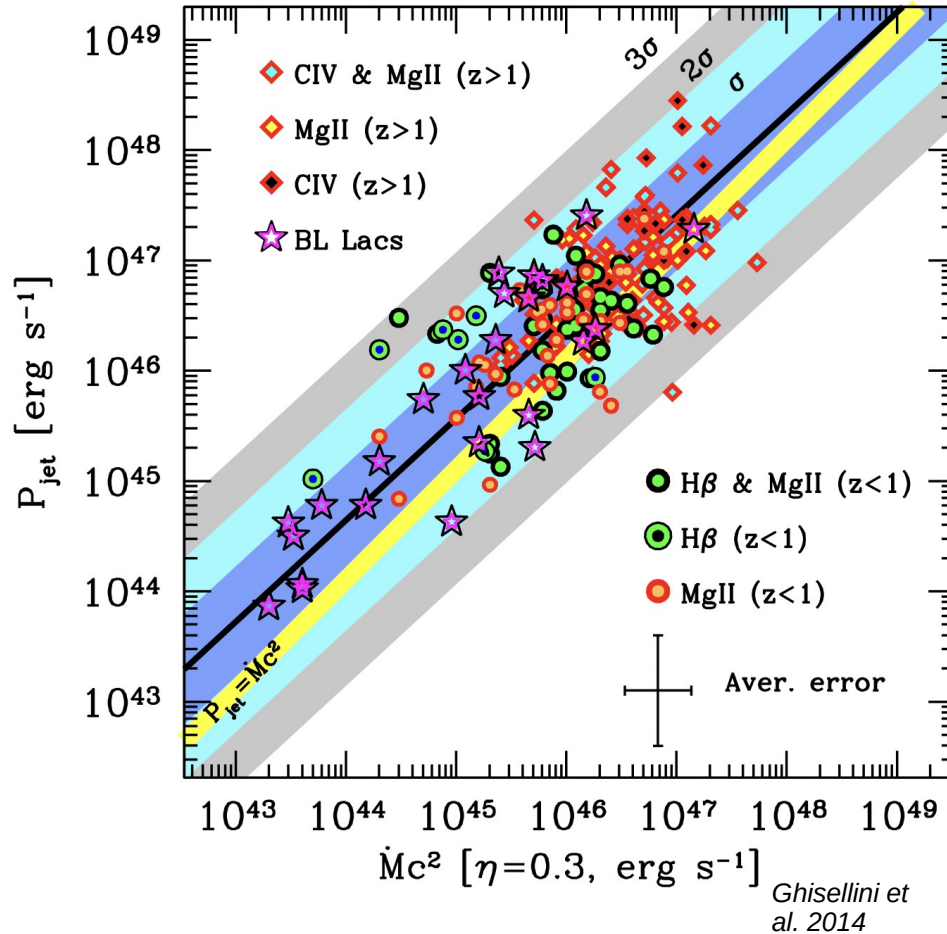
+ make the connection with neutrinos and cosmic rays

+ solutions for certain data sets, where leptonic models struggle

- require high jet powers ( $\sim L_{\text{edd}}$  or above)

- description of rapid flares difficult: longer acceleration and cooling time scales  
( factor  $(m_p / m_e)^4$  for synchrotron cooling ! )

# disk-jet connection in blazars



There is a clear correlation between jet power (measured through the  $\gamma$ -ray luminosity) and accretion luminosity (measured by the broad emission lines), with the  $P_{\text{jet}}$  dominating over the  $L_{\text{acc}}$ , in agreement with numerical simulations, in which the average outflowing power in jets and winds reaches 140% of  $\dot{M}c^2$  for dimensionless spin values  $a = 0.99$ . The presence of the jet implies that the gravitational potential energy of the falling matter can not only be transformed into heat and radiation, but can also amplify the magnetic field, allowing the field to access the large store of black hole rotational energy and transform part of it into jet mechanical power.

# particle acceleration in jets

---

Several acceleration processes are being discussed to explain the non-thermal particle distribution in blazar jets.

## 1. Diffusive shock acceleration & Shock drift acceleration (“Fermi I”)

- acceleration on standing or moving shocks (that might be identified with radio knots)
- power-law distribution of particle energies with an index of  $\sim 2.2$  for mildly relativistic shocks
- requires low magnetization to be efficient:  $\sigma = \frac{u_B}{u_{particles}} < 10^{-2}$

## 2. Stochastic acceleration by turbulence (“Fermi II”)

- acceleration on turbulences that can be caused by Kelvin-Helmholtz instabilities at interfaces between different jet layers or knots, or by magnetic instabilities.
- power-law / logparabola distribution of particle energies with hard spectra
- in general, less efficient than Fermi I

# particle acceleration in jets

---

## 3. Shear acceleration

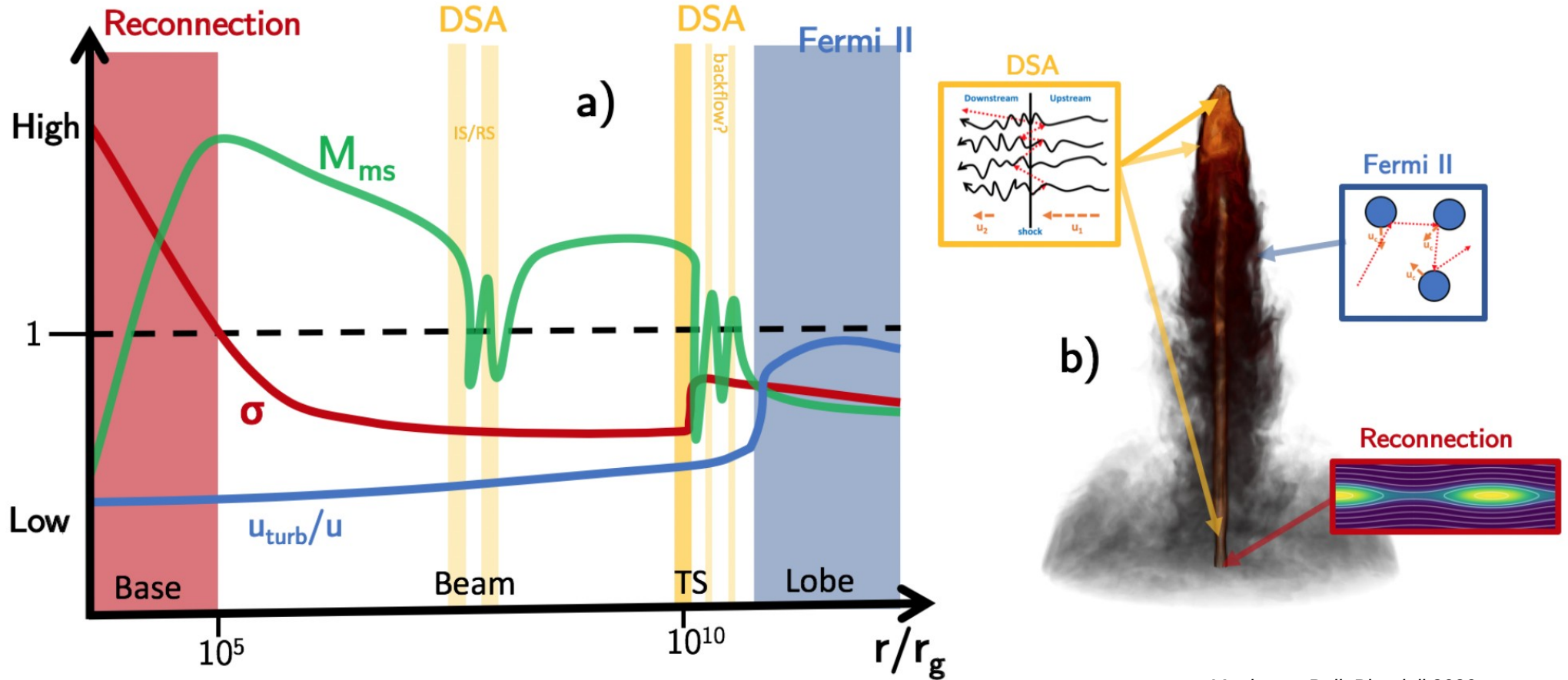
- acceleration through scattering of shearing flows at different velocities (interface jet / ambient medium , interface between different jet layers...) through Fermi-like process.
- The distribution of accelerated particles tends to a power law with index depending on the properties of the underlying turbulence.

## 4. Magnetic reconnection

- acceleration through energy release in regions of reorganisation of magnetic field lines
- can lead to power-law distribution with very hard index  $\sim 1.5 - 1$  for high magnetization
- requires high jet magnetization to be efficient  $\sigma \gg 1$

# particle acceleration in jets

Possibly there is no single mechanism at play, but several mechanisms contribute in different regions of the jet.



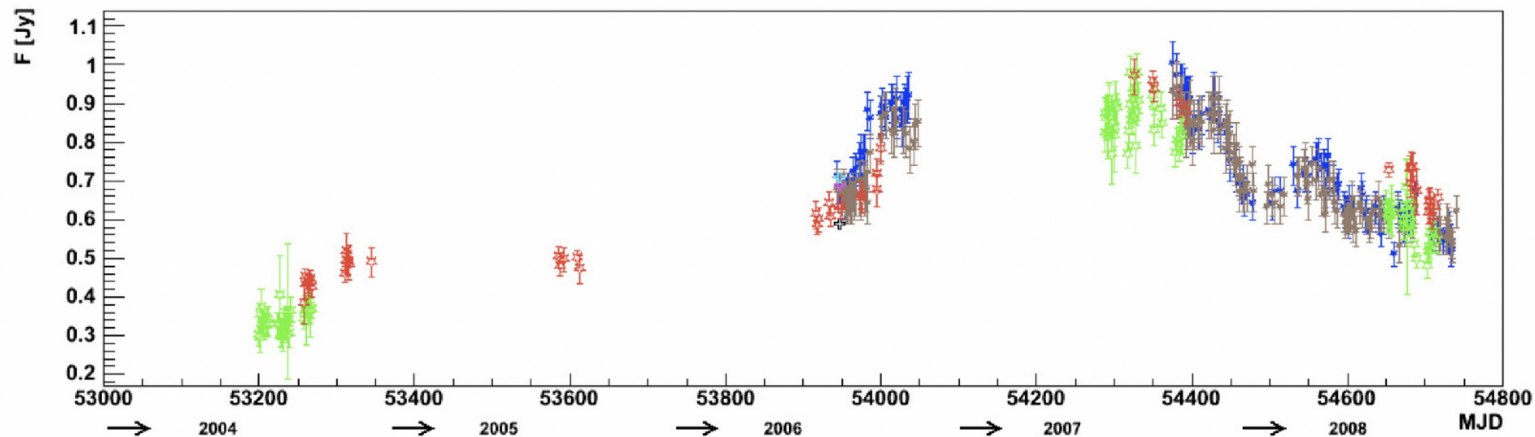
Matthews, Bell, Blundell 2020

4) variability from the jet

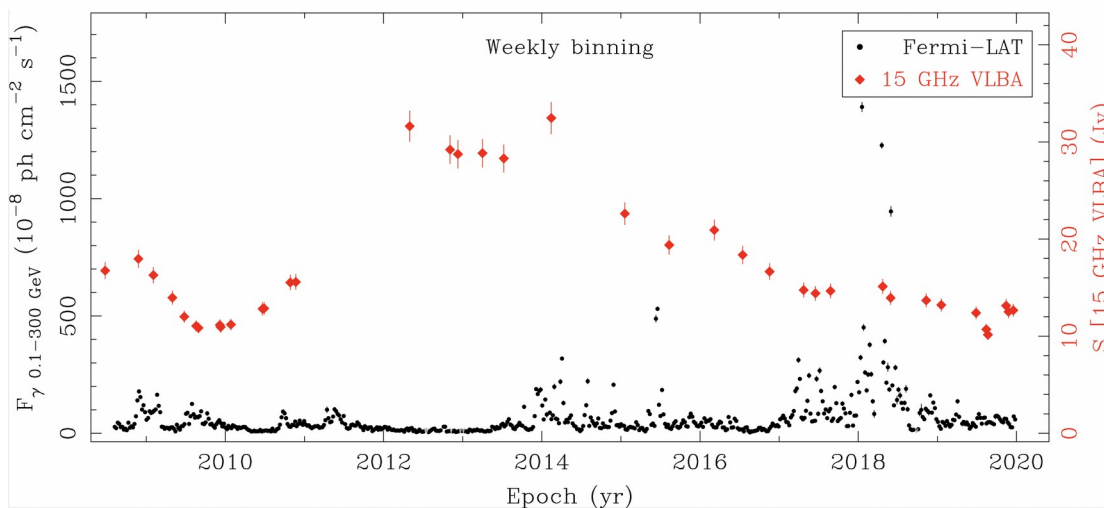


# long-term variability in blazars

longest variability time scales in the radio band : long radiative cooling times, emission from a large region (extended jet)



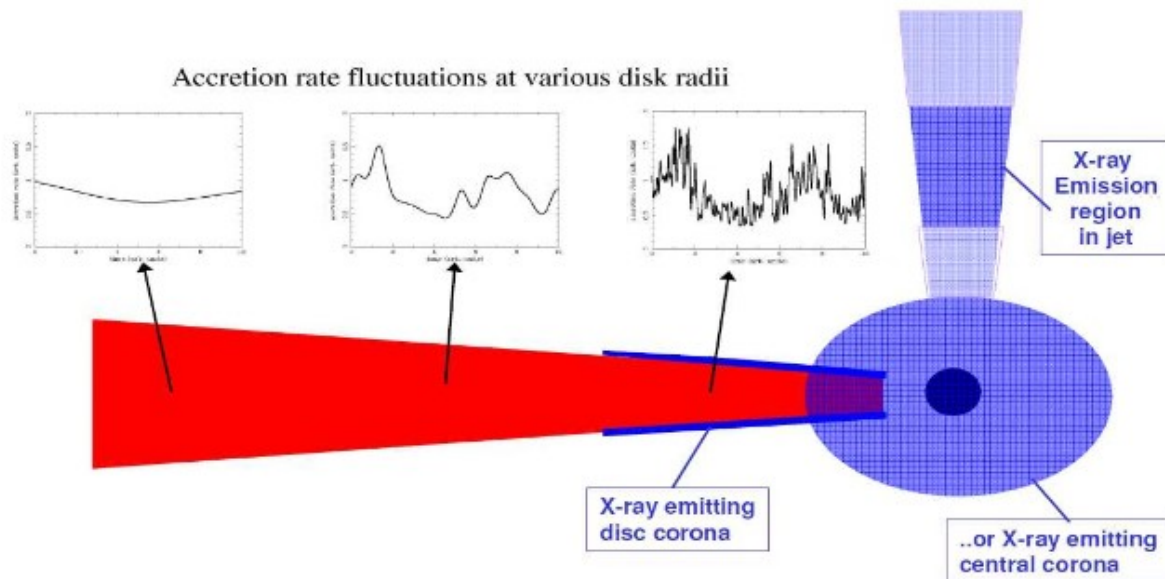
radio light curve of  
PKS 2155-304  
(3.5 – 21 cm)  
(HESS Collab. 2012)



radio light curve of 3C 279 in radio  
and gamma-rays (MOJAVE web site)

# a link between disk and jet variability ?

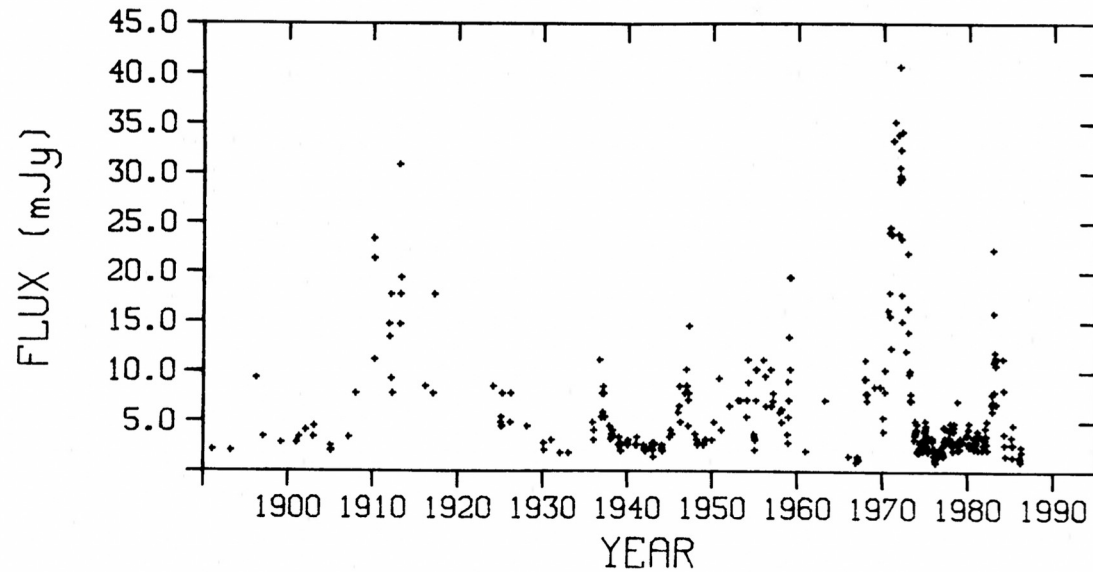
- **red-noise / pink noise** power spectrum observed in Fermi-LAT data from blazar jets
  - **log-normal flux distributions** are commonly observed in gamma-ray light curves  
(*Ulaczykont et al. 2010; Ackermann et al. 2015; Shah et al. 2018*)
- variations in the accretion rate might propagate into the jet to modulate its emission



McHardy  
(2008)

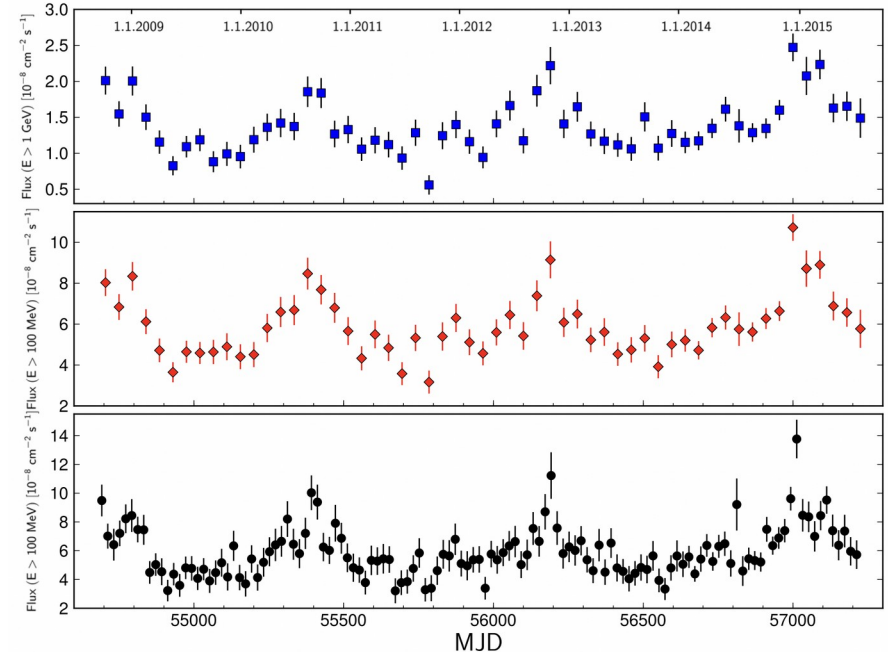
# long-term variability in blazars : QPOs

Evidence for **quasi-periodic oscillations (QPOs)** on time scales of the order of years has been detected in several blazars from radio to gamma-ray wavelengths.



A collection of optical (V-band) data from the blazar OJ 287 showing oscillations with a period of  $\sim 12$  years.

(Sillanpää et al. 1988)



Fermi-LAT light curves from the blazar PG 1553+113 showing peaks with a period of  $\sim 2$  years.

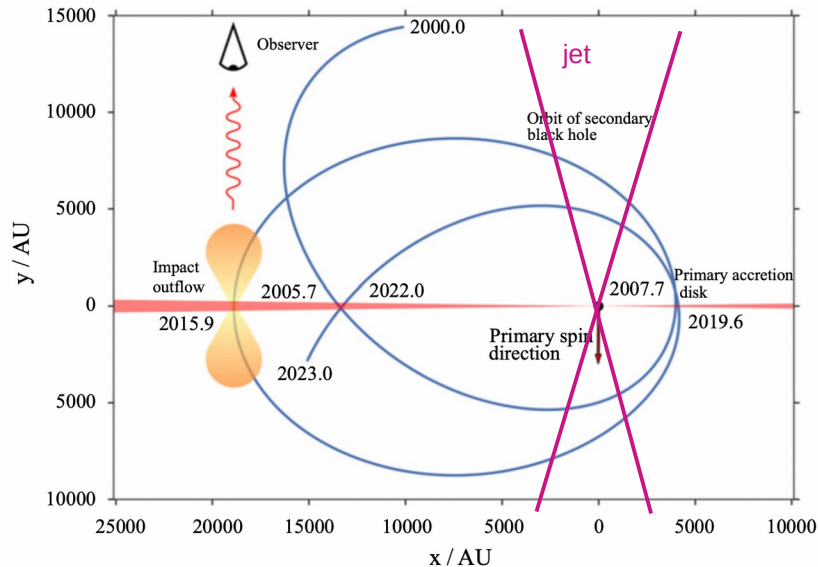
This signature is also seen in MWL observations in radio, optical, X-rays.

(Ackermann et al. 2015)

# long-term variability in blazars : QPOs

Several scenarios have been evoked to explain these periodic variations :

- **Jet precession, rotation or helical structure** could lead to quasi-periodic variations of the viewing angle and thus Doppler boosting.
- Pulsational **accretion flow instabilities** could lead to quasi-periodic variations of the energy outflow. Mechanisms similar to the accretion-outflow coupling observed in high-mass X-ray binaries or microquasars are also proposed.
- A gravitationally bound **SMBH binary system** could lead to quasi-periodic variations through accretion perturbations or jet nutation (from misalignment of SMBH spins or gravitational torque on disc).

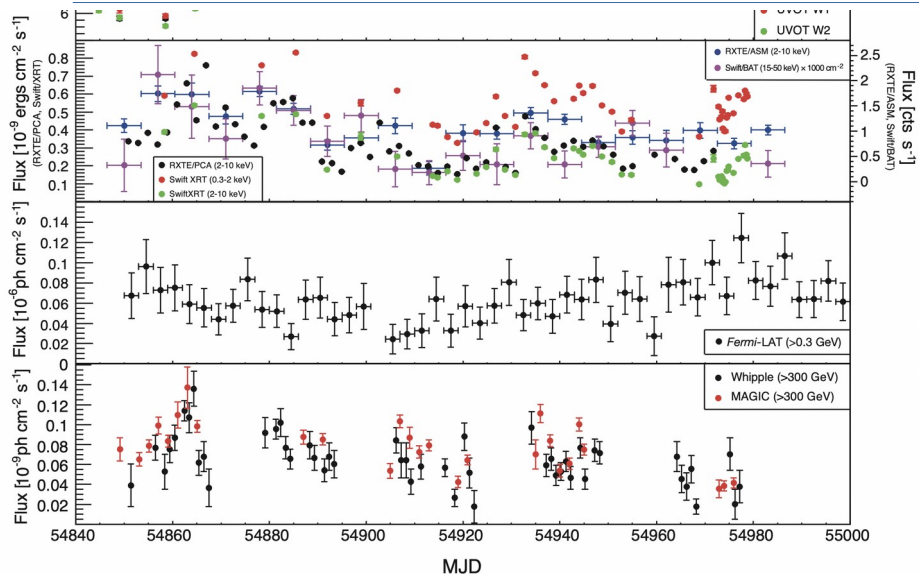


A binary SMBH model proposed for OJ 287 :

- quasi-period thermal outbursts (bremsstrahlung) due to the **crossing of the accretion disk** of the primary BH by the secondary BH
- non-thermal emission from the jet of the primary BH

(Valtonen et al. 2016)

# short-term variability during low flux state



Analysis of the high-energy light curve during the **low flux state** of the blazar Mrk 421:

- PSDs can be described by power-laws without a break, and with indices consistent with **pink/red-noise** behavior.

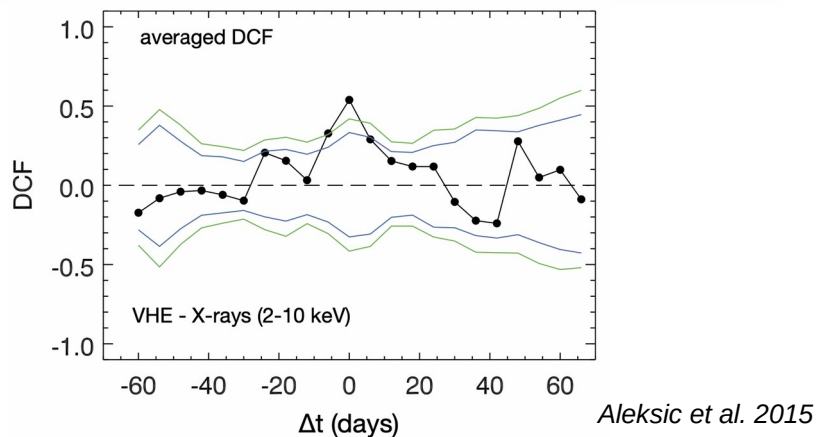
- similar mechanisms at play as in radio-quiet sources ?

- **positive correlation between VHE and X-ray** fluxes with zero time lag.

- argument in favor of leptonic scenarios dominating the broadband emission of Mrk 421 during non-flaring activity

- Moreover, a negative correlation in the (long-term) temporal evolution of the optical/UV and X-ray bands was also observed

- change in the magnetization ?



# blazar flares

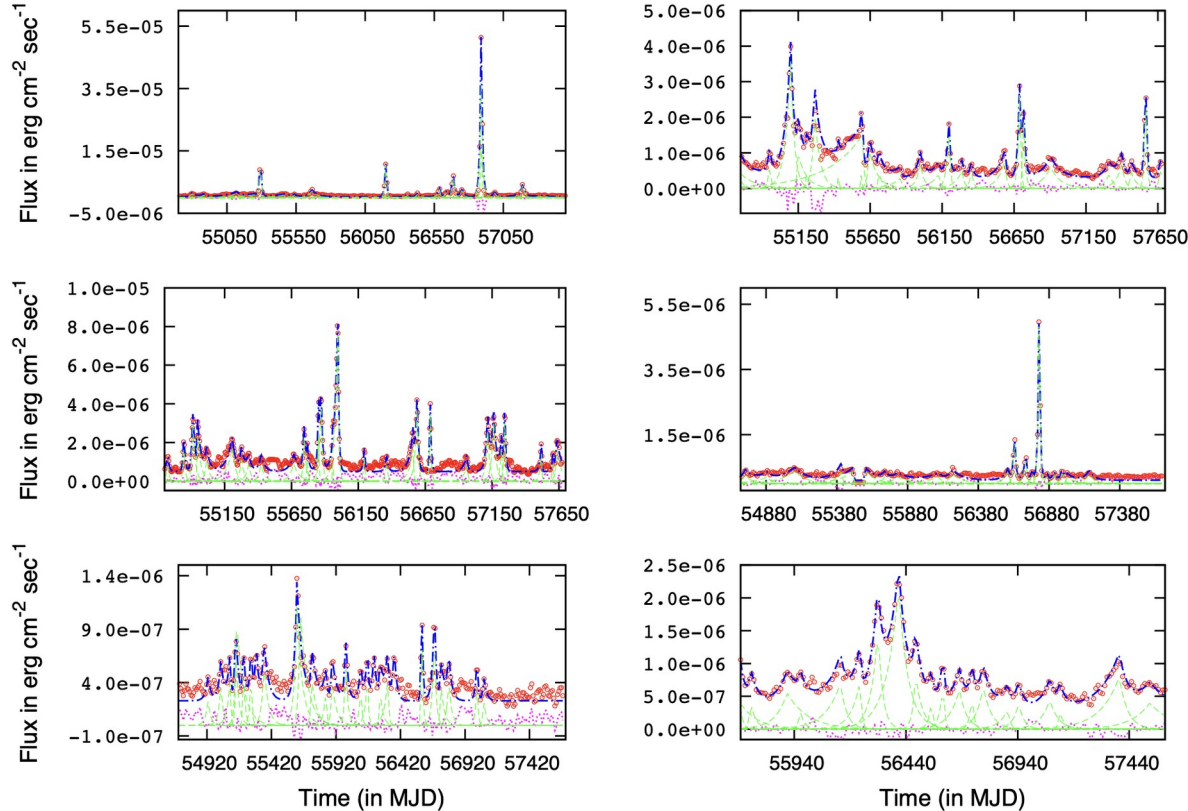


**Figure 1.** Top left – 3C 279; top right – 3C 273; middle left – 1510-089; middle right – Mrk 501; bottom left – PKS 2155-304; bottom right – PKS 1424-41. The red open circles denote the *Fermi*-LAT light curves of the above blazars at the energy range 0.1–300 GeV, which are smoothed with a Gaussian function of width 10 days; green long-dashed lines represent the individual decomposed flares (see the text), the blue dot-dashed line is the best fit to the model function given in Section 3.1, which is the sum of the individual flares, while the magenta dotted line is the residue after the fit.

Roy et al. 2019

Study of ~200 long-term (~weeks–months) GeV and R-band outbursts and ~25 short-term (~hour–day) GeV flares in a sample of 10 blazars from the *Fermi*-LAT and the Yale/SMARTS monitoring programme.

→ Most of the **long-term outbursts** are **symmetric**, indicating that the observed variability is dominated by the **crossing time-scale of a disturbance**.

→ A larger fraction of **short-term flares** are **asymmetric** with an approximately equal fraction of longer and shorter decay than rise time-scale.  
Signature of **gradual particle acceleration and cooling** ?

# causality constraints with relat. beaming

---

The causality constraint applies also to emission zones within the jet, but one has to apply the effect of Doppler beaming :

$$R \leq \frac{c t_{var,obs} \delta}{(1+z)}$$

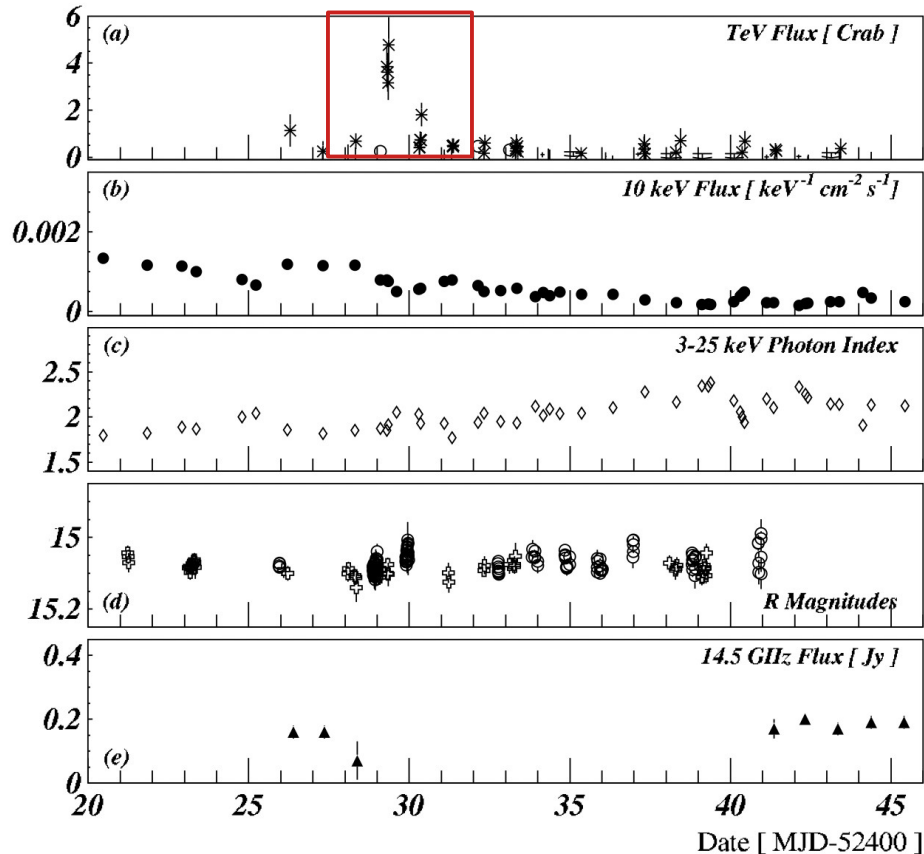
The larger the Doppler factor, the more one can relax the constraint on the size of the emission region, if the perturbation is caused by **processes within the jet**.

$$t_{var,obs} = t_{var,jet} (1+z) / \delta$$

For a perturbation caused in the source frame (e.g. a **perturbation from the accretion disk**), the observed variability time scale is **not** shortened by the Doppler factor if  $\delta \sim \Gamma$ .

$$t_{var,obs} = \Gamma t_{var,source} (1+z) / \delta \approx t_{var,source} (1+z)$$

# “orphan” flares



“orphan” TeV flare from the blazar 1ES 1959+650  
(Krawczynski et al. 2004)

Detections of “orphan” flares from several blazars are difficult to interpret with standard SSC emission scenarios.

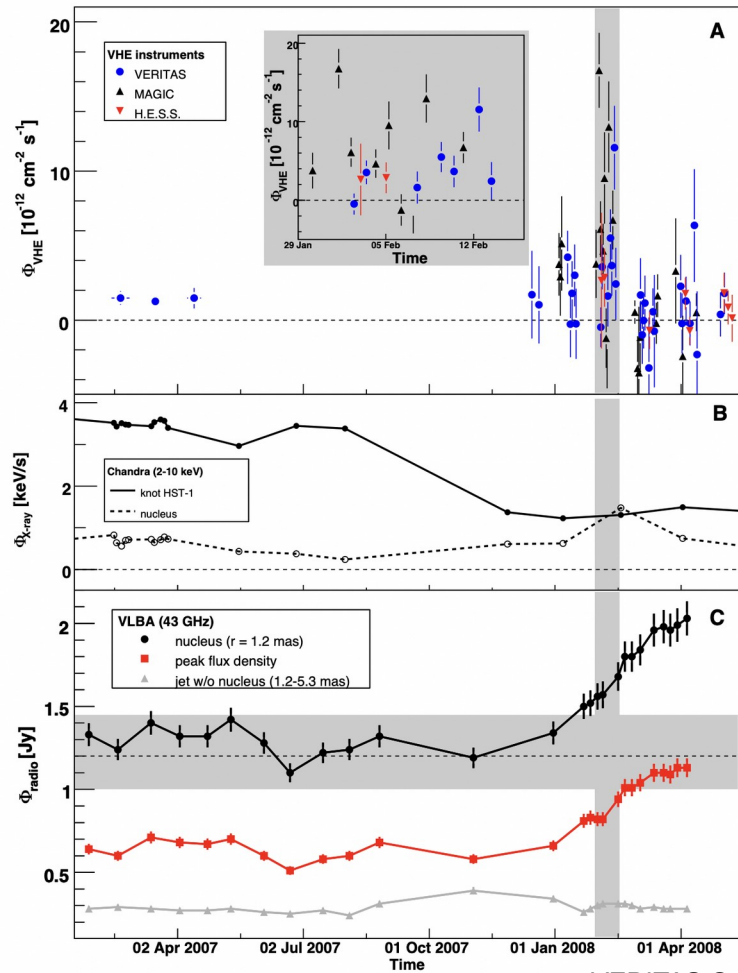
Here, an important flare in a high-energy band is not accompanied by any significant variation in the other MWL bands.

Different scenarios have been evoked to explain such events:

- **multi-component SSC models** : a very compact region is responsible for a TeV flare, while a more extensive region dominates the emission at longer wavelengths
- EIC emission from **rapidly varying external photon field** could lead to TeV flare, while the synchrotron emission is unchanged
- **hadronic models** : relativistic electrons dominate emission at low energies, while protons are responsible for the TeV flare



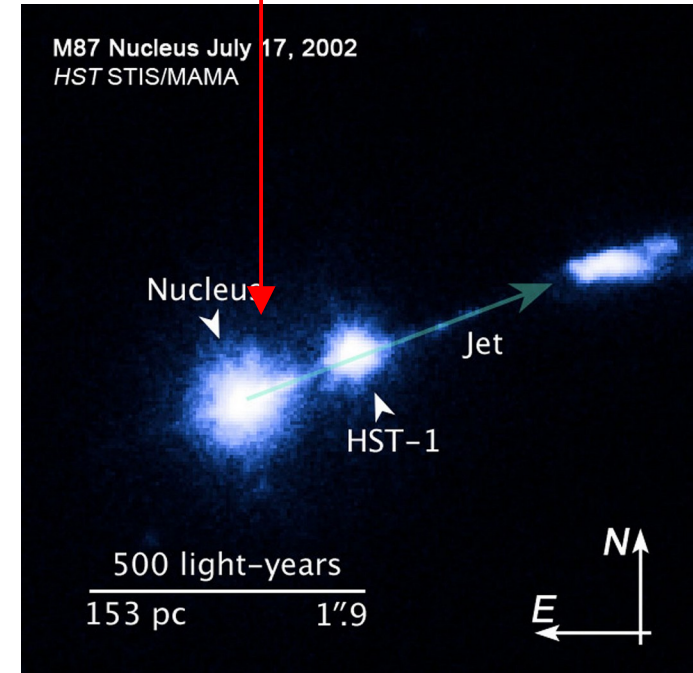
# the VLBI – high-energy connection



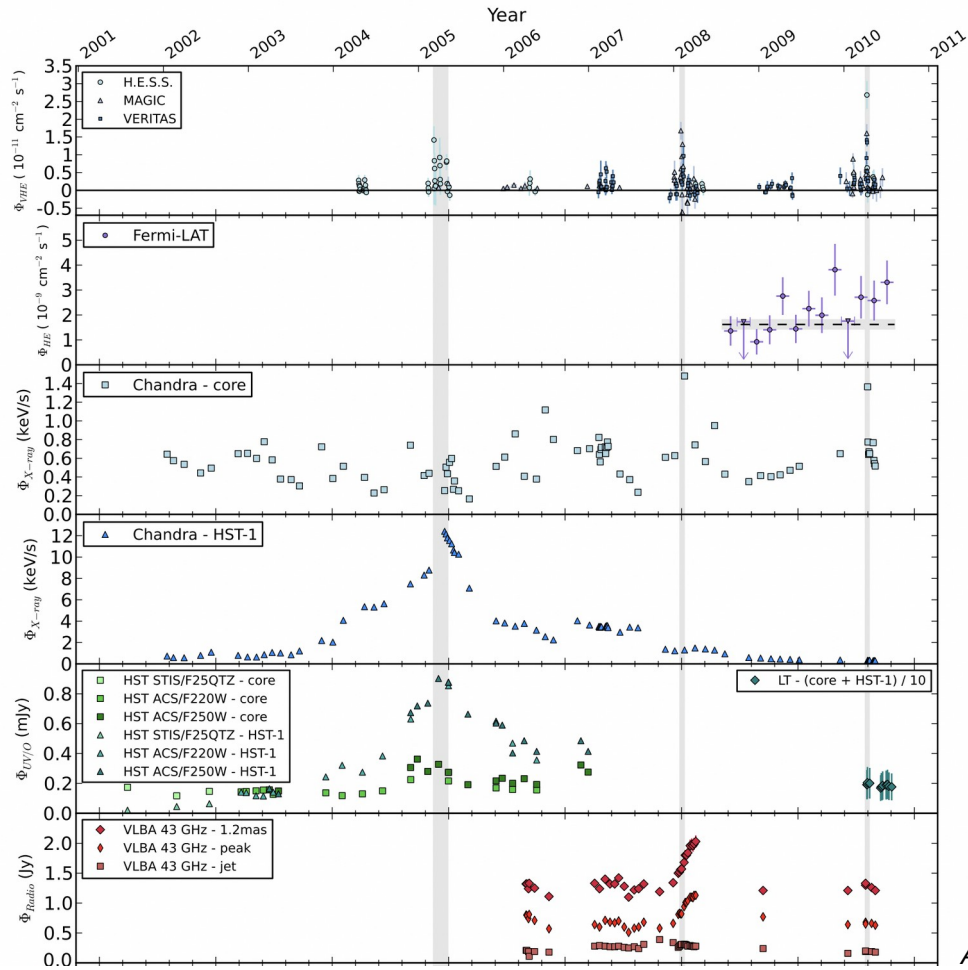
VERITAS Collab. et al. 2009

2008 VHE flare of the radio galaxy M87 :

Correlation with high activity  
(radio VLBI, X-rays) from the nucleus  
(radio core).



# the VLBI – high-energy connection

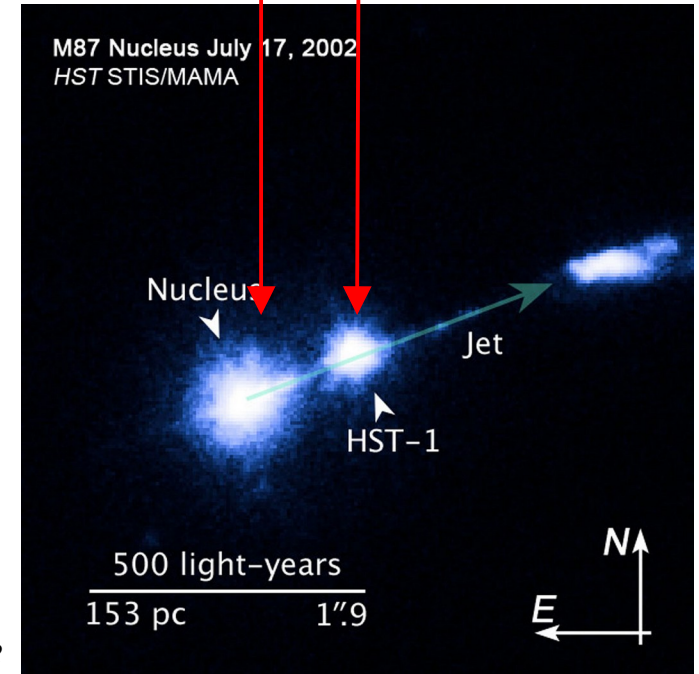


Abramowski. et al. 2012

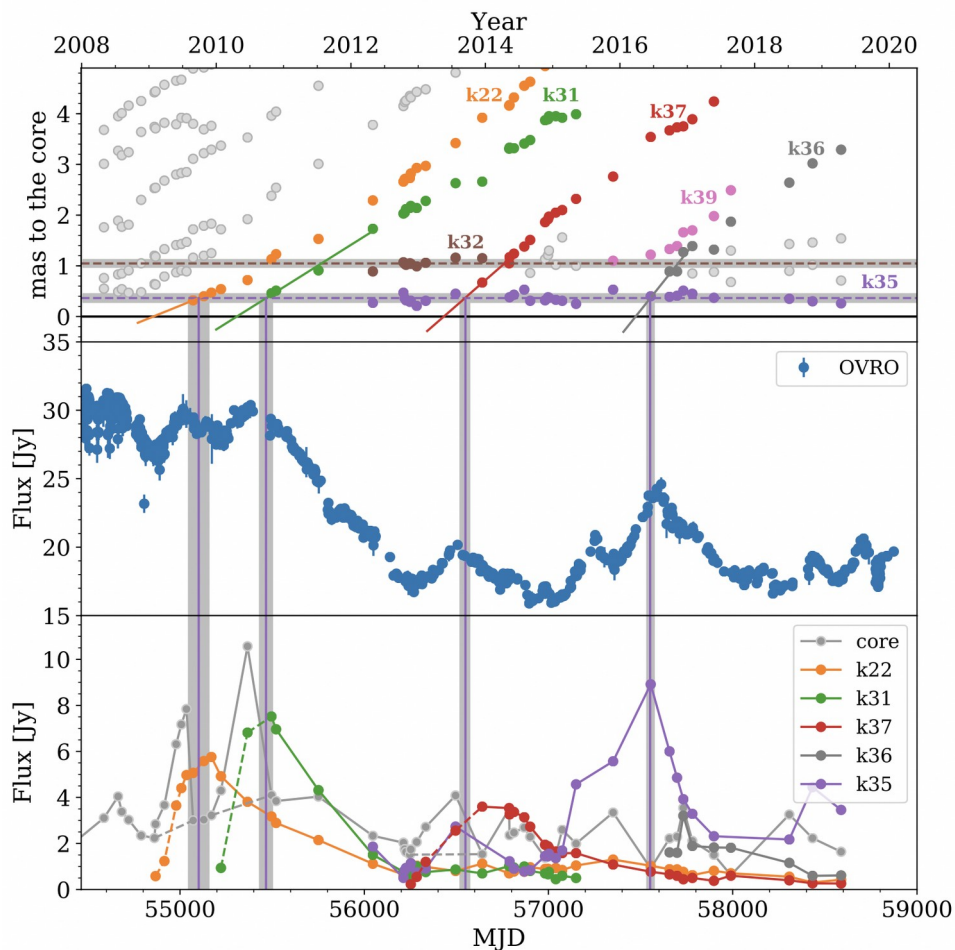
BUT :

2005 VHE flare of the same source: Correlation with high activity (optical, X-rays) from the radio knot HST1.

Correlation of the 2010 VHE flares with the nucleus.



# the VLBI – high-energy connection



*blazar 3C 273 observed at 15.3 GHz*

upper panel : identification of moving and standing radio knots with the Mojave VLBI survey

middle panel : light curve of the overall radio flux from the jet

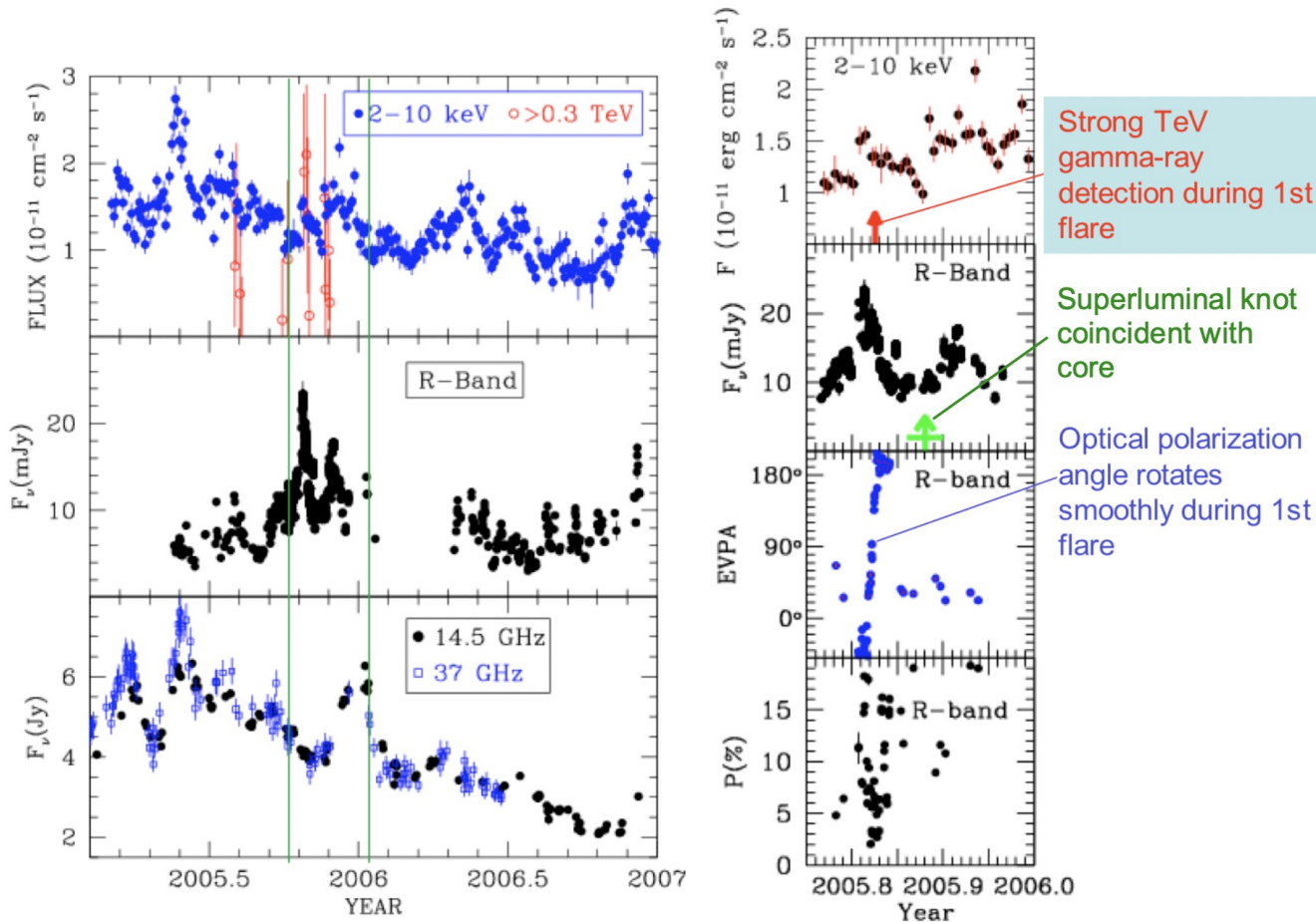
bottom panel : light curves of radio fluxes from individual knots

→ The crossing of moving knots through the position of standing knots coincides with flux increases in the moving knots. These are also visible in the overall emission, if they are isolated events.

→ Indication of **shock-shock interactions** inside the jet.

*Fichet de Clairfontaine et al. (2020)*

# optical polarization signatures ?



double optical flare of the blazar BL Lac in 2005 ( Marscher 2008 )

Rotation of the electric vector polarisation angle (EVPA) coincides with flare events.

→ Signature of the disturbance causing the flare following **a helical motion through a helical magnetic field** in the jet.

Monitoring of blazars with the Robopol telescope finds indications for a **general correlation between gamma-ray flares and EVPA rotations**

( D. Blinov et al. 2017 ).

# X-ray polarization

Detection of X-ray polarization is now possible thanks to the IXPE space telescope.

Observations of the blazar Mrk 501 (during a low state) show a **polarization degree that is increasing from the radio to optical to X-rays** and a **polarization angle aligned with the jet axis**.

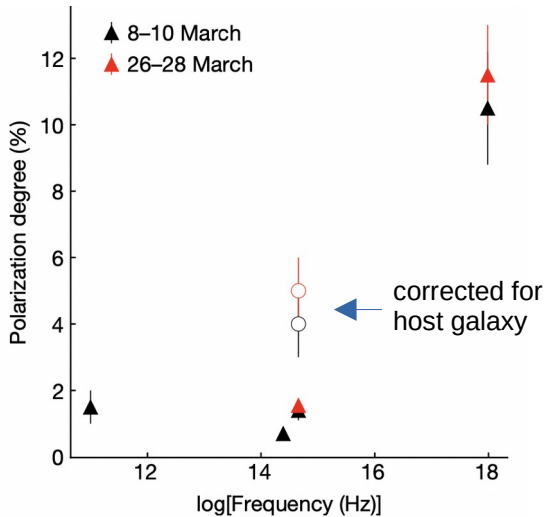
Interpretation through **shock acceleration** :

A shock partially orders the magnetic field of the plasma crossing it

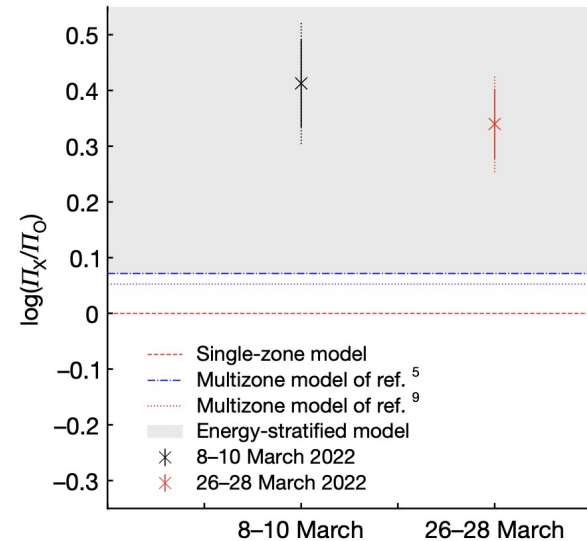
→ net polarization vector aligns with the jet

Particles accelerated on shock, progressively lose energy and emit at lower and lower frequencies as they diffuse away from the shock. Farther from the shock, the plasma becomes increasingly turbulent.

→ polarization decreases from high to low energy emission

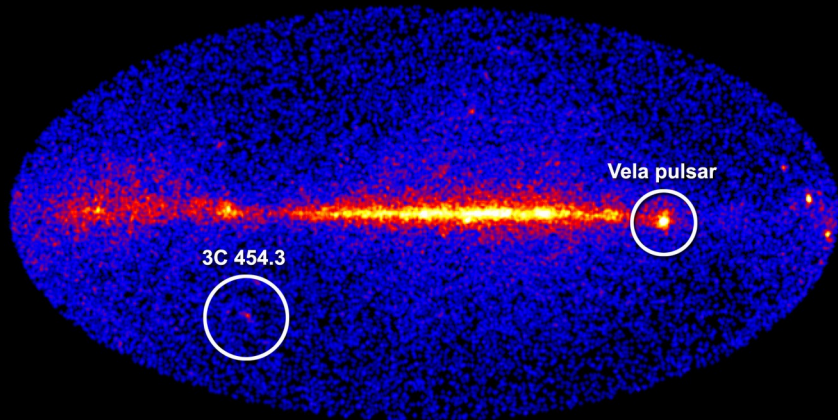


polarization from Mrk 501 from radio to X-rays  
(Lioudakis et al. 2022)

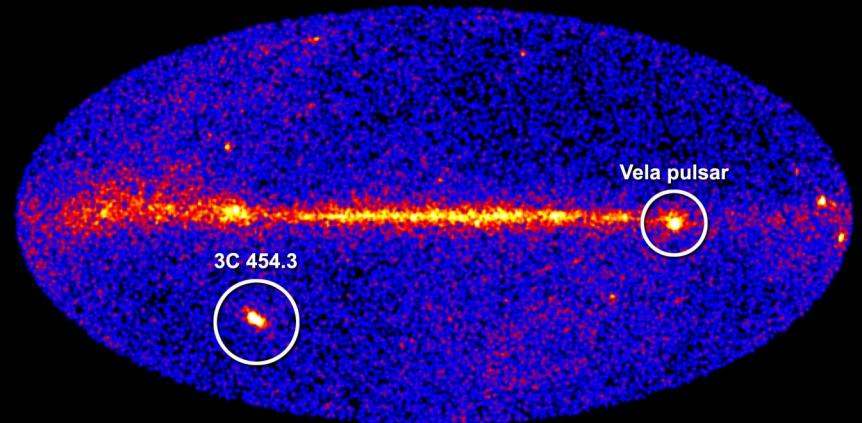


polarization ratio X-ray / optical compared to different emission models  
(Lioudakis et al. 2022)

## 5) modelling blazar flares



November 3, 2009



December 2, 2009

# origin of flares in the one-zone model

---

possible physical origin of flares :

- change in size of emission region  $R \rightarrow$  density  $n$ , magnetic field  $B$  (expansion, contraction)
- change in magnetic field  $B$
- change in Doppler beaming (Lorentz factor, viewing angle)
- particle injection (pre-accelerated particle distribution)
- particle acceleration (shock, turbulence, shear, magnetic reconnection)

# origin of flares in the one-zone model

electron evolution: 
$$\frac{\partial N_e}{\partial t} = \frac{\partial}{\partial \gamma} [(\beta \gamma^2 - 2D_0 \gamma - a \gamma + b \gamma) N_e] + \frac{\partial}{\partial \gamma} \left( D_0 \gamma^2 \frac{\partial N_e}{\partial \gamma} \right) - \frac{N_e}{t_{esc}} - \frac{N_e}{t_{ad}} + Q_{inj}$$
 Fokker-Planck equation

$Q_{inj}(\gamma, t)$  particle injection rate ,  $-\frac{N_e}{t_{esc}}$  particle escape rate,  $-\frac{N_e}{t_{ad}}$  adiabatic expansion rate

acceleration terms :

- Fermi I :  $a = 1/t_{shock}$  with  $t_{shock}$  the acceleration time scale
- Fermi II :  $D_0 = 1/t_{turb}$  with  $t_{turb}$  the acceleration time scale

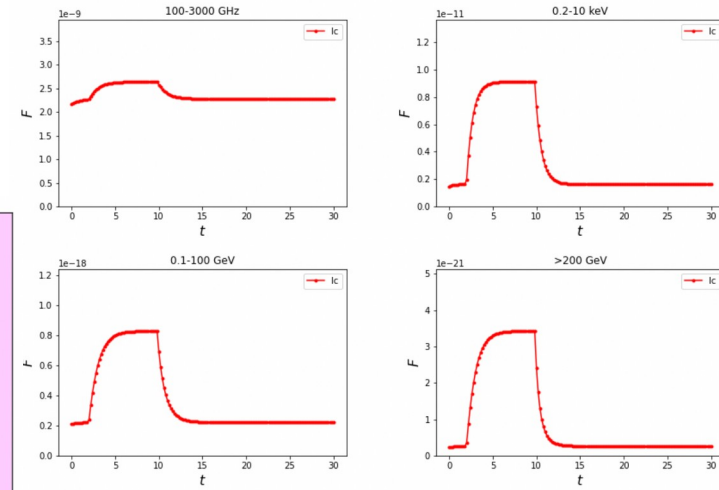
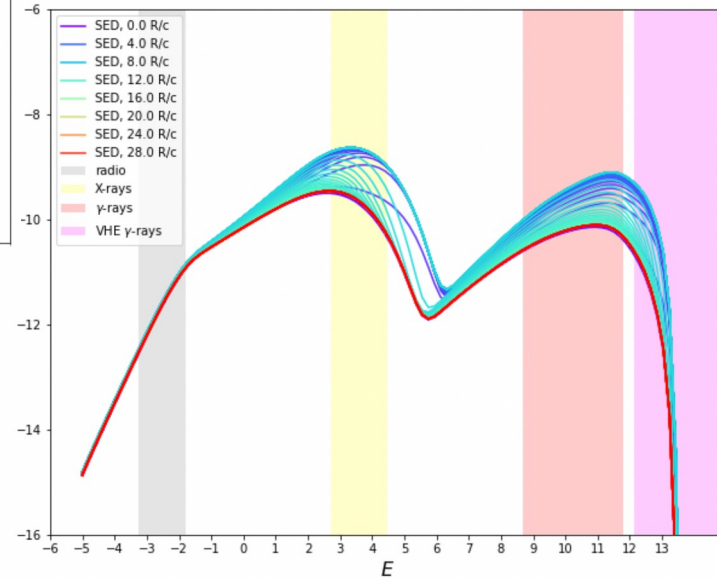
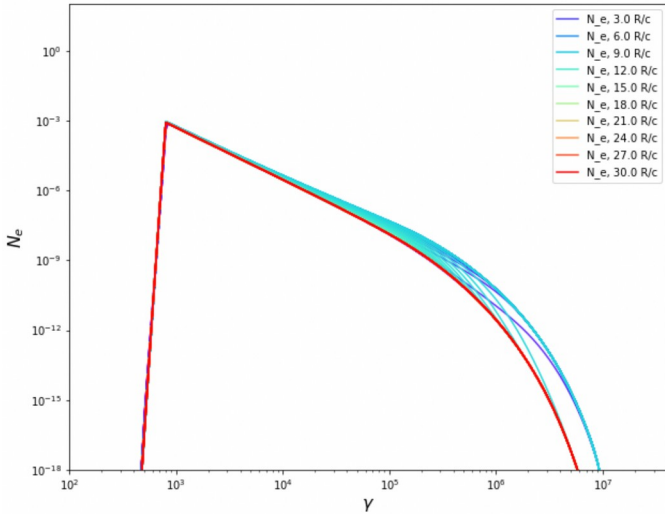
cooling terms :

- adiabatic  $\dot{\gamma}_{ad}(t) = \frac{\dot{V}}{3V} \gamma = \frac{\dot{R}(t)}{R(t)} \gamma = \frac{\beta_{exp} c}{R(t)} \gamma = b \gamma$
  - synchrotron  $\dot{\gamma}_{synch}(t) = \frac{4 \sigma_T c}{3 m_e c^2} \gamma^2 U_B(t)$  with  $U_B = \frac{B^2}{8 \pi}$
  - Inverse Compton (Thomson regime)  $\dot{\gamma}_{IC}(t) = \frac{4 \sigma_T c}{3 m_e c^2} \gamma^2 U_{ph}(t)$  with  $U_{ph}$  the (target) photon energy density
- }  $\beta \gamma^2$



# origin of flares in the one-zone model

example: flare through injection, radiative cooling, escape



Light curves

Spectral Energy Distribution

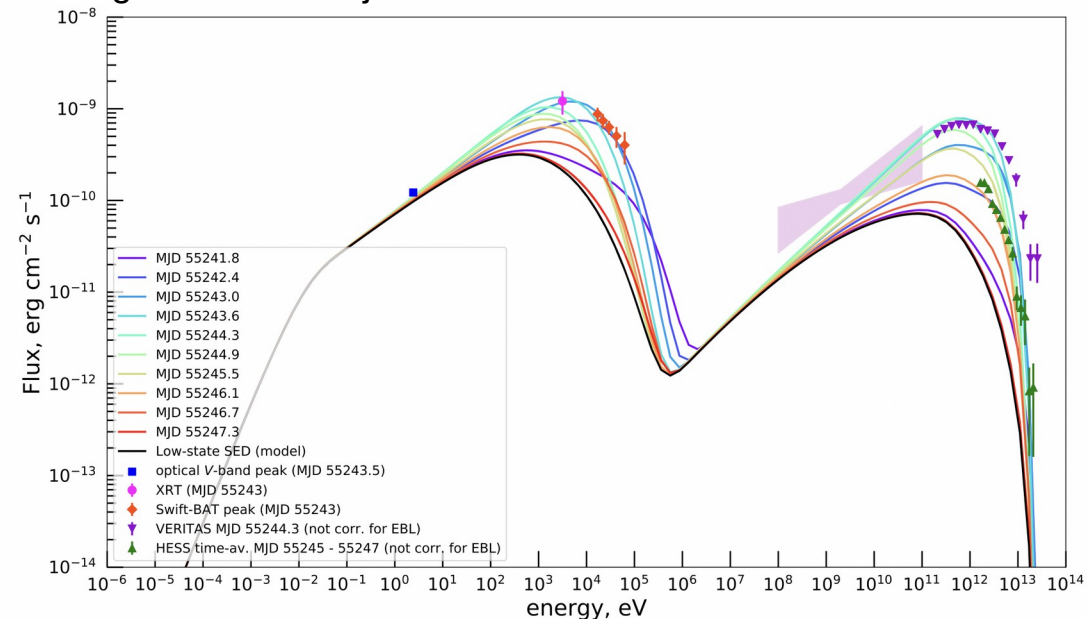
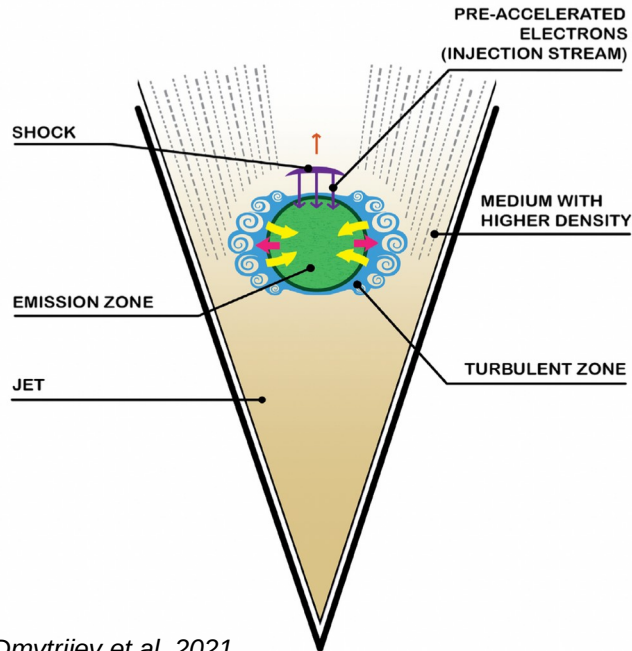
**e- distribution** : steady state (violet) + injection, radiative cooling, escape

*P. Thevenet,  
internship, 2023*

# an example : modelling a flare from Mrk 421

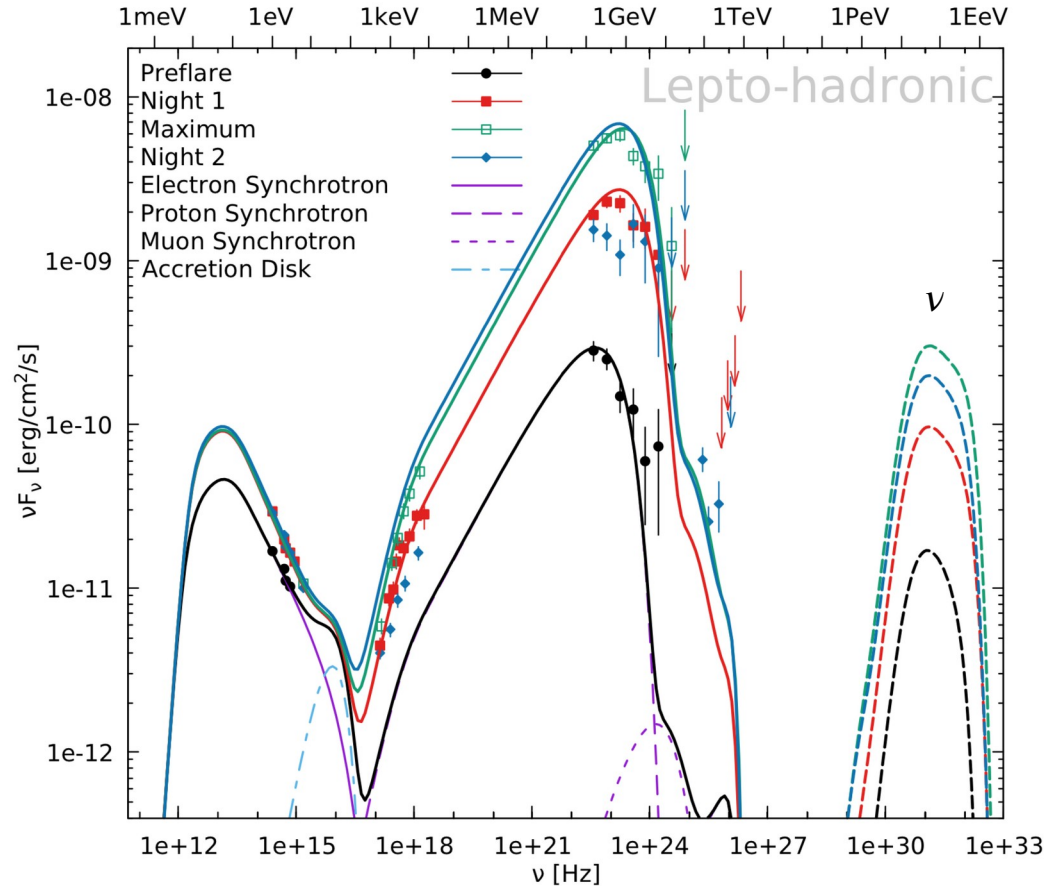
In this model, the continuous low-state emission from Mrk 421 is connected with a flare in Feb. 2010 :

- low state is modelled with a continuous injection (+ cooling, escape) of electrons accelerated on a (bow) shock into the emitting blob
- the hard spectrum during the flare requires additional Fermi II acceleration from a turbulent emission region surrounding the blob as it passes through an inhomogeneous region inside the jet.



Broad-band emission from Mrk 421 during low state and flare + model curves. (A. Dmytriiev et al. 2021)

# hadronic one-zone models



Model for a flare from the blazar 3C 279 in 2015  
(HESS Collaboration 2019)

- 3C 279 is a bright FSRQ-type blazar  
-> important photon fields

- $\gamma$ -ray emission region is at a distance  
> 0.06 pc from the central black hole,  
i.e. beyond BLR

- attempts to model this flare with one-zone  
leptonic or lepto-hadronic models are not  
entirely satisfactory...

- predicted number of  $\nu$  detectable with IceCube  
during flare very small ( $\sim 5 \times 10^{-4}$ )

# open-access codes to model flares

Various open-source packages exist to model the broad-band emission of extragalactic sources from radio up to the highest gamma ray energies.

software	sources	approach	particles			processes						temp. ev.	emission region
			thermal	non-thermal		synch.	leptonic			Brems.	hadronic pp		
				$e^\pm$	p			SSC	EC				
naima	PWN, SNR, GRB	numerical	✗	✓	✓	✓	✓	✓(CMB)	✓	✓ <sup>†</sup>	✓(EBL)	✗	not specified
GAMERA	PWN, SNR, AGN microquasars	numerical	✗	✓	✓	✓	✓	✓ <sup>⊙</sup>	✓	✓ <sup>†</sup>	✓ <sup>*</sup>	✓ (only cool.)	multiple uniform
JetSeT	jetted AGN, PWN microquasars, SNR	numerical	✗	✓	✓	✓	✓	✓	✓	✓ <sup>‡</sup>	✓(EBL)	✓ (acc. + cool.)	multiple uniform acc. + rad.
agnpy	jetted AGN	numerical	✗	✓	✗	✓	✓	✓ <sup>*</sup>	✗	✗	✓ <sup>*</sup>	✗	single uniform
BHJet	binaries, AGN	numerical semi-analytical	✓	✓	✗	✓	✓	✓	✗	✗	✗	✗	whole jet
FLAREMODEL	synch. sources	numerical ray-tracing	✓	✓	✗	✓	✓	✗	✗	✗	✗	✓ (only cool.)	single radial dep.

<sup>†</sup> pp interaction: computing only gammas from  $\pi_0$  decay.

<sup>‡</sup> pp interaction: computation of radiation from secondaries of charged pions (pairs evolved in time to equilibrium) and of  $\nu$  spectra.

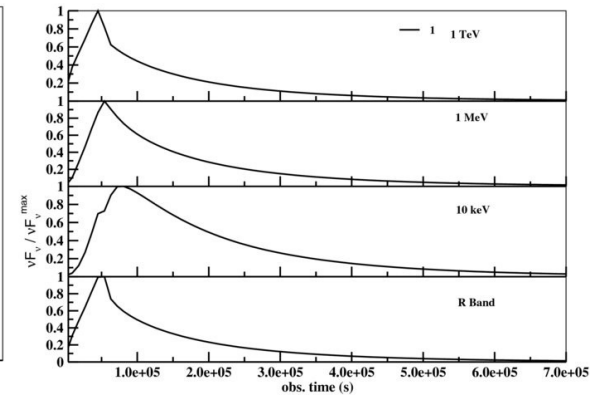
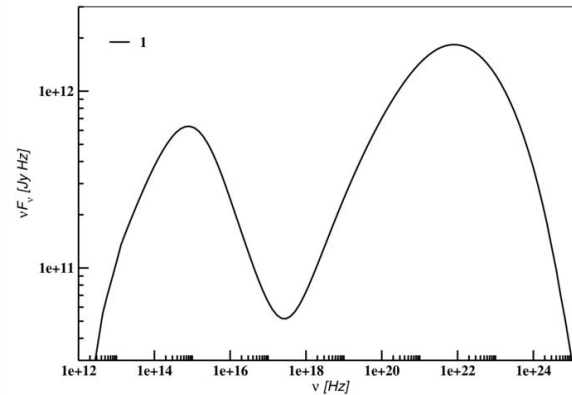
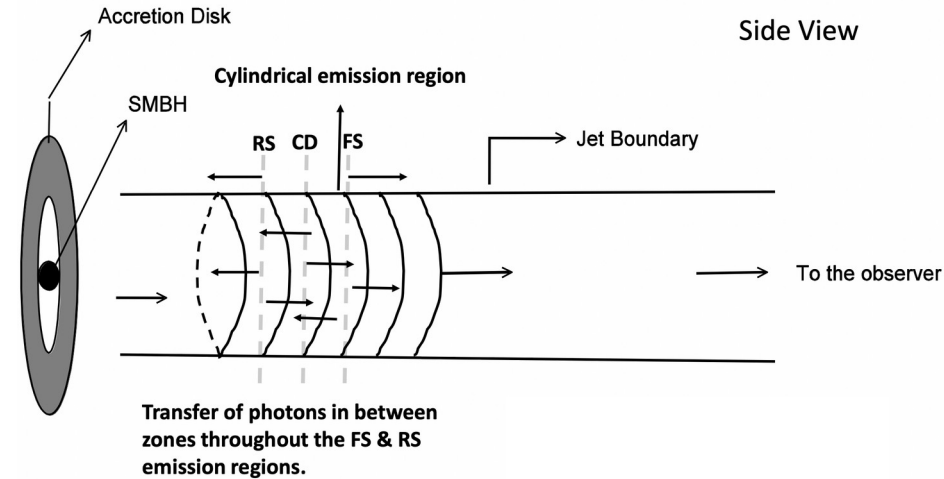
<sup>⊙</sup> full angular dependency of the Compton cross section: anisotropic electrons and anisotropic photon fields.

<sup>\*</sup> full angular dependency of the Compton or  $\gamma\gamma$  cross sections: anisotropic photon fields.

# beyond the one-zone model

## the internal shock scenario

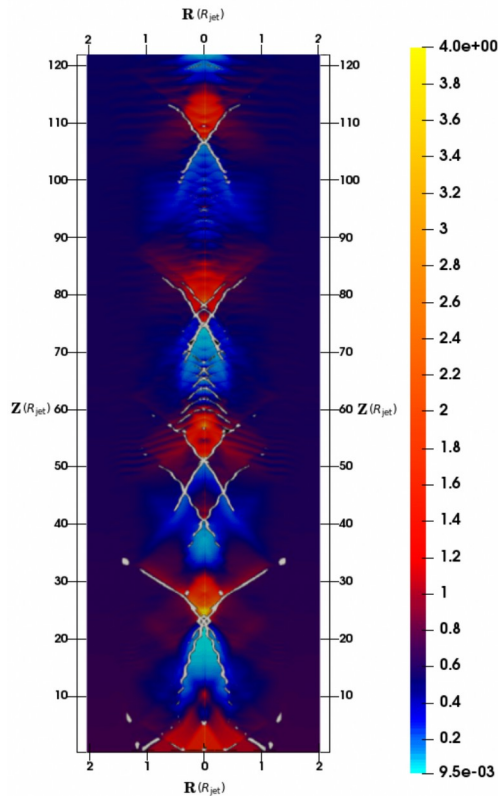
- emission of a series of relativistic plasma shells with different Lorentz factors into the jet
- faster inner shells catch up with slower outer cells → inelastic collisions produce internal shocks  
→ particle acceleration on the reverse and forward shock → emission of synchrotron and SSC radiation
- similar scenarios are used to explain the prompt emission in GRBs



Joshi M. & Boettcher M., 2011, ApJ, 727, 21

# beyond the one-zone model

## shock-shock interactions in an MHD jet

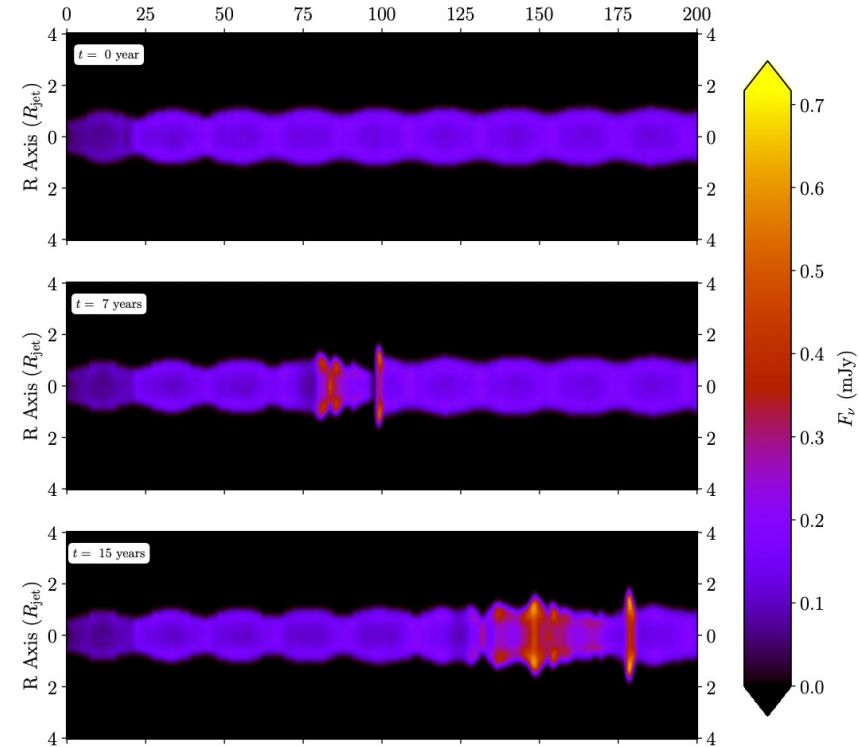


In this example, an overpressured jet propagates in the ambient medium.

→ formation of a series of recollimation shocks (left)

A perturbation (= zone with elevated Lorentz factor or density) is injected at the base of the jet. A bow shock forms in front of the perturbation as it propagates through the jet.

→ shock-shock interactions lead to enhanced emission (i.e. flares), here observed in the radio band



rarefaction (light blue) and compression (red) regions and associated standing shocks (white)

*G. Fichtel de Clairfontaine et al. 2021*

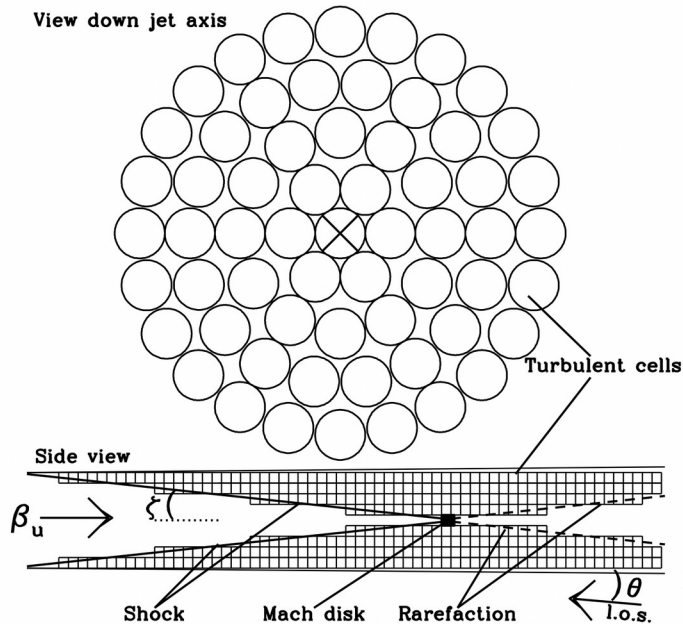
radio (synchrotron) emission from a perturbation crossing standing shocks

*G. Fichtel de Clairfontaine et al. 2022*

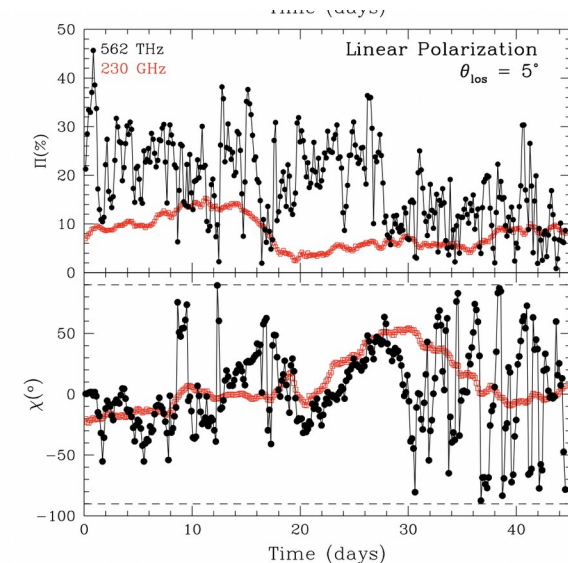
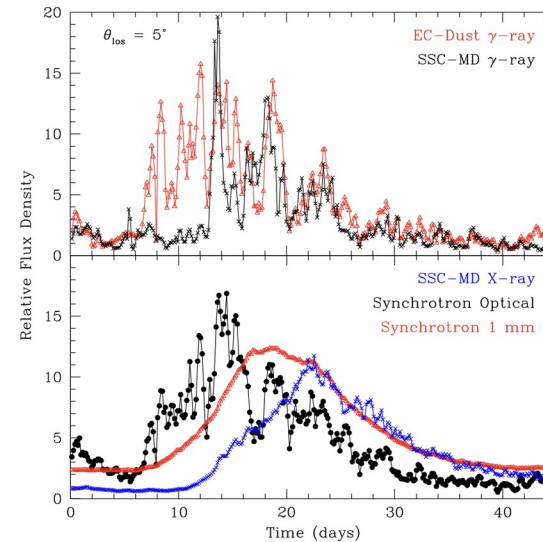
# beyond the one-zone model

## a turbulent flow through a standing shock

- turbulent plasma flowing at a relativistic speed down a jet crosses a standing conical shock.
  - The shock compresses the plasma and accelerates electrons to energies up to  $\gamma_{\max} \sim 10^4$
  - The turbulence is approximated in a computer code as many cells, each with a uniform magnetic field whose direction is selected randomly.
  - The density of high-energy electrons in the plasma changes randomly with time in a manner consistent with the power spectral density from observations of blazars.
- The **variations in flux and polarization** are therefore caused by continuous noise processes rather than by singular events such as explosive injection of energy at the base of the jet.



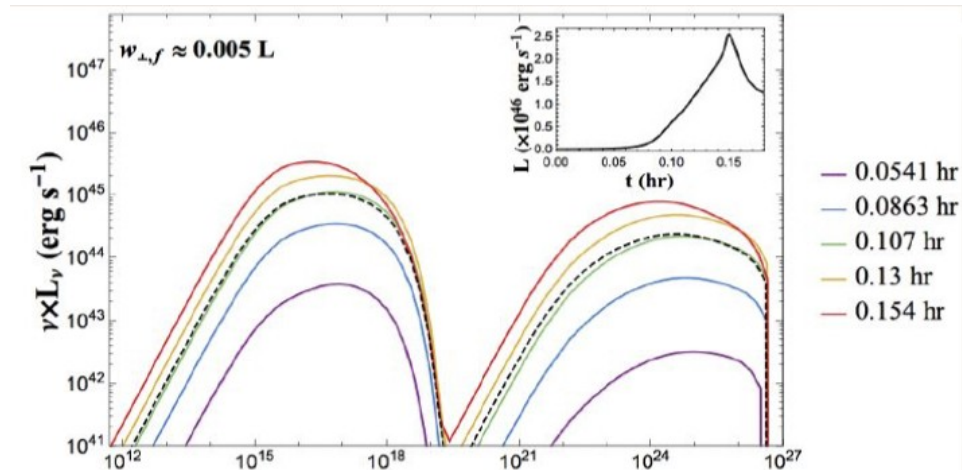
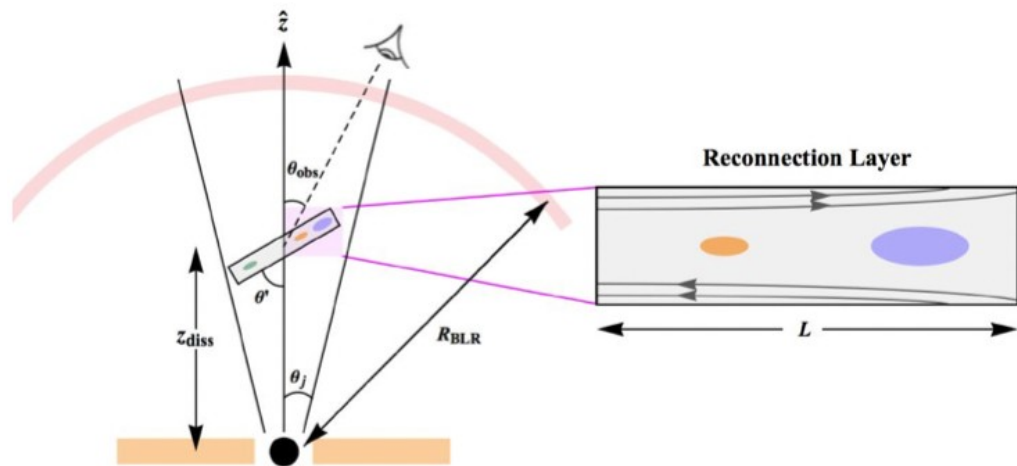
A.P. Marscher 2014



# beyond the one-zone model

## magnetic reconnection models

- reconnection events within the jet lead to particle acceleration and flares  
→ requires high jet magnetization  $\sigma \geq 1$  ( ↔ shock acceleration requires low magnetization  $\sigma \leq 10^{-2}$  )
- simulation of plasmoids with PIC codes



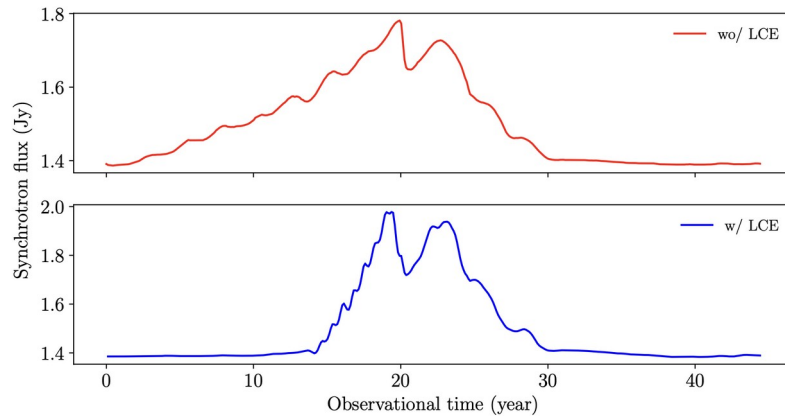
Petropoulou, Giannios, Sironi, 2016, MNRAS, 462, 3325  
Sironi, Giannios, Petropoulou, 2016, MNRAS, 462, 48  
Christie, Petropoulou, Sironi, Giannios, 2019, MNRAS, 482



# caveat : internal light crossing effect

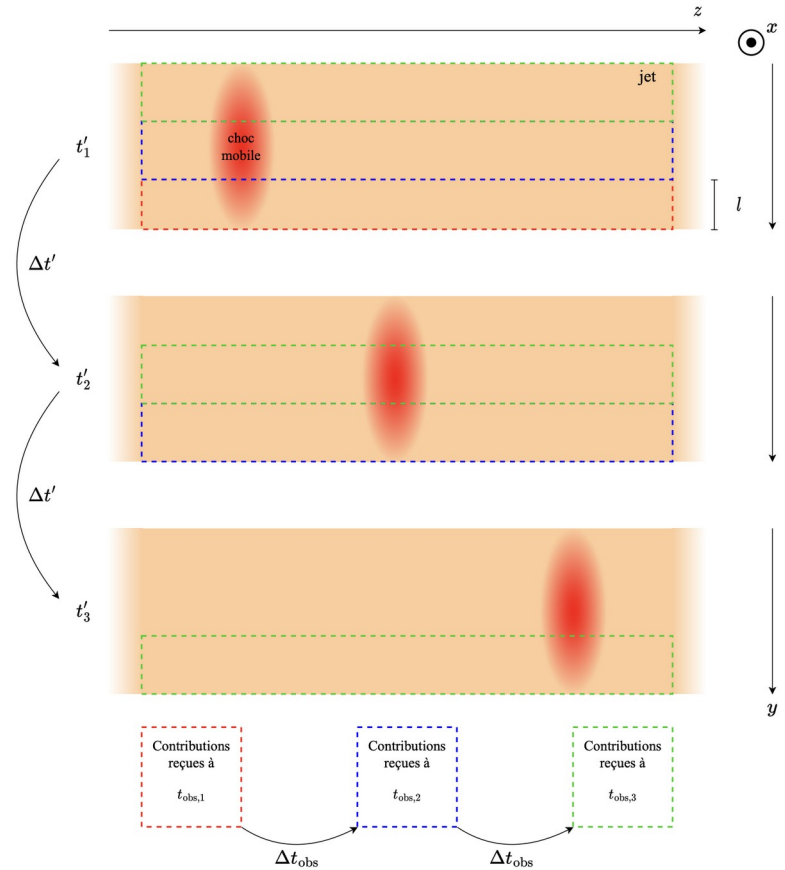
Models with extended emission regions (beyond the one-zone approach) need to evaluate the impact of time delays due to internal light crossing effects ( cf. *Chiaberge & Ghisellini 1999* ).

For relativistically moving perturbations travelling along the jet, the time it takes light from the distant edge of the jet to traverse the jet can distort the observed shape of flares.



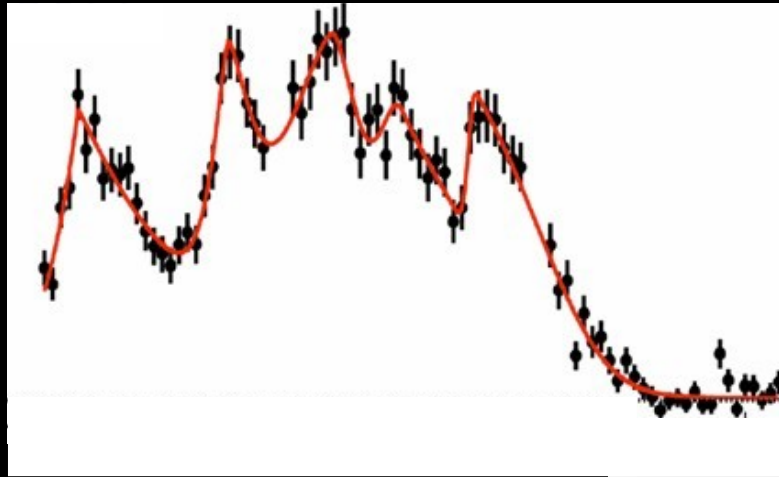
simulated radio light curves for a viewing angle of 20 deg (observer frame) with and without light crossing effect

G. Fichet de Clairfontaine 2022



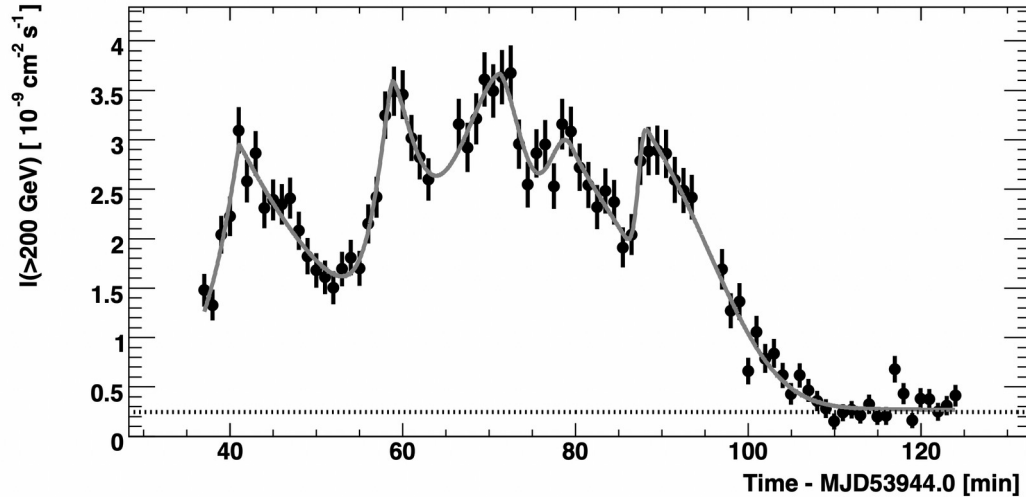
G. Fichet de Clairfontaine 2022

## 6) the puzzle of very rapid flares



# observations of very rapid flares

A few TeV flares with flux variability down to the **minute time scale** have been observed from different sources. These are difficult to reconcile with the causality constraint.  
e.g. 2006 flares from PKS 2155-304:



An exceptional flare from the blazar PKS 2155-304 seen in 2006 with the H.E.S.S. array. (F. Aharonian et al. 2007)

- measure of characteristic variability time scale with flux doubling time for any pair of points (i,j) in the light curve

$$T_2 \equiv \left| \frac{(I_j + I_i)}{2} \frac{T_j - T_i}{I_j - I_i} \right|$$

shortest  $T_2 = 224 \pm 60$  s

- similar result for the fastest rise-time from generalized Gaussian fit functions :  $\tau_r = 173 \pm 28$  s

→ Applying the **causality constraint** leads to :

$$R / \delta \leq 4.65 \times 10^{12} \text{ cm} \leq 0.31 \text{ AU}$$

while the Schwarzschild radius of the source is :

$$R_S \sim 3 \times 10^5 \text{ cm} / M_\odot \times 10^9 M_\odot \sim 3 \times 10^{14} \text{ cm}$$

For  $R \leq R_S$ , this would imply  $\delta \sim 100$  !

# rapid variability from reconnection ?

Several scenarios (mini-jet, jet-in-jet, needle-in-jet) are proposed to achieve compact emission regions within the jet and very large Doppler factors.

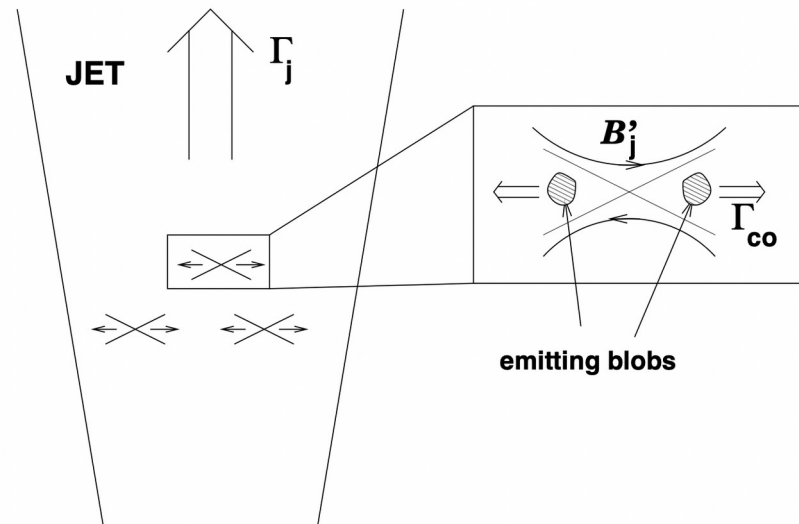
e.g. the **jet-in-jet model** assumes that **reconnection events** within the Poynting-flux dominated jet. Small plasma blobs are ejected from such events with angle  $\theta'$  against the jet axis and with Lorentz factor  $\Gamma_{co}$  in the comoving (jet) frame. For an observer in the source frame, this leads to

$$\Gamma_{tot} = \Gamma_j \Gamma_{co} (1 + \beta_j \beta_{co} \cos \theta')$$

$$\tan \theta = \frac{\beta_{co} \sin \theta'}{\Gamma_j (\beta_{co} \cos \theta' + \beta_j)}$$

For angles of  $\theta'$  around  $\pi/2$ , this would lead to  $\Gamma_{tot} \approx \Gamma_j \Gamma_{co}$  and a viewing angle of  $\theta \approx 1/\Gamma_j$ . Very high Lorentz factors of  $\Gamma_{tot} \approx 100$  may be achievable in this way.

A very large magnetisation is required ( $\sigma \sim 100$ ,  $B \sim 10$  G) in such scenarios (cf. Nalewajko et al. 2011).



geometry of the jets-in-jet model  
*Giannios et al. 2009*

# stochastic characteristics of the mini-jet model

The flux distribution from blazars is shown to follow a lognormal distribution (i.e.  $\log(\text{flux})$  is normally distributed).

Lognormal distributions are related to multiplicative processes, BUT the flux distribution of a large number of minijets is shown to experimentally resemble a lognormal distribution.

→ Even though the minijet model proposes an **additive mechanism for variability** (sum of independent boosted emitting regions, isotropically oriented within the bulk relativistic flow of a jet.), it leads to an **approximately lognormal flux distribution**.

It is also shown that the flux from minijets is proportional to their rms.

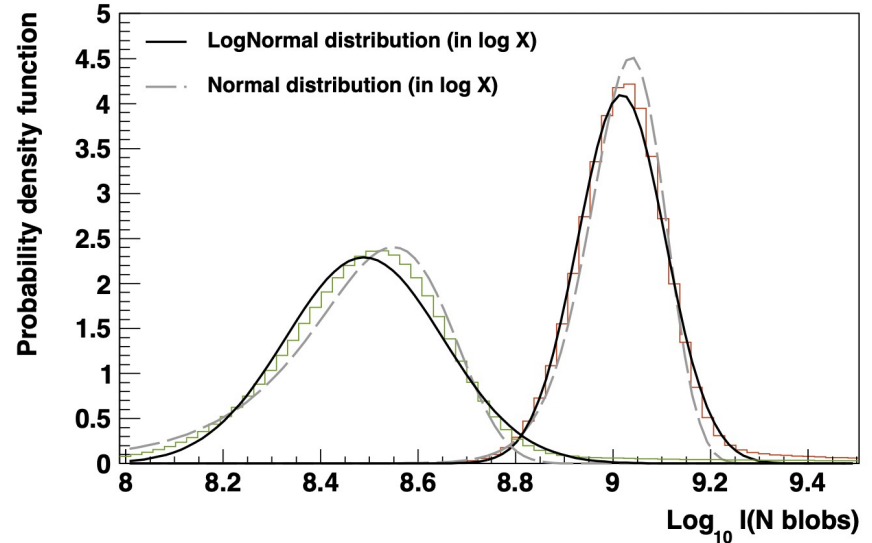


**Fig.5.** Distribution of the logarithm of the flux of  $N$  minijets for  $N = 3 \times 10^3$  (left) and  $N = 10^4$  (right), as in Fig. 4. The continuous black and grey dashed lines represent the best fit with a log-normal and normal flux distributions, respectively.

*Biteau & Giebels 2012*

# rapid variability from the BH magnetosphere ?

Rapid variability detected from the **radio galaxy IC 310** with doubling time scales of  $< 5$  min and **small Doppler factor  $< 10$** .

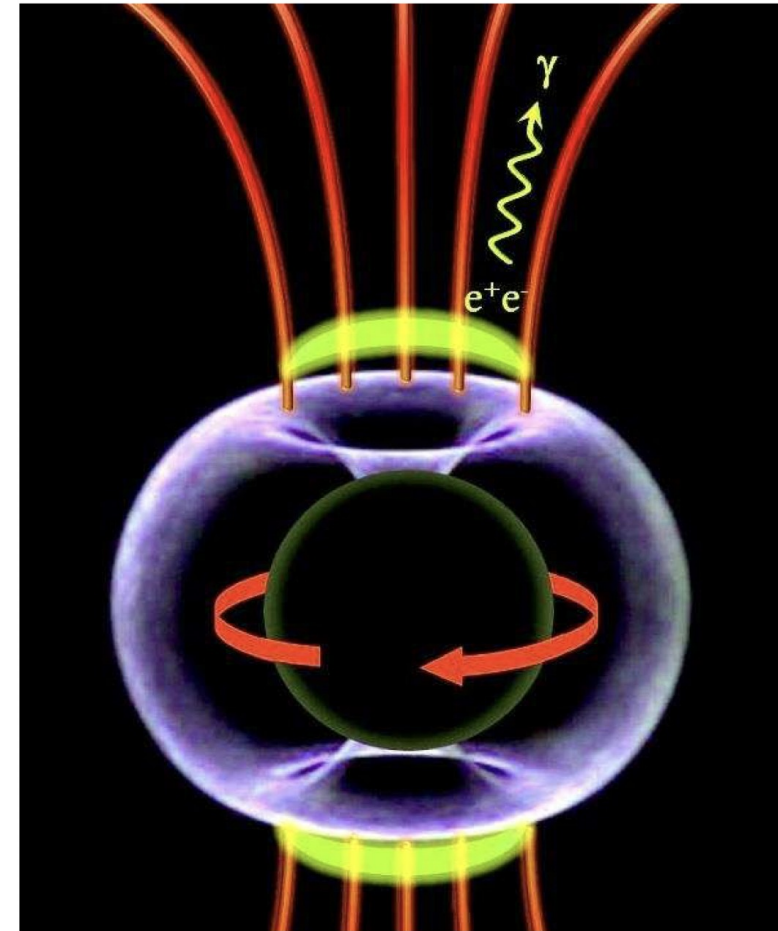
→ Causality constrains the size of the emission region to be smaller than 20% of the gravitational radius of its central BH.

Proposed scenario : **pulsar-like particle acceleration** by the electric field across a magnetospheric gap at the base of the radio jet.

- A maximally rotating BH with event horizon  $r_g$  (black sphere) accretes plasma. In the ergosphere (blue) extending to  $2r_g$  in the equatorial plane, Poynting flux is generated by the frame-dragging effect (→ Blandford-Znajek)

- The rotation of the BH induces a magnetosphere (red) with polar vacuum gap regions (yellow). In the gaps, the **electric field of the magnetosphere has a component parallel to the magnetic field** accelerating particles to ultra-relativistic energies.

- **Inverse-Compton scattering and pair production** due to interactions with low-energy thermal photons from the accretion disk leads to the observed gamma rays.

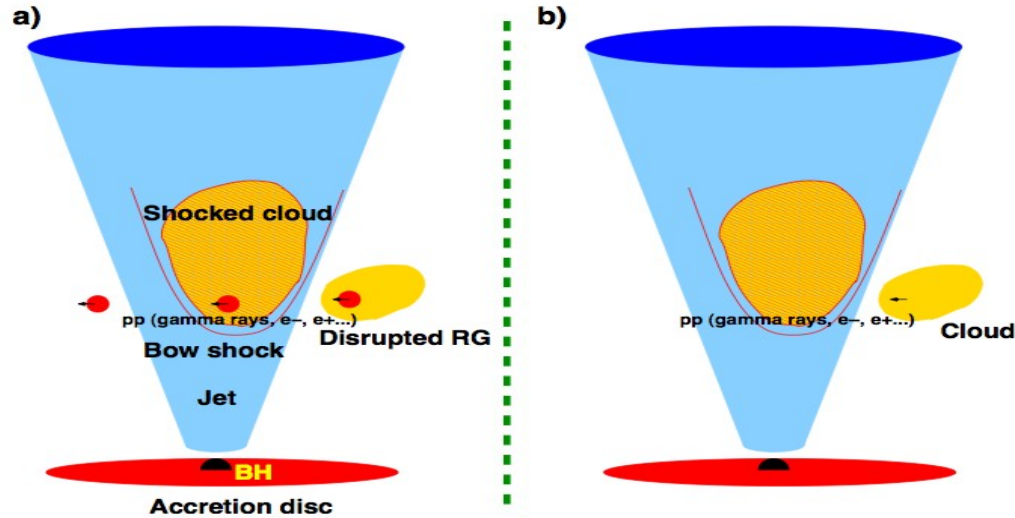


(Aleksic et al. 2014)

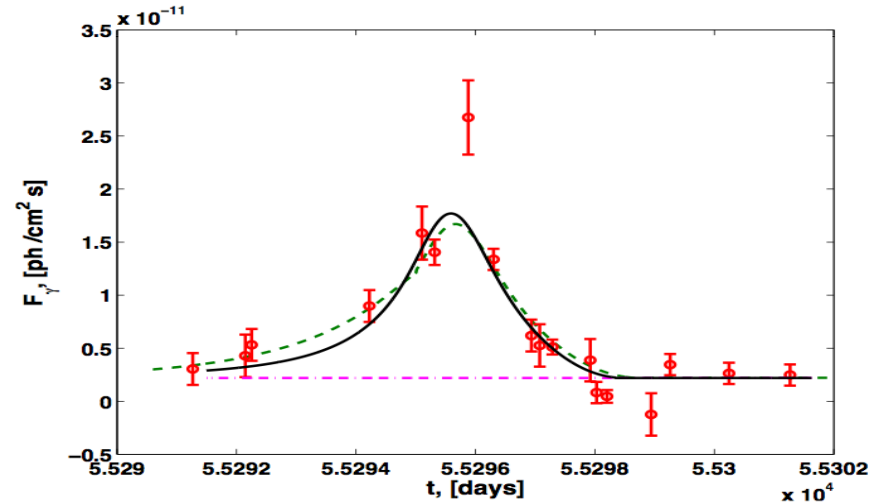
# jet/cloud interaction

very rapid variability seems possible if relativistic hadrons in the jet interact with stellar envelopes (red giants) or gas clouds (BLR) via p-p, p- $\gamma$  or p-synchrotron.

(e.g. D.V. Khangulyan, M.V. Barkov, V. Bosch-Ramon, F.A. Aharonian, A.V. Dorodnitsyn 2013)



Bosch-Ramon, Perucho, Barkov, A&A (2012)

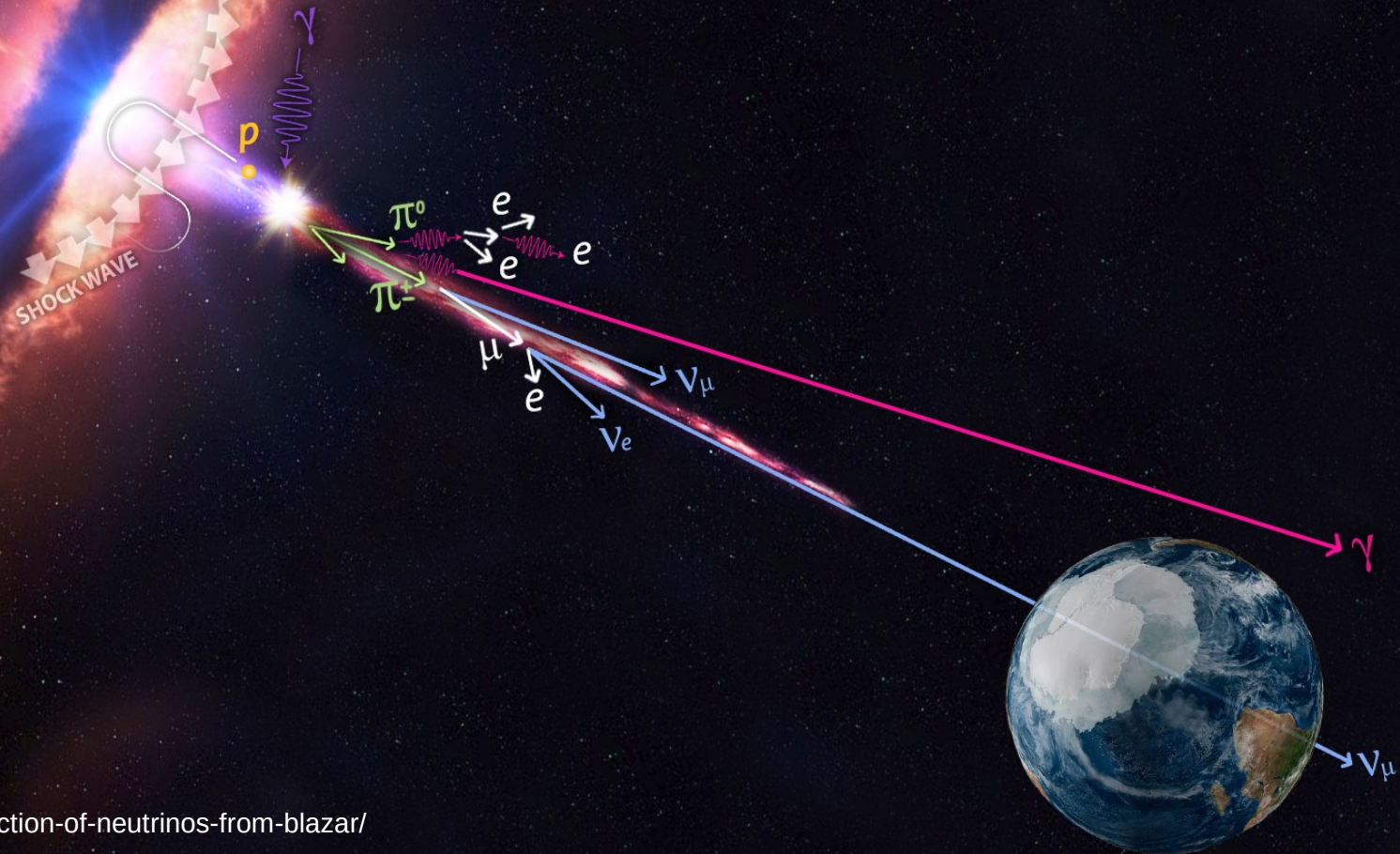


VHE flare of M87 in 2010

Barkov, Bosch-Ramon, Aharonian, ApJ (2012)

problems: collision rate realistic?, jet stability...

## 7) flares and multi-messengers



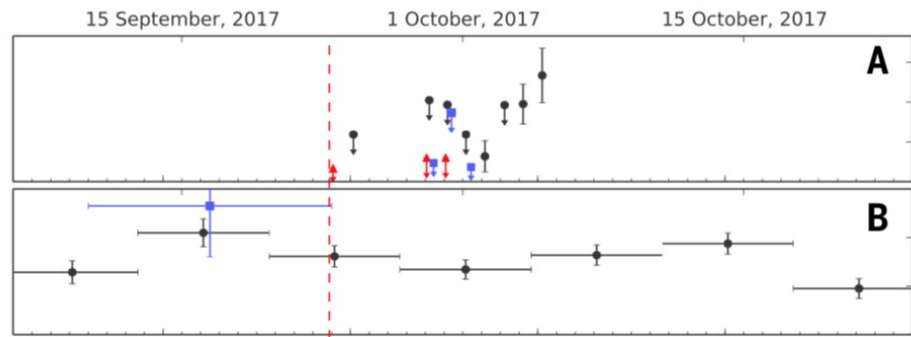
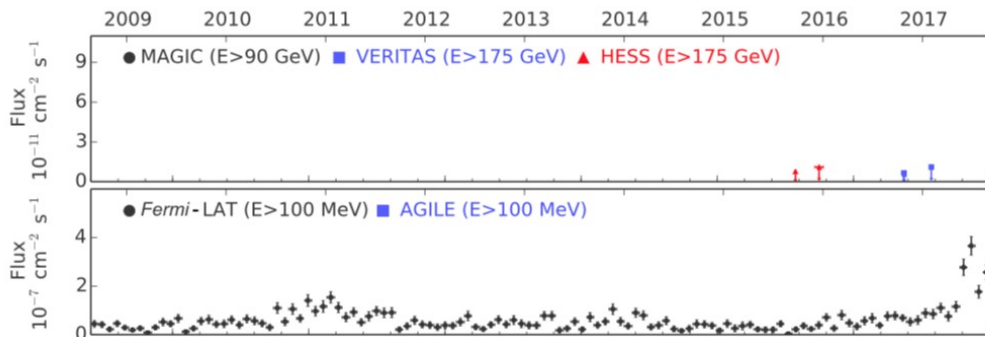
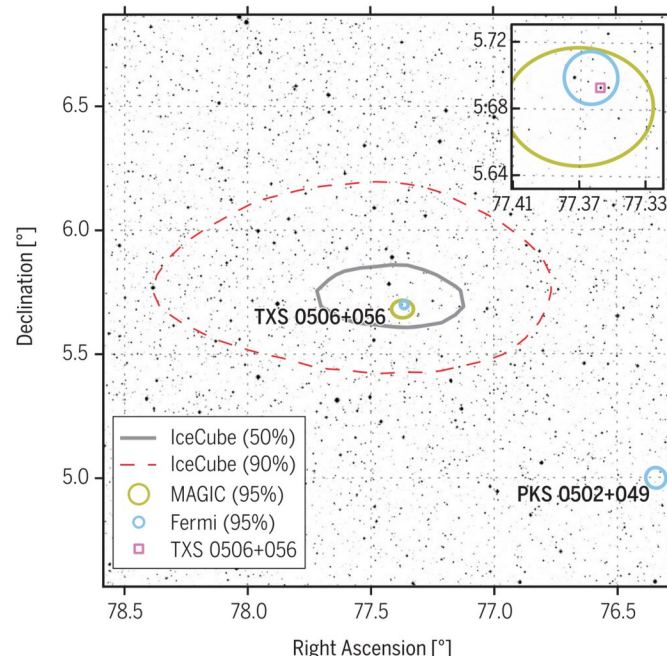


# TXS 0506+056: first extragalactic neutrino source?

First detection of a high-energy neutrino ( $\sim 290$  TeV) with IceCube from a known blazar during a  $\gamma$ -ray outburst (duration  $\sim 6$  months) in 2017, followed by a VHE flare seen with MAGIC.

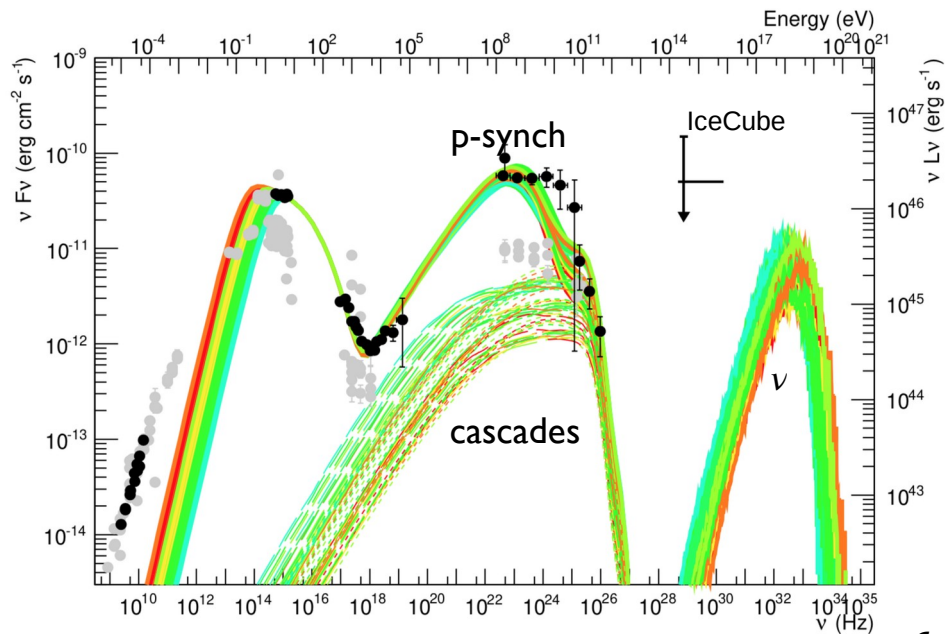
-> chance coincidence at  $3\sigma$  level

Later also detection with the VERITAS Cherenkov telescopes.



Aartsen et al. 2018

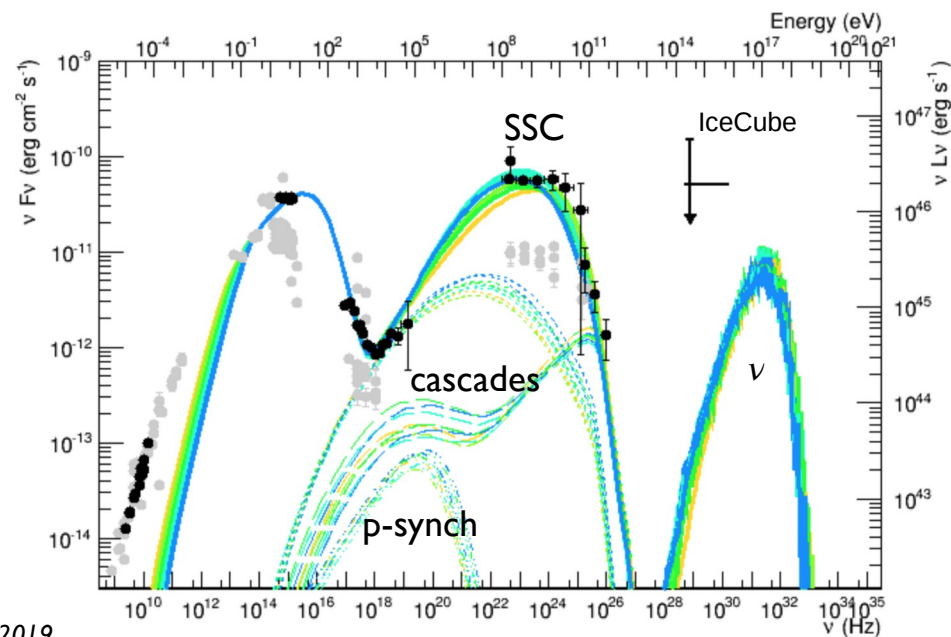
# interpretation with one-zone lepto-hadronic code



(a) Proton synchrotron modeling of TXS 0506+056

$\gamma$ -rays mostly p-synchrotron  
+ cascade emission

->  $\nu$  rate too low to be consistent with IceCube



(b) Lepto-hadronic modeling of TXS 0506+056

$\gamma$ -rays mostly SSC + cascade emission

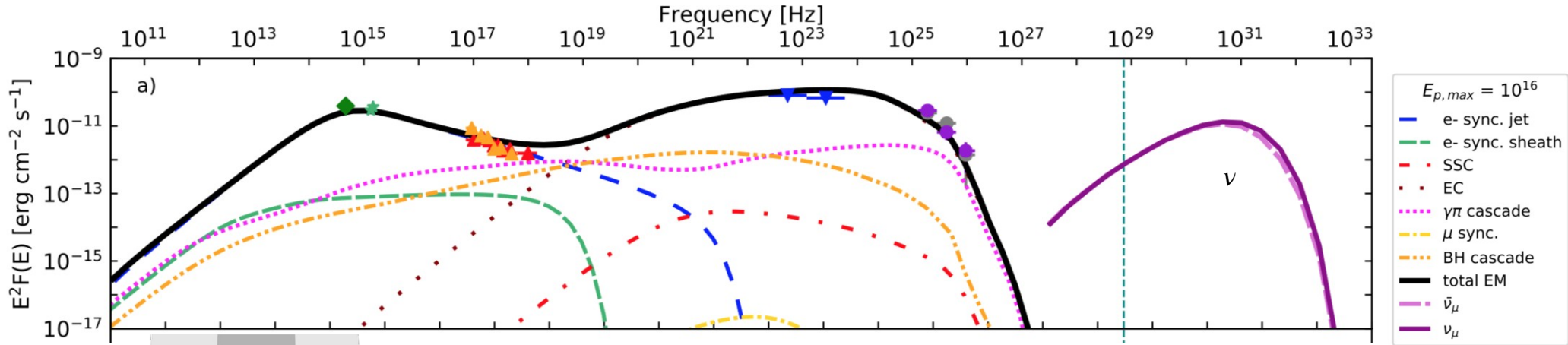
->  $\nu$  flux marginally consistent with IceCube (prob. ~2%)

-> very high jet power

*Cerruti et al. 2019*

# external photon fields ?

e.g. *Ansoldi et al. 2018*: interactions of e- and p+ co-accelerated in the jet with external photons originating from a **slow-moving plasma sheath surrounding the faster jet spine**.

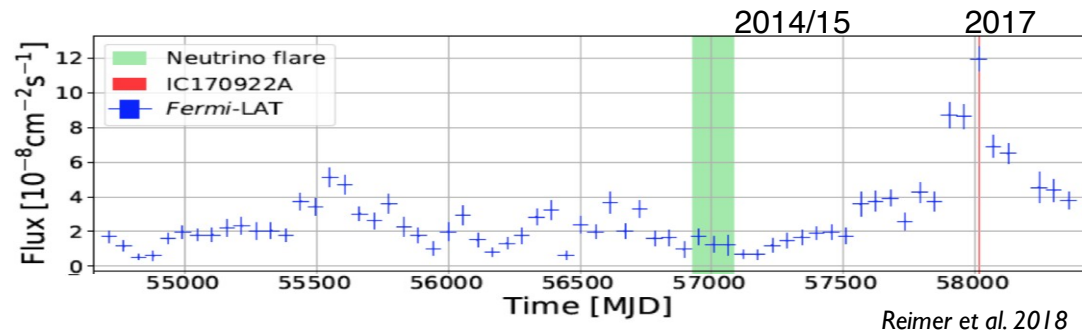
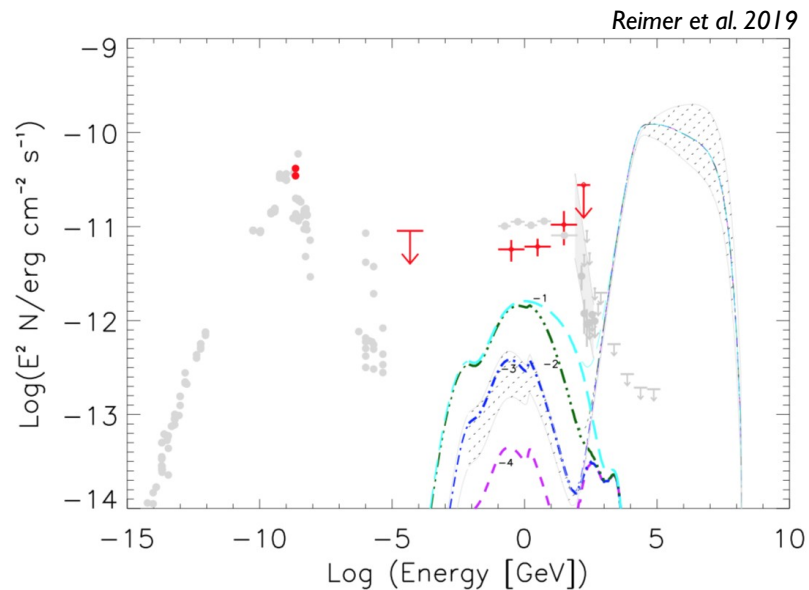


-> Good reproduction of MWL SED and neutrino rate (~0.2 events for flare), with acceptable jet power.

->  $\gamma$ -rays mostly from Inverse Compton up-scattering of the external ("layer") field.

# the 2014/15 “orphan” neutrino flare

Archival searches in IceCube then found a flare in the 2014/15 data ( $\sim 3.5\sigma$ ), not accompanied by any  $\gamma$ -ray flaring.

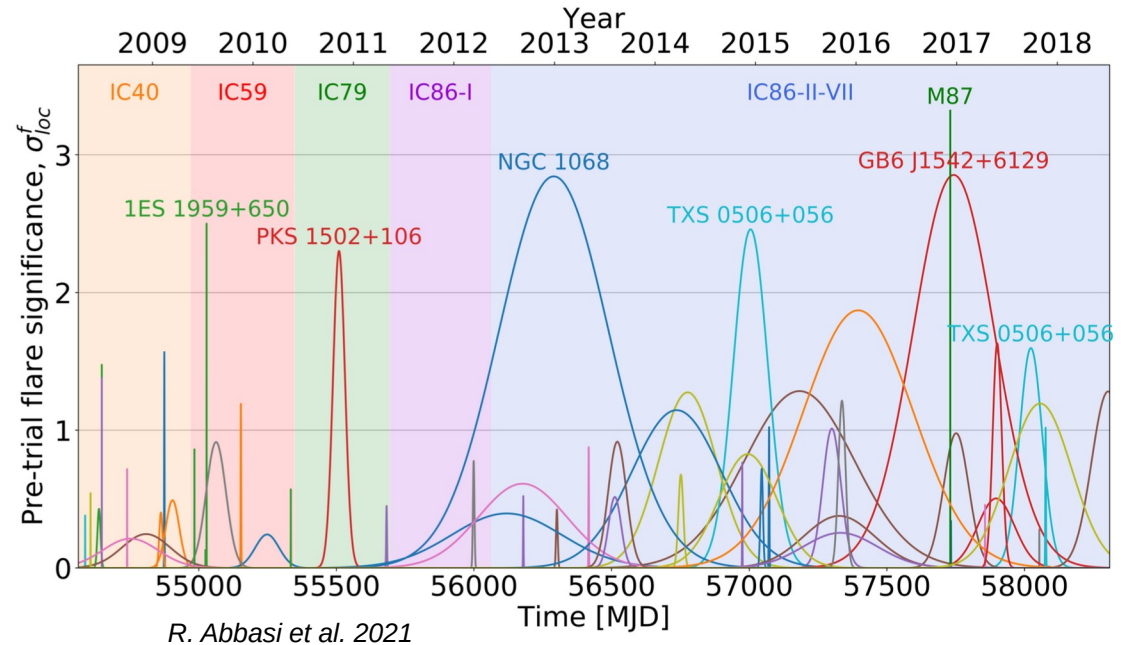


-> no direct causal connection between  $\gamma$ -ray flares and neutrino events

Only solution to explain  $\nu$  flare implies that the majority of  $\gamma$ -rays are emitted from another region in the source !

# neutrinos correlated with AGN flares ?

Search for time-dependent correlations between 10 years of IceCube data and a pre-defined catalog of 110 neutrino candidate sources.

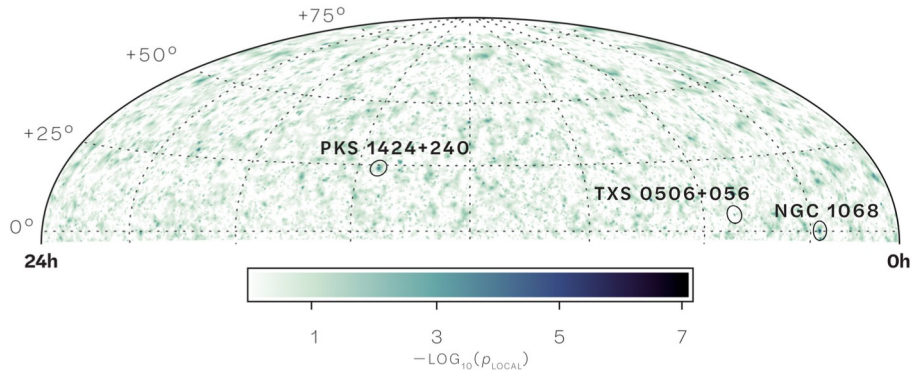


- Time-dependent statistical test of the Northern hemisphere suggests an incompatibility at **3.0  $\sigma$  significance** of the neutrino events from **four sources** with respect to the overall Northern background expectation :  
NGC 1068 (Seyfert2 & starburst) , TXS 0506+056 (blazar), GB6 J1542+6129 (blazar), M87 (radio-galaxy)

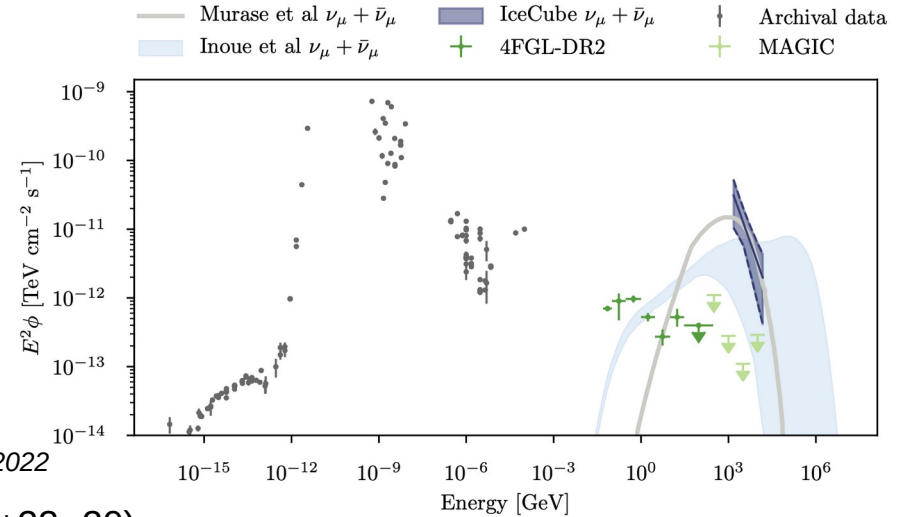
- The three first sources are also seen in time-independent studies, but not M87.

- No significant result in the Southern hemisphere → consistent with the lower sensitivity due to the substantially larger background of atmospheric muons in the Southern hemisphere.

# neutrinos from NGC 1068



IceCube Collaboration 2022



Systematic analysis of IceCube events found an excess of 79 (+22 -20) high-energy neutrinos associated with the nearby **active / starburst galaxy** NGC 1068 at a significance of **4.2  $\sigma$** .

NGC 1068 is a nearby Seyfert II galaxy with a core that is optically thick. It has strong starburst activity and outflows.

Emission scenarios :

- particle acceleration linked to the **active nucleus** (e.g. disk wind) **or starburst region**
- environment allows production of neutrinos and strong absorption of gamma rays

# blazars as sources of UHECRs ?

Blazars are probably not the dominant source of observed TeV/PeV neutrinos (Aartsen et al. 2017).

But they might dominate the UHECR spectrum.

BL Lac objects:

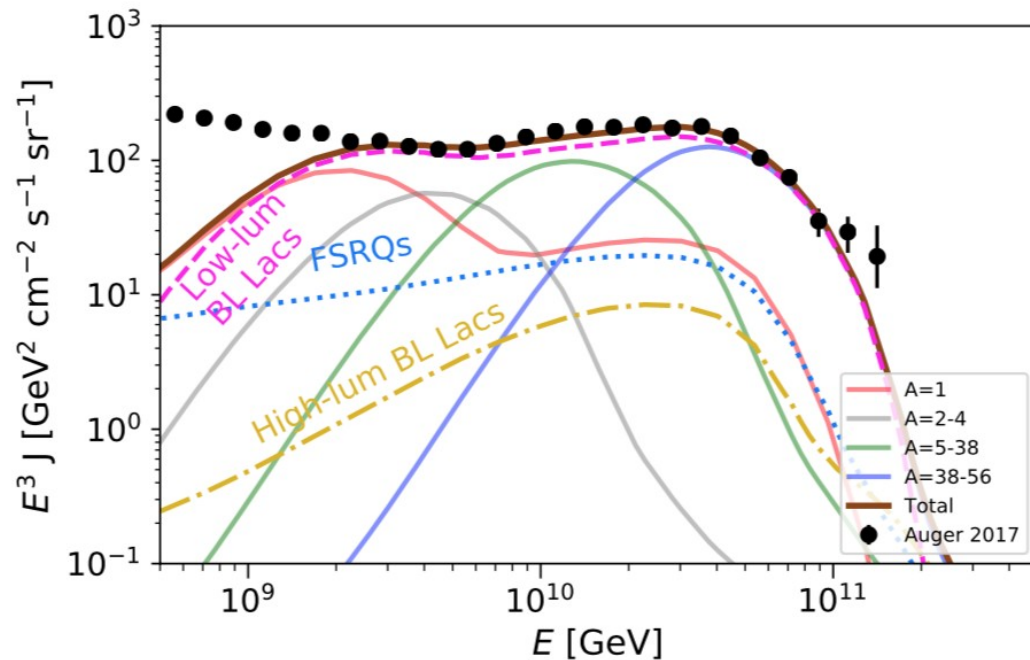
- nearby sources (mostly  $z < 0.5$ )
- low external photon fields
- > survival & escape of nuclei

-> should be **efficient UHECR emitters**

FSRQs:

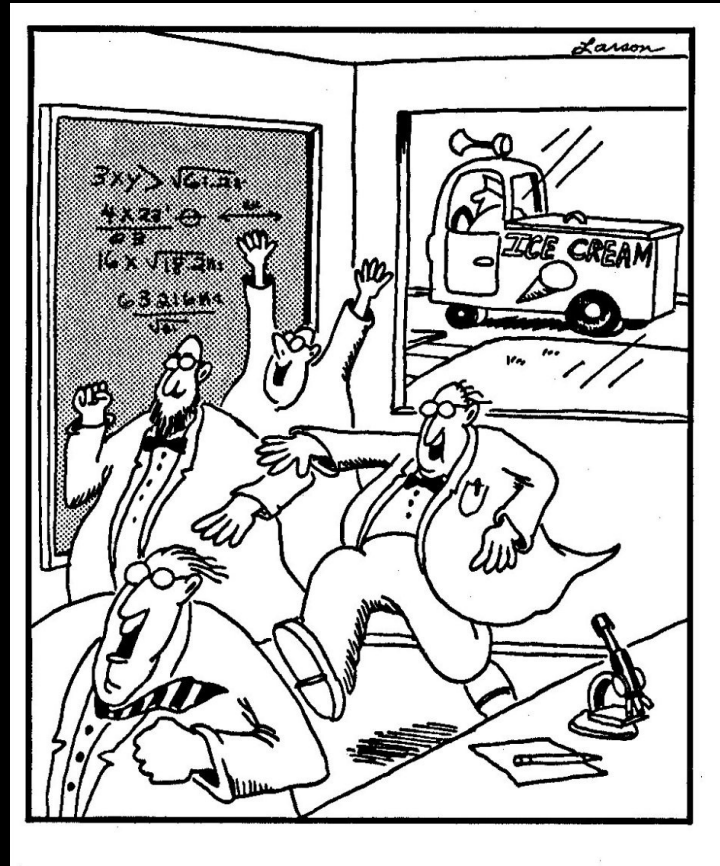
- high external photon fields
- > strong pion production

-> should be **efficient  $\nu$  emitters at EeV energies**



Rodrigues X. et al. 2021

## 8) conclusions & outlook





# variability – attempt at a short summary

---

- Flux variability is detected in all types of AGNs at all wavelengths and time scales (shortest time scales at the highest energies).
- The origin is not clearly understood, but probably **multiple mechanisms** are responsible:
  - geometric effects → long-term variability, QPOs
  - shocks, turbulence in the jet ; variation of the accretion rate → medium- and short-term variability
  - reconnection, turbulence in the jet ; particle acceleration in the BH magnetosphere → very short-term variability
- Links seem to exist between flares and multi-messenger emission, but the correlation is not trivial.

# what observational approach ?

---

- Need to combine
  - **MWL and VLBI monitoring** of AGNs with regular sampling
    - characterisation of variability at different scales, study of temporal evolution of the jet structure (radio knots...)
  - **MWL and multi-messenger ToOs** on AGN flares
- There is probably a lot more to be learnt from optical and X-ray polarisation studies

# take-home message : blazars are cool !



<https://invisibleaudio.bandcamp.com/album/reach-out>

## → Meet **BLAZAR**

Posted: October 7, 2020 by Soda in [Blazar](#), [Feature](#), [Indie](#), [New Release](#), [Pop](#), [Single](#)

I'm tellin' ya, you gotta give it to a patient, consistent and polite artist. Jerad Finck is THAT guy. And, to top it off he's got some great sounds to go right along with it. Jerad and I have been back and forth for a few months to get him a feature on M-S-G and well, life happens and it's already October, (BOO!). I am happy to finally give them/him a bump.



Blazar is hot on the heels of brand new single "Precious". Great timing too, it's upbeat, fun, danceable. All the things needed to close your eyes for a few moments on such a soulless year. No surprise it's as good as it is, the work has been put in and quite a team was behind it.

<https://musicsurvivalguide.org/category/blazar/>



<https://www.facebook.com/TheSilkenBlazar/>